Displacement and stress intensity factors of elliptical and ribbon-like cracks in a transformed transversely isotropic matrix

Jean-François Barthélémy[1]

2026

[1] *Cerema, Univ Gustave Eiffel, UMR MCD, F-77171 Sourdun, France*

This paper is devoted to the analytical derivation of the displacement intensity factor (DIF) and stress intensity factor (SIF) vectors for elliptical and ribbon-like cracks embedded in an infinite matrix, with particular focus on the case of a transformed transversely isotropic (TraTI) matrix. The approach is based on an integral equation framework applied to the crack opening displacement (COD), from which general expressions for the DIF and SIF are established for an arbitrary elastic matrix symmetry. The method of linear transformation of elastic boundary value problems – connecting the TraTI problem to a transversely isotropic (TI) reference problem in which the crack is aligned with the isotropy plane – is then applied to derive closed-form analytical expressions of the DIF and SIF for both elliptical and ribbon-like cracks. This extends a previous paper restricted to the compliance contribution tensor and average COD tensor of a crack in a TraTI matrix, to the full local COD profile and the associated DIF and SIF distributions along the crack front. A numerical application illustrates the analytical results through the computation of the local energy release rate around an elliptical crack in a monoclinic TraTI matrix. Validations against semi-analytical and finite element simulations are provided.

Author-accepted manuscript (postprint). This is the accepted version of an article published by Elsevier in *International Journal of Solids and Structures*. The version of record is available at doi:10.1016/j.ijsolstr.2026.114293. Please cite as: J.-F. Barthélémy, "Displacement and stress intensity factors of elliptical and ribbon-like cracks in a transformed transversely isotropic matrix", *International Journal of Solids and Structures* (2026) 114293.

Nomenclature

	Symbol	Description
General notations		
	s, t	Scalar

Symbol	Description
$\vec{v}$	Vector (1st order tensor)
$\mathbf{A}$	2^{nd} order tensor
$\boldsymbol{C}$	4^{th} order tensor
$\mathbf{1}$	2^{nd} order identity tensor
Tensor operations	
$\otimes$	Tensor product: $(\vec{a} \otimes \vec{b})_{ij} = a_i b_j$
$\overset{s}{\otimes}$	Symmetrized tensor product: $(\vec{a} \overset{s}{\otimes} \vec{b})_{ij} = \frac{1}{2}(a_i b_j + a_j b_i)$
$\overset{s}{\boxtimes}$	Modified tensor product: $(\mathbf{a} \overset{s}{\boxtimes} \mathbf{b})_{ijkl} = \frac{1}{2}(a_{ik} b_{jl} + a_{il} b_{jk})$
$\cdot$	Single contraction: $(\mathbf{A} \cdot \vec{b})_i = A_{ij} b_j$
$:$	Double contraction: $\mathbf{A} : \mathbf{B} = A_{ij} B_{ij}$; $(\boldsymbol{A} : \mathbf{B})_{ij} = A_{ijkl} B_{kl}$
$\vec{n} \cdot \boldsymbol{Q} \cdot \vec{n}$	Normal double contraction: $(\vec{n} \cdot \boldsymbol{Q} \cdot \vec{n})_{ij} = n_k Q_{kijl} n_l$
$\cdot^{\intercal}$	Transpose
$\cdot^{-1}$	Inverse
$\cdot^{-\intercal}$	$\equiv \left(\cdot^{-1}\right)^{\intercal} \equiv \left(\cdot^{\intercal}\right)^{-1}$
$\cdot^{\dagger}$	Moore-Penrose pseudo-inverse
$\wedge$	Cross product
Decorations and conventions	
$\hat{\cdot}$	Fourier transform
$\cdot^{\star}$	In-plane component perpendicular to $\vec{n}$, e.g. $\vec{v} = \vec{v}^{\star} + v_n \vec{n}$ with $\vec{v}^{\star} \cdot \vec{n} = 0$ Fourier transform reduced to $\vec{n}^{\perp}$ plane $\hat{\phi}^{\star}(\vec{\xi}^{\star}) = \frac{1}{2\pi} \int_{\xi_n=-\infty}^{+\infty} \hat{\phi}(\vec{\xi}^{\star} + \xi_n \vec{n})\, \mathrm{d}\xi_n$
$\cdot^{\sharp}$	Quantity in the reference (transformed) problem
$[\![\vec{u}]\!]$	Displacement discontinuity (jump) across crack surface
Crack geometry	
$\mathscr{I}$	Crack (generic notation)
$\mathscr{E}, \mathscr{R}$	Elliptical and ribbon-like crack geometries
$\mathbf{A}$	Crack shape tensor (rank-deficient)
$\mathbf{S}, \mathbf{R}$	Shape and rotation tensors from polar decomposition of $\mathbf{A}$
$\vec{n}$	Unit normal to crack plane
$\vec{l}, \vec{m}$	Unit vectors along major and minor axes
a, b	Major and minor semi-axes ($a \geqslant b$)
$\eta = b/a$	Aspect ratio
$\vec{\nu}, \vec{\tau}$	Outer normal and tangent at crack border $\partial\mathscr{I}$
Elasticity	
$\boldsymbol{C}, \boldsymbol{S} = \boldsymbol{C}^{-1}$	Elastic stiffness and compliance tensors
$\boldsymbol{\sigma}, \boldsymbol{\varepsilon}$	Stress and strain fields
$\boldsymbol{\Sigma}, \mathbf{E}$	Remote (prescribed) stress and strain
$\vec{t} = \boldsymbol{\sigma} \cdot \vec{n}$	Stress vector on the crack plane
Integral equation kernels	
$\hat{\boldsymbol{\Gamma}}(\vec{\xi}), \hat{\boldsymbol{Q}}(\vec{\xi})$	Green kernels in Fourier space
$\hat{\mathbf{Q}}^{\star}_{nn}(\vec{\xi}^{\star})$	Reduced kernel: $\frac{1}{2\pi} \int_{-\infty}^{+\infty} \vec{n} \cdot \hat{\boldsymbol{Q}}(\vec{\xi}^{\star} + \xi_n \vec{n}) \cdot \vec{n}\, \mathrm{d}\xi_n$
$\boldsymbol{\Lambda}$	Kernel in crack integral equation
Crack mechanics	
$[\![\vec{u}]\!]$	Crack opening displacement (COD)
$\vec{\beta}$	Maximum COD vector
χ	Dimensionless average COD coefficient ($\frac{2}{3}$ for $\mathscr{E}$, $\frac{\pi}{4}$ for $\mathscr{R}$)
$\mathbf{B}^{\mathscr{E}}, \mathbf{B}^{\mathscr{R}}$	Normalized COD tensors (elliptical and ribbon-like)

Symbol	Description
$\bar{\mathbf{B}}$	COD tensor for a closed frictionless crack
$\vec{N}\ (N_I, N_{II}, N_{III})$	Displacement intensity factor (DIF) vector and modal components
$\vec{K}\ (K_I, K_{II}, K_{III})$	Stress intensity factor (SIF) vector and modal components
$G = \vec{K} \cdot \vec{N}$	Local energy release rate
Linear transformation	
$\mathbf{P}$	Linear transformation tensor: $\vec{x}^\sharp = \mathbf{P}^{-1} \cdot \vec{x}$
Undecorated symbols	Initial anisotropic problem
TI	Transversely isotropic (reference material class)
TraTI	Transformed transversely isotropic (initial material class)

1 Introduction

The displacement and stress intensity factors (DIF and SIF) of elliptical and ribbon-like cracks embedded in an infinite matrix of transformed transversely isotropic (TraTI) symmetry are analytically derived in this paper. The approach combines the integral equation framework of Kunin (1983) and Kanaun and Levin (2009) with the linear transformation technique between elastic boundary value problems, thereby extending to TraTI the set of anisotropies for which fully closed-form expressions of DIF and SIF are available.

Stress intensity factors, originally introduced by Irwin (1957) to characterize the singular stress field near a crack front, are central to fracture mechanics. Their connection with the path-independent J-integral of Rice (1968) provides an important energetic interpretation. In the context of micromechanics of cracked media (Dormieux and Kondo, 2016; Kachanov, 1993, 1992; Kachanov and Sevostianov, 2018; Nemat-Nasser and Hori, 1999), the SIF are also intimately related to the crack opening displacement (COD) and compliance contribution tensors, as discussed in Rice (1975), Kachanov and Sevostianov (2018) and Sevostianov and Kachanov (2021). Kassir and Sih (1966) showed that, for an elliptical crack in an infinite isotropic matrix, the stress state near the crack front decomposes into a combination of local plane-strain and antiplane-shear problems, a result that has since formed the basis of many SIF analyses (Budiansky and O'Connell, 1976; Hoenig, 1978; Rice, 1968). Closed-form formulas for the SIF in isotropic media can be found in, e.g., Kachanov et al. (2003) and Fabrikant (1987).

The problem of a crack in an anisotropic matrix was pioneered by Willis (1968) who expressed, via Fourier transforms, the stress field and COD for an arbitrary crack in a compact contour-integral form. Kassir and Sih (1968) computed the three-dimensional stresses around elliptical cracks in transversely isotropic (TI) solids, showing that the local plane-strain/antiplane-shear decomposition remains valid when the crack is aligned with the isotropy plane. Hoenig (1978) derived integral-form expressions for the SIF and COD in a generally anisotropic medium, establishing that closed-form evaluation is feasible for a crack aligned with the isotropy plane of a TI matrix. Further closed-form results for such geometries were provided by Laws (1985) and Sevostianov et al. (2005). The relationship between the asymptotic coefficient of the COD and the SIF in the framework of an arbitrary crack shape in an anisotropic matrix was derived by Kanaun (1981) under an integral form. For a planar crack aligned with the plane of isotropy of a TI matrix, this relationship was obtained from a boundary integral equation approach by Zhao et al. (1998), and subsequently extended to coupled multi-field problems by Zhao et al. (2007) and Li et al. (2020). The effective elastic properties of anisotropic materials with arbitrary orientations of multiple cracks, relying on the SIF and COD tensors, were studied by Mauge and Kachanov (1994a), Mauge and Kachanov (1994b), Tsukrov and Kachanov (2000) and Gruescu et al. (2005) among others. A systematic integral equation approach for elliptical cracks in 3D anisotropic media was developed by Kanaun and Levin (2009), leading to compact expressions for the COD via a reduced Fourier transform. When closed-form solutions are out of reach, the semi-analytical method of Barthélémy (2009), requiring only a one-dimensional numerical quadrature, offers an efficient alternative for elliptical cracks in arbitrary anisotropy.

A powerful strategy to extend the class of anisotropies amenable to analytical treatment consists in applying a linear transformation to the elastic boundary value problem, as introduced by Pouya (2000) and developed by Pouya and Zaoui (2006). This technique establishes a correspondence between two elastic problems through an invertible linear mapping of the spatial coordinates, so that the solution of a complex anisotropy problem can be inferred from that of a simpler reference problem on a body of different geometry. Pouya (2007) showed that the TraTI symmetry is linearly connected to transverse isotropy and provided the first explicit analytical expression of the Green tensor for TraTI materials. The approach was exploited for ellipsoidal inhomogeneities in elliptically orthotropic (EO) matrices by Sevostianov and Kushch (2020) and Kushch and Sevostianov (2020). In the crack context, Barthélémy et al. (2021) used this strategy to derive the compliance contribution tensor of an elliptical crack in an EO matrix, and Barthélémy et al. (2023) extended it to the compliance contribution tensor and average COD tensor of an arbitrarily oriented crack in a TraTI matrix, covering configurations in which the COD tensor is not diagonal in the crack frame.

The present paper extends the framework of Barthélémy et al. (2023) by going beyond average compliance quantities to derive the full local COD profile and the associated DIF and SIF distributions along the crack front, for both elliptical and ribbon-like cracks in a TraTI matrix. The derivation follows a different resolution strategy from Barthélémy et al. (2021) and Barthélémy et al. (2023), relying directly on the integral equation formulation of Kunin (1983) and Kanaun and Levin (2009). The paper is organized as follows. Section 2 recalls the integral equation framework and establishes general expressions for the COD tensor, DIF and SIF of elliptical and ribbon-like cracks in a matrix of arbitrary anisotropy; the framework is further extended to the practically important case of a closed frictionless crack. Section 3 presents the linear transformation method, derives the corresponding transformation rules for the COD tensor, DIF and SIF, and applies them to the EO and TraTI cases to yield fully closed-form analytical expressions. Section 4 illustrates the approach through a numerical example: the local energy release rate is computed around an elliptical crack embedded in a monoclinic TraTI matrix. Semi-analytical and finite element computations are used to validate the closed-form solution. The appendices provide auxiliary material used throughout the text: among them, Appendix 6.3 collects closed-form expressions of the COD tensor for the reference cases of an isotropic matrix (Appendix 6.3.1) and a TI matrix with the crack aligned with the isotropy plane (Appendix 6.3.2); these expressions are rewritten in a unified notation that makes the limiting transitions from the TI to the isotropic case, and from elliptical to circular or ribbon-like crack shapes, straightforward.

2 Isolated crack in an anisotropic unbounded elastic matrix: background and extension to a closed frictionless crack

Within the framework of linear elasticity, the present paper deals with the problem of a plane *elliptical* crack embedded in a homogeneous unbounded anisotropic 3D matrix and subjected to remote prescribed tractions (see Fig. 1), especially when purely analytical solutions are available. A *ribbon-like* (translation-invariant) crack is also considered as a limiting case and plays an important role in the framework of the calculation of stress intensity factors even in the case of an elliptical shape.

This section aims at recalling the background of the resolution of this problem leading to the crack opening displacement tensor and stress intensity factors with a carefully detailed proof. Such a derivation prepares the application of the transformation method in Section 3 to extend the set of anisotropic behaviors for which analytical solutions are reachable.

In Section 2.1, the crack is defined from a rank-deficient quadratic positive form. Then the linear elastic equilibrium of this crack is considered in Section 2.2 followed by a reformulation of the problem as an integral equation in Section 2.3 without any particular assumptions made on the material symmetries. The general expressions of the crack-opening displacement tensor and stress and displacement intensity vectors are then derived in subsequent sections for any elastic matrix and any orientation and aspect-ratio of the elliptical crack.

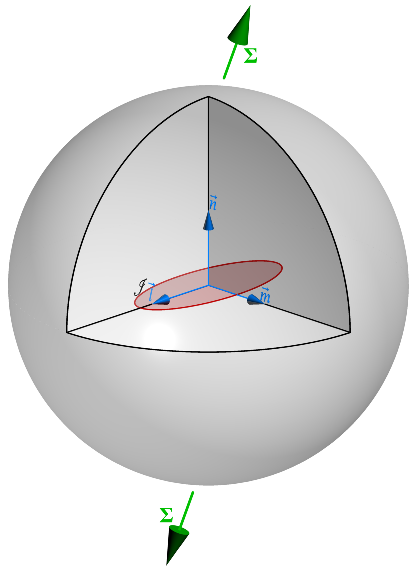

Fig. 1: Graphical illustration of the problem under investigation. The crack $\mathscr{I}$ is embedded in an infinite matrix and subjected to remote stresses. Note that at this stage, no asumption is made on the material symmetries of the matrix, nor on the direction of loading.

2.1 Geometric description of the crack

The crack $\mathscr{I}$ under consideration is embedded in the unbounded space $\mathbb{R}^3$. It is defined as the following set of points

$$\vec{x} \in \mathscr{I} \quad \Longleftrightarrow \quad \vec{x} \cdot \vec{n} = 0 \quad \text{and} \quad \vec{x} \cdot (\mathbf{A}^{\intercal} \cdot \mathbf{A})^{\dagger} \cdot \vec{x} \leqslant 1 \tag{1}$$

where $\mathbf{A}$ is a second-order, singular tensor of rank 1 or 2 such that $\vec{n} \in \operatorname{Ker}\mathbf{A}$, $\|\vec{n}\| = 1$ and $(\mathbf{A}^{\intercal} \cdot \mathbf{A})^{\dagger}$ denotes the Moore-Penrose inverse (pseudoinverse) of $\mathbf{A}^{\intercal} \cdot \mathbf{A}$ (not invertible in the usual sense because $\mathbf{A}$ is not of rank 3). It results from the above definition that crack $\mathscr{I}$ is embedded in the plane perpendicular to $\vec{n}$.

In the elliptical case (see Fig. 2, left), the crack is denoted $\mathscr{E}$ and the tensor $\mathbf{A}$ is of rank 2 ($\operatorname{Ker}\mathbf{A} = \operatorname{Span}(\vec{n})$). In the ribbon-like case (see Fig. 2, right), the crack is denoted $\mathscr{R}$ and the tensor $\mathbf{A}$ is of rank 1 ($\operatorname{Ker}\mathbf{A} = \operatorname{Span}(\vec{l}, \vec{n})$, where $\vec{l}$ is a unit vector, orthogonal to $\vec{n}$). The general definition (1) of an ellipse/ribbon might seem overly complicated. It will be seen later that it is well-suited to further applications of linear transforms. It is briefly verified below that it indeed defines an ellipse (resp. a ribbon) when $\mathbf{A}$ is of rank 2 (resp. 1) and some useful characteristics of $\mathbf{A}$ are particularly extracted. The general form of $\mathbf{A}$ is (see Appendix 6.1)

$$\mathbf{A} = a\,\vec{U} \otimes \vec{l} + b\,\vec{V} \otimes \vec{m} \tag{2}$$

where $a, b \geqslant 0$ and $\vec{l}$, $\vec{m}$, $\vec{U}$ and $\vec{V}$ are unit vectors such that

$$\vec{l} \cdot \vec{m} = \vec{m} \cdot \vec{n} = \vec{n} \cdot \vec{l} = \vec{U} \cdot \vec{V} = 0 \tag{3}$$

completed by $\vec{W} = \vec{U} \wedge \vec{V}$ so that $(\vec{U}, \vec{V}, \vec{W})$ form a right-handed orthonormal basis.

It results from (2) and (3) that

$$\mathbf{A}^{\intercal} \cdot \mathbf{A} = \mathbf{S}^2 \quad \text{with} \quad \mathbf{S} = a\,\vec{l} \otimes \vec{l} + b\,\vec{m} \otimes \vec{m}$$

as well as

$$\mathbf{A}^{\dagger} = \frac{\vec{l} \otimes \vec{U}}{a} + \frac{\vec{m} \otimes \vec{V}}{b} \quad \text{and} \quad (\mathbf{A}^{\intercal} \cdot \mathbf{A})^{\dagger} = \frac{\vec{l} \otimes \vec{l}}{a^2} + \frac{\vec{m} \otimes \vec{m}}{b^2} \tag{4}$$

If $\mathbf{A}$ is of rank 2, then both a and b are positive and it can be assumed that $a \geqslant b > 0$. If $\mathbf{A}$ is of rank 1, then only b is positive and a cancels out. However it would be an error to write $\mathbf{A}$ with $a = 0$ in (2) since the right mechanism to topologically deform an ellipse to a ribbon is actually $a \to +\infty$ while keeping in memory the direction of $\vec{l}$. In fact the limit when $a \to +\infty$ may be taken in the pseudo-inverses $\mathbf{A}^\dagger$ or $(\mathbf{A}^\intercal \cdot \mathbf{A})^\dagger$ so that

$$\lim_{a \to +\infty} \mathbf{A}^\dagger = \frac{\vec{m} \otimes \vec{V}}{b} \quad \text{and} \quad \lim_{a \to +\infty} (\mathbf{A}^\intercal \cdot \mathbf{A})^\dagger = \frac{\vec{m} \otimes \vec{m}}{b^2} \tag{5}$$

It follows that definition (1) writes

$$\vec{x} \in \mathscr{I} \quad \Longleftrightarrow \quad \vec{x} \cdot \vec{n} = 0 \quad \text{and} \quad \begin{cases} \dfrac{\left(\vec{x} \cdot \vec{l}\right)^2}{a^2} + \dfrac{\left(\vec{x} \cdot \vec{m}\right)^2}{b^2} \leqslant 1 & \text{if } \mathbf{A} \text{ is of rank 2} \\ \dfrac{|\vec{x} \cdot \vec{m}|}{b} \leqslant 1 & \text{if } \mathbf{A} \text{ is of rank 1} \end{cases} \tag{6}$$

The above characterization indeed defines an ellipse when $\mathbf{A}$ is of rank 2 and a ribbon when $\mathbf{A}$ is of rank 1. When $\mathbf{A}$ is of rank 2, the orthogonal unit vectors $\vec{l}$ and $\vec{m}$ are directed along respectively the major and minor axes, a is the major radius and b is the minor radius. It will be convenient to also introduce the dimensionless aspect ratio $\eta = b/a \leqslant 1$ of the ellipse. When $\mathbf{A}$ is of rank 1, the crack is translation-invariant (ribbon) along $\vec{l}$ and its in-plane width is $2b$. As mentioned above, the ribbon $\mathscr{R}$ appears as the limiting case of an ellipse $\mathscr{E}$ with infinite major radius ($a \to +\infty$) or, equivalently, vanishing aspect ratio $\eta \to 0$. In the ellipse case, the knowledge of $\mathbf{A}$ is sufficient to fully define the crack since, on the one hand, it contains all information about the directions of the axes and the radii and, on the other hand, $\vec{n}$ spans its kernel. This is no longer true for a ribbon since $\mathbf{A}$ only defines the direction $\vec{m}$ in (5) whereas it does not contain any more information allowing to locate $\vec{l}$ and $\vec{n}$ in the plane orthogonal to $\vec{m}$. The direction of either of these two vectors is therefore additionally required. This observation highlights the interest of considering a ribbon as a limit case of an ellipse.

The following definitions of the crack $\mathscr{I}$, which are rigorously equivalent to (1), will also prove useful in the sequel

$$\mathscr{I} = \left\{ \vec{x} = \mathbf{A}^\intercal \cdot \vec{y}, \quad \vec{y} \in \left(\operatorname{Ker} \mathbf{A}^\intercal\right)^\perp = \operatorname{Im} \mathbf{A} = \vec{W}^\perp, \quad \|\vec{y}\| \leqslant 1 \right\} = \left\{ \vec{x} \in \vec{n}^\perp, \quad \|(\mathbf{A}^\intercal)^\dagger \cdot \vec{x}\| \leqslant 1 \right\} \tag{7}$$

or alternatively

$$\mathscr{I} = \left\{ \vec{x} = \mathbf{S} \cdot \vec{y}, \quad \vec{y} \in \vec{n}^\perp, \quad \|\vec{y}\| \leqslant 1 \right\} = \left\{ \vec{x} \in \vec{n}^\perp, \quad \|\mathbf{S}^\dagger \cdot \vec{x}\| \leqslant 1 \right\} \tag{8}$$

where $\mathbf{S}^\dagger$ denotes the pseudo-inverse of the (singular) tensor $\mathbf{S}$

$$\mathbf{S}^\dagger = \frac{\vec{l} \otimes \vec{l}}{a} + \frac{\vec{m} \otimes \vec{m}}{b} \quad (\mathscr{I} = \mathscr{E}) \qquad \text{and} \qquad \mathbf{S}^\dagger = \frac{\vec{m} \otimes \vec{m}}{b} \quad (\mathscr{I} = \mathscr{R})$$

To close this section, we introduce a useful notation. It is recalled that the direct orthogonal sum $\mathbb{R}^3 = \operatorname{Span}(\vec{n}) \overset{\perp}{\oplus} \vec{n}^\perp$ holds. In other words, any vector $\vec{v}$ of $\mathbb{R}^3$ can be decomposed uniquely as $\vec{v} = \vec{v}^\star + v_n \vec{n}$ with $\vec{v}^\star \cdot \vec{n} = 0$. In the remainder of this paper, quantities living in the plane that contains $\mathscr{I}$ will systematically be starred, like $\vec{v}^\star$ in the previous orthogonal decomposition.

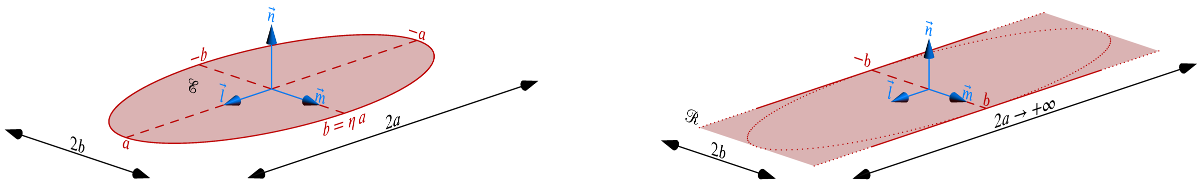

(a) Elliptical crack

(b) Ribbon-like crack

Fig. 2: Models of cracks

2.2 Linear elastic equilibrium of the crack and definition of COD tensor

Equilibrium of the cracked system under consideration is governed by the following boundary-value problem $\mathscr{P}$

$$(\mathscr{P}) \quad \begin{cases} \vec{\operatorname{div}}\, \boldsymbol{\sigma} = \vec{0} & (\mathbb{R}^3 \setminus \mathscr{I}) \\ \boldsymbol{\sigma} = \boldsymbol{C} : \boldsymbol{\varepsilon} & (\mathbb{R}^3 \setminus \mathscr{I}) \\ \boldsymbol{\varepsilon} = \frac{1}{2}(\mathbf{grad}\, \vec{u} + \mathbf{grad}\, \vec{u}^{\mathsf{T}}) & (\mathbb{R}^3 \setminus \mathscr{I}) \\ \boldsymbol{\sigma} \to \boldsymbol{\Sigma} & (\|\vec{x}\| \to +\infty) \\ \boldsymbol{\sigma} \cdot \vec{n} = \vec{0} & (\mathscr{I}) \end{cases} \tag{9}$$

where $\boldsymbol{\Sigma}$ is a prescribed, symmetric, second-order tensor (see also Fig. 1). The last equation of (9) means that the stress vector acting on the crack $\mathscr{I}$ cancels out, which corresponds to a hypothesis of open crack. The extension to a closed frictionless crack will be addressed in Section 2.6. For an open crack, the kinematic counterpart of a null stress vector entails that the displacements are discontinuous at the crack $\mathscr{I}$: the displacement of the upper lip (directed towards $+\vec{n}$) is $\vec{u}^+$, while the displacement of the lower lip is $\vec{u}^- \neq \vec{u}^+$. The displacement jump $[\![\vec{u}]\!] = \vec{u}^+ - \vec{u}^-$ is referred to as the *crack opening displacement* (COD). For problem $\mathscr{P}$, the general expression of the COD is known for both elliptical and ribbon-like cracks ($\mathscr{I} = \mathscr{E}, \mathscr{R}$) (Hoenig, 1978; Kanaun and Levin, 2009; Willis, 1968) after the pioneering work of Eshelby (1957) considering that the ellipse is a degenerated form of an ellipsoid in which the smallest radius tends towards 0

$$\forall \vec{x}^\star \in \mathscr{I}, \quad [\![\vec{u}]\!](\vec{x}^\star) = \sqrt{1 - \vec{x}^\star \cdot \mathbf{S}^{2\dagger} \cdot \vec{x}^\star}\, \vec{\beta} = \sqrt{1 - \|\mathbf{S}^\dagger \cdot \vec{x}^\star\|^2}\, \vec{\beta} \tag{10}$$

where $\vec{\beta}$ denotes the maximum COD. Introducing the cartesian coordinates $x = \vec{x}^\star \cdot \vec{l}$ and $y = \vec{x}^\star \cdot \vec{m}$ of point $\vec{x}^\star$, the above equation also reads

$$\forall \vec{x}^\star \in \mathscr{I}, \quad [\![\vec{u}]\!](\vec{x}^\star) = \sqrt{1 - \frac{x^2}{a^2} - \frac{y^2}{b^2}}\, \vec{\beta} \quad (\mathscr{I} = \mathscr{E}) \qquad \text{and} \qquad [\![\vec{u}]\!](\vec{x}^\star) = \sqrt{1 - \frac{y^2}{b^2}}\, \vec{\beta} \quad (\mathscr{I} = \mathscr{R}) \tag{11}$$

Of particular interest is the *average* COD over the crack. Indeed, it allows the evaluation of the crack compliance contribution tensor, which is central for the homogenization of cracked media within the framework of classical micromechanical models (see Barthélémy et al. (2023) and references therein). It results from the above expressions that the average COD is proportional to $\vec{\beta}$

$$\langle [\![\vec{u}]\!] \rangle_{\mathscr{I}} = \chi\, \vec{\beta} \tag{12}$$

where the dimensionless coefficient $\chi = \chi^{\mathscr{E}}, \chi^{\mathscr{R}}$ reads, for elliptical and ribbon-like cracks

$$\chi^{\mathscr{E}} = \frac{1}{\pi\, a\, b} \int_{\frac{x^2}{a^2} + \frac{y^2}{b^2} \leqslant 1} \sqrt{1 - \frac{x^2}{a^2} - \frac{y^2}{b^2}}\, \mathrm{d}x\, \mathrm{d}y = \frac{2}{3} \qquad \text{and} \qquad \chi^{\mathscr{R}} = \frac{1}{2\, b} \int_{y=-b}^{b} \sqrt{1 - \frac{y^2}{b^2}}\, \mathrm{d}y = \frac{\pi}{4} \tag{13}$$

Owing to the linearity of problem $\mathscr{P}$, $\vec{\beta}$ depends linearly on the loading parameter $\mathbf{\Sigma}$. In addition, the superposition principle allows to show that the COD is the same if the remote loading vanishes and is replaced by a traction $\mathbf{\Sigma} \cdot \vec{n}$ on the upper lip and $-\mathbf{\Sigma} \cdot \vec{n}$ on the lower lip so that $\vec{\beta}$ actually depends only on the components of $\mathbf{\Sigma} \cdot \vec{n}$. The following expression of the average COD then holds

$$\frac{\langle [\![\vec{u}]\!] \rangle_{\mathcal{I}}}{b} = \mathbf{B} \cdot \mathbf{\Sigma} \cdot \vec{n}, \tag{14}$$

where $\mathbf{B} = \mathbf{B}^{\mathscr{E}}, \mathbf{B}^{\mathscr{R}}$ denotes the *normalized COD tensors* (Kachanov, 1993, 1992). Note that in the present work, for both elliptical and ribbon-like cracks, the COD tensor is normalized by the width b so that $\mathbf{B}$ is size-independent (it depends only on the *shape* of the crack, through its aspect ratio). For an elliptical crack, $\mathbf{B}^{\mathscr{E}}$ is a function of the crack orientation (defined by the vectors $\vec{n}$ and $\vec{m}$) and aspect ratio η: $\mathbf{B}^{\mathscr{E}}(\vec{m}, \vec{n}, \eta)$. For a ribbon-like crack, $\mathbf{B}^{\mathscr{R}}$ is a function of $\vec{n}$ and $\vec{m}$ only: $\mathbf{B}^{\mathscr{R}}(\vec{m}, \vec{n})$. When no confusion is possible, the arguments $\vec{m}$, $\vec{n}$ and η will be ommitted.

Before deriving in the sequel the strategy to exhibit $\mathbf{B}$ tensors, it is worth here emphasizing the importance of taking two different notations for elliptical and ribbon-like cracks since $\mathbf{B}^{\mathscr{R}}$ is *not* the limit of $\mathbf{B}^{\mathscr{E}}$ when $\eta \to 0$ (as already observed by Barthélémy et al. (2021), albeit with a different normalization of the COD tensors). Geometrically speaking, the ribbon is indeed the limiting case of the ellipse when the major radius tends to infinity and the expressions of the COD in (11) are also consistent by the same limit. However the asymptotic expression of the area of an ellipse differs from that of a finite-length ribbon of the same major length, which entails different normalization factors and thus different χ coefficients in (13). Considering (12) together with the definition (14) leads to

$$\frac{\vec{\beta}}{b} = \frac{\mathbf{B}}{\chi} \cdot \mathbf{\Sigma} \cdot \vec{n}, \tag{15}$$

so that the consistency between the elliptical and ribbon-like shapes is given by the limit

$$\mathbf{B}^{\mathscr{R}}(\vec{m}, \vec{n}) = \frac{\chi^{\mathscr{R}}}{\chi^{\mathscr{E}}} \lim_{\eta \to 0} \mathbf{B}^{\mathscr{E}}(\vec{m}, \vec{n}, \eta) = \frac{3\pi}{8} \lim_{\eta \to 0} \mathbf{B}^{\mathscr{E}}(\vec{m}, \vec{n}, \eta) \tag{16}$$

2.3 Reformulation of Problem $\mathscr{P}$ as an integral equation

This section recalls an efficient strategy based on integral equations (Kanaun and Levin, 2009; Kunin, 1983) for solving the problem of a single crack embedded in an infinite matrix and in particular the crack opening displacement and stress intensity factors induced by a remote stress state.

The starting point is Eshelby's *problem of the inclusion* (Eshelby, 1957) embedded in an infinite, homogeneous, linearly elastic matrix ($\boldsymbol{C}$ denotes the elastic stiffness and $\boldsymbol{S} = \boldsymbol{C}^{-1}$ the elastic compliance). It is recalled that an inclusion is defined by Eshelby (1957) as a bounded domain $\mathscr{D} \subset \mathbb{R}^3$ subjected to the eigenstress $\boldsymbol{\sigma}^*$. A uniform remote strain $\mathbf{E}$ being applied at infinity, the local strains at equilibrium read[1]

$$\boldsymbol{\varepsilon}(\vec{x}) = \mathbf{E} - \int_{\vec{x}' \in \mathscr{D}} \boldsymbol{\Gamma}(\vec{x} - \vec{x}') : \boldsymbol{\sigma}^*(\vec{x}')\, \mathrm{d}\Omega_{x'} = \mathbf{E} - \int_{\vec{x}' \in \mathscr{D}} \boldsymbol{\Gamma}(\vec{x} - \vec{x}') : \big(\boldsymbol{\sigma}(\vec{x}') - \boldsymbol{C} : \boldsymbol{\varepsilon}(\vec{x}')\big)\, \mathrm{d}\Omega_{x'} \tag{17}$$

where $\boldsymbol{\Gamma}$ is the fourth-order Green kernel associated to $\boldsymbol{C}$ in $\mathbb{R}^3$. Without entering into details not necessary in the present work (see for example Willis (1977) or Mura (1987)), it is recalled that $\boldsymbol{\Gamma}$ is the sum of a local singular part supported by a Dirac distribution (Gel'fand and Shilov, 1964; Schwartz, 1966) and a regular part defined as the opposite of the symmetrized hessian of the Green tensor associated to $\boldsymbol{C}$ in $\mathbb{R}^3$. By invariance by translation in an infinite medium, $\boldsymbol{\Gamma}$ operates over any prestress field as a convolution product in (17).

[1] Note that by convention integration elements are denoted by $\mathrm{d}\Omega$ (resp. by $\mathrm{d}S$) for volume (resp. surface) elements with a subscript about the integration variable.

A dual version involving the stress field $\boldsymbol{\sigma}$ consistent with (17) can be obtained by introducing the remote stress $\boldsymbol{\Sigma} = \boldsymbol{C} : \mathbf{E}$, the eigenstrain $\boldsymbol{\varepsilon}^* = -\boldsymbol{S} : \boldsymbol{\sigma}^*$ and the second Green kernel $\boldsymbol{Q}(\vec{x}) = \boldsymbol{C}\,\delta(\vec{x}) - \boldsymbol{C} : \boldsymbol{\Gamma}(\vec{x}) : \boldsymbol{C}$ (where δ denotes the Dirac distribution)

$$\boldsymbol{\sigma}(\vec{x}) = \boldsymbol{\Sigma} - \int_{\vec{x}'\in\mathscr{D}} \boldsymbol{Q}(\vec{x}-\vec{x}') : \boldsymbol{\varepsilon}^*(\vec{x}')\,\mathrm{d}\Omega_{x'} = \boldsymbol{\Sigma} - \int_{\vec{x}'\in\mathscr{D}} \boldsymbol{Q}(\vec{x}-\vec{x}') : \left(\boldsymbol{\varepsilon}(\vec{x}') - \boldsymbol{S} : \boldsymbol{\sigma}(\vec{x}')\right)\,\mathrm{d}\Omega_{x'} \tag{18}$$

The idea is now to apply (18) to the case of an interface $\mathscr{I}$ supported by a surface of normal unit vector $\vec{n}$. Although not strictly required in the general integral expression, it is assumed here that $\vec{n}$ is uniform over the interface consistently with the description of Section 2.1, which means that $\mathscr{I}$ is included in the plane $\vec{n}^{\perp}$ orthogonal to $\vec{n}$.

In the sense of distributions, a displacement jump $[\![\vec{u}]\!] = \vec{u}^+ - \vec{u}^-$ across a surface domain $\mathscr{I}$ corresponds to a strain field $\boldsymbol{\varepsilon} = [\![\vec{u}]\!]\overset{s}{\otimes}\vec{n}\,\delta_{\mathscr{I}}$ where $\overset{s}{\otimes}$ is the symmetrized tensor product[2] and $\delta_{\mathscr{I}}$ is the surface Dirac distribution supported by $\mathscr{I}$. Assuming that the stress state is regular at the interface, its contribution to the integral of (18) vanishes and as shown by Kunin (1983), (18) becomes, using the minor symmetries[3] of $\boldsymbol{Q}$

$$\boldsymbol{\sigma}(\vec{x}) = \boldsymbol{\Sigma} - \int_{\vec{x}'^{\star}\in\mathscr{I}} \left(\boldsymbol{Q}(\vec{x}-\vec{x}'^{\star})\cdot\vec{n}\right)\cdot[\![\vec{u}]\!](\vec{x}'^{\star})\,\mathrm{d}S_{x'^{\star}} \tag{19}$$

Note that the variable integration in (19) has been changed in $\vec{x}'^{\star}$ so as to recall that the integration is performed over the plane surface $\mathscr{I}$. The stress vector applied on a facet of normal $\vec{n}$ i.e. $\vec{t} = \boldsymbol{\sigma}\cdot\vec{n}$ of the same plane as that of the crack writes

$$\vec{t}(\vec{x}^{\star}) = \boldsymbol{\Sigma}\cdot\vec{n} - \int_{\vec{x}'^{\star}\in\mathscr{I}} \left(\vec{n}\cdot\boldsymbol{Q}(\vec{x}^{\star}-\vec{x}'^{\star})\cdot\vec{n}\right)\cdot[\![\vec{u}]\!](\vec{x}'^{\star})\,\mathrm{d}S_{x'^{\star}} \tag{20}$$

Although analytical expressions of $\boldsymbol{\Gamma}$ or $\boldsymbol{Q}$ are not available in the general anisotropic case, it is possible to resort to the reduced Fourier transform introduced in (106) in Appendix 6.2, to transform (19) to

$$\boldsymbol{\sigma}(\vec{x}^{\star}) = \boldsymbol{\Sigma} - \frac{1}{4\pi^2}\int_{\vec{x}'^{\star}\in\mathscr{I}}\int_{\vec{\xi}^{\star}\in\vec{n}^{\perp}} \mathrm{e}^{i\,\vec{\xi}^{\star}\cdot(\vec{x}^{\star}-\vec{x}'^{\star})}\left(\frac{1}{2\pi}\int_{\xi_n=-\infty}^{+\infty}\hat{\boldsymbol{Q}}(\vec{\xi}^{\star}+\xi_n\,\vec{n})\cdot\vec{n}\,\mathrm{d}\xi_n\right)\cdot[\![\vec{u}]\!](\vec{x}'^{\star})\,\mathrm{d}S_{\xi^{\star}}\,\mathrm{d}S_{x'^{\star}} \tag{21}$$

where $\hat{\boldsymbol{\Gamma}}$ and $\hat{\boldsymbol{Q}}$ are the first and second fourth-order Green kernels, expressed in Fourier space (Mura, 1987; Willis, 1977)

$$\hat{\boldsymbol{\Gamma}}(\vec{\xi}) = \vec{\xi}\overset{s}{\otimes}\left(\vec{\xi}\cdot\boldsymbol{C}\cdot\vec{\xi}\right)^{-1}\overset{s}{\otimes}\vec{\xi} \quad\text{and}\quad \hat{\boldsymbol{Q}}(\vec{\xi}) = \boldsymbol{C} - \boldsymbol{C} : \hat{\boldsymbol{\Gamma}}(\vec{\xi}) : \boldsymbol{C} \tag{22}$$

The stress vector (20) is also conveniently rewritten

$$\vec{t}(\vec{x}^{\star}) = \boldsymbol{\Sigma}\cdot\vec{n} - \frac{1}{4\pi^2}\int_{\vec{x}'^{\star}\in\mathscr{I}}\int_{\vec{\xi}^{\star}\in\vec{n}^{\perp}} \mathrm{e}^{i\,\vec{\xi}^{\star}\cdot(\vec{x}^{\star}-\vec{x}'^{\star})}\,\hat{\mathbf{Q}}^{\star}_{nn}(\vec{\xi}^{\star})\cdot[\![\vec{u}]\!](\vec{x}'^{\star})\,\mathrm{d}S_{\xi^{\star}}\,\mathrm{d}S_{x'^{\star}} \tag{23}$$

where

$$\hat{\mathbf{Q}}^{\star}_{nn}(\vec{\xi}^{\star}) = \frac{1}{2\pi}\int_{\xi_n=-\infty}^{+\infty} \vec{n}\cdot\hat{\boldsymbol{Q}}(\vec{\xi}^{\star}+\xi_n\,\vec{n})\cdot\vec{n}\,\mathrm{d}\xi_n \tag{24}$$

The convergence of the integrals over ξ_n in (21) and (24) requires to be analyzed. It comes after some algebra that

$$\begin{aligned}\hat{\boldsymbol{Q}}(\vec{\xi}^{\star}+\xi_n\,\vec{n})\cdot\vec{n} = \hat{\boldsymbol{Q}}\left(\frac{\vec{\xi}^{\star}}{\xi_n}+\vec{n}\right)\cdot\vec{n} &= \frac{1}{\xi_n}\left(\left(\boldsymbol{C}\cdot\vec{n}\right)\cdot\left(\vec{n}\cdot\boldsymbol{C}\cdot\vec{n}\right)^{-1}\cdot\left(\vec{n}\cdot\boldsymbol{C}\cdot\vec{\xi}^{\star}\right) - \boldsymbol{C}\cdot\vec{\xi}^{\star}\right) + \mathscr{O}\left(\frac{1}{\xi_n^2}\right)\\ &= -\frac{1}{\xi_n}\hat{\boldsymbol{Q}}(\vec{n})\cdot\vec{\xi}^{\star} + \mathscr{O}\left(\frac{1}{\xi_n^2}\right)\end{aligned} \tag{25}$$

[2] $(\vec{a}\overset{s}{\otimes}\vec{b})_{ij} = (a_i b_j + a_j b_i)/2$

[3] Minor symmetries: $Q_{jikl} = Q_{ijlk} = Q_{ijkl}$. Major symmetry: $Q_{klij} = Q_{ijkl}$

and thus

$$\vec{n} \cdot \hat{\boldsymbol{Q}}(\vec{\xi}^\star + \xi_n \vec{n}) \cdot \vec{n} = \mathcal{O}\left(\frac{1}{\xi_n^2}\right) \tag{26}$$

It follows immediately that, as mentioned in Kanaun and Levin (2009), the integral (24) converges since the integrand is $\mathcal{O}(1/\xi_n^2)$. It also appears that some components of $\hat{\boldsymbol{Q}}(\vec{\xi}^\star + \xi_n \vec{n}) \cdot \vec{n}$ vary in $1/\xi_n$ at infinity. However the integral is performed over the whole real set $]-\infty, +\infty[$ so that a regularization based on the replacement of the integrand by its even part $(\hat{\boldsymbol{Q}}(\vec{\xi}^\star + \xi_n \vec{n}) + \hat{\boldsymbol{Q}}(\vec{\xi}^\star - \xi_n \vec{n})) \cdot \vec{n}/2$ ensures the convergence. Although interesting to reach all components of the stress state in the crack plane, the sequel relies only on (23) and thus (24) to derive the COD tensor and the intensity factors.

Introducing (10) in (23) while adopting a change of variables $\vec{y}^\star = \mathbf{S}^\dagger \cdot \vec{x}^\star$ and $\vec{y}'^\star = \mathbf{S}^\dagger \cdot \vec{x}'^\star$ belonging to the unit disk of the plane $\vec{n}^\perp$ as shown in (8) as well as $\vec{\zeta}^\star = \mathbf{S} \cdot \vec{\xi}^\star$ describing all the plane $\vec{n}^\perp$, yields

$$\vec{t}(\vec{x}^\star) = \boldsymbol{\Sigma} \cdot \vec{n} - \boldsymbol{\Lambda}(\vec{x}^\star) \cdot \vec{\beta} \tag{27}$$

with

$$\boldsymbol{\Lambda}(\vec{x}^\star = \mathbf{S} \cdot \vec{y}^\star) = \frac{1}{4\pi^2} \int_{\substack{\vec{y}'^\star \in \vec{n}^\perp \\ \|\vec{y}'^\star\| \leqslant 1}} \int_{\vec{\zeta}^\star \in \vec{n}^\perp} \mathrm{e}^{i\,\vec{\zeta}^\star \cdot (\vec{y}^\star - \vec{y}'^\star)} \sqrt{1 - \|\vec{y}'^\star\|^2}\, \hat{\mathbf{Q}}^\star_{nn}(\mathbf{S}^\dagger \cdot \vec{\zeta}^\star)\, \mathrm{d}S_{\zeta^\star}\, \mathrm{d}S_{y'^\star} \tag{28}$$

Using (109) and integrating with respect to $\vec{y}'^\star$ provides

$$\boldsymbol{\Lambda}(\vec{x}^\star = \mathbf{S} \cdot \vec{y}^\star) = \frac{1}{2\pi} \int_{\vec{\zeta}^\star \in \vec{n}^\perp} \mathrm{e}^{i\,\vec{\zeta}^\star \cdot \vec{y}^\star} \frac{j_1(\|\vec{\zeta}^\star\|)}{\|\vec{\zeta}^\star\|} \hat{\mathbf{Q}}^\star_{nn}(\mathbf{S}^\dagger \cdot \vec{\zeta}^\star)\, \mathrm{d}S_{\zeta^\star} \tag{29}$$

To simplify (29) it is useful to introduce $\vec{\zeta}^\star = r\,\vec{\kappa}^\star$ with $r = \|\vec{\zeta}^\star\|$ and $\vec{\kappa}^\star$ which describes the unit circle of $\vec{n}^\perp$ (with an angle $\varphi_{\kappa^\star}$ varying from 0 to 2π) and to remark from (108) that $\hat{\mathbf{Q}}^\star_{nn}$ is positively homogeneous of degree 1, i.e. $\hat{\mathbf{Q}}^\star_{nn}(\lambda\,\vec{\xi}^\star) = |\lambda| \hat{\mathbf{Q}}^\star_{nn}(\vec{\xi}^\star)$ for all $\lambda \neq 0$, so that

$$\boldsymbol{\Lambda}(\vec{x}^\star = \mathbf{S} \cdot \vec{y}^\star) = \frac{1}{2\pi} \int_{\varphi_{\kappa^\star}=0}^{2\pi} \int_{r=0}^{+\infty} r\, j_1(r)\, \mathrm{e}^{i\,r\,\vec{\kappa}^\star \cdot \vec{y}^\star}\, \hat{\mathbf{Q}}^\star_{nn}(\mathbf{S}^\dagger \cdot \vec{\kappa}^\star)\, \mathrm{d}r\, \mathrm{d}\varphi_{\kappa^\star} \tag{30}$$

Using the properties $\hat{\mathbf{Q}}^\star_{nn}(-\vec{\xi}^\star) = \hat{\mathbf{Q}}^\star_{nn}(\vec{\xi}^\star)$ and $j_1(-r) = -j_1(r)$, (30) rewrites

$$\boldsymbol{\Lambda}(\vec{x}^\star = \mathbf{S} \cdot \vec{y}^\star) = \frac{1}{4\pi} \int_{\varphi_{\kappa^\star}=0}^{2\pi} \int_{r=-\infty}^{+\infty} r\, j_1(r)\, \mathrm{e}^{i\,r\,\vec{\kappa}^\star \cdot \vec{y}^\star}\, \hat{\mathbf{Q}}^\star_{nn}(\mathbf{S}^\dagger \cdot \vec{\kappa}^\star)\, \mathrm{d}r\, \mathrm{d}\varphi_{\kappa^\star} \tag{31}$$

which finally yields thanks to the Fourier transform result (110)

$$\boldsymbol{\Lambda}(\vec{x}^\star = \mathbf{S} \cdot \vec{y}^\star) = \frac{1}{4} \int_{\varphi_{\kappa^\star}=0}^{2\pi} \Big(\mathrm{H}(\vec{\kappa}^\star \cdot \vec{y}^\star + 1) - \mathrm{H}(\vec{\kappa}^\star \cdot \vec{y}^\star - 1) - \delta(\vec{\kappa}^\star \cdot \vec{y}^\star + 1) - \delta(\vec{\kappa}^\star \cdot \vec{y}^\star - 1) \Big)\, \hat{\mathbf{Q}}^\star_{nn}(\mathbf{S}^\dagger \cdot \vec{\kappa}^\star)\, \mathrm{d}\varphi_{\kappa^\star} \tag{32}$$

where H is the Heaviside function (104) and δ is the Dirac distribution (102).

2.4 Crack opening displacement tensor for an open crack

The interface $\mathscr{I}$ behaves as a frictionless open crack: the traction $\vec{t}$ vanishes at any point of the interior of $\mathscr{I}$. Moreover, taking $\|\vec{y}^\star\| < 1$ and thus $\vec{\kappa}^\star \cdot \vec{y}^\star < 1$ in (32) entails that, among the terms depending on $\vec{\kappa}^\star \cdot \vec{y}^\star$ in the expression of $\boldsymbol{\Lambda}$ in (32), only the first Heaviside function remains and is equal to 1, which confirms that $\boldsymbol{\Lambda}$ is uniform within $\mathscr{I}$. Finally inserting (32) in (27) provides a result already found in Kanaun and Levin (2009)

$$\boldsymbol{\Sigma} \cdot \vec{n} = \boldsymbol{\Lambda} \cdot \vec{\beta} \tag{33}$$

with

$$\mathbf{\Lambda} = \frac{1}{4} \int_{\varphi_{\kappa^\star}=0}^{2\pi} \hat{\mathbf{Q}}^\star_{nn}(\mathbf{S}^\dagger \cdot \vec{\kappa}^\star)\, \mathrm{d}\varphi_{\kappa^\star} \tag{34}$$

The comparison between (15) and (33) allows to identify the COD tensor as

$$\mathbf{B} = \chi\, (b\, \mathbf{\Lambda})^{-1} \tag{35}$$

which will take different values depending on the shape (elliptical or ribbon-like) of the crack.

Recalling that $\hat{\mathbf{Q}}^\star_{nn}$ is positively homogeneous of degree 1, it follows from (34) that $\mathbf{\Lambda}$ is inversely proportional to the size of the crack, which could have been deduced from a simple dimensional analysis. Indeed $\mathbf{\Lambda}$ writes in the case of an elliptical crack with bounded radii

$$\begin{aligned} b\, \mathbf{\Lambda}^{\mathscr{E}}(\vec{m}, \vec{n}, a, b) &= \frac{b}{4} \int_{\varphi_{\kappa^\star}=0}^{2\pi} \hat{\mathbf{Q}}^\star_{nn} \left(\frac{\cos\varphi_{\kappa^\star}}{a}\, \vec{l} + \frac{\sin\varphi_{\kappa^\star}}{b}\, \vec{m} \right) \mathrm{d}\varphi_{\kappa^\star} \\ &= \frac{1}{4} \int_{\varphi_{\kappa^\star}=0}^{2\pi} \hat{\mathbf{Q}}^\star_{nn} \left(\eta\, \cos\varphi_{\kappa^\star}\, \vec{l} + \sin\varphi_{\kappa^\star}\, \vec{m} \right) \mathrm{d}\varphi_{\kappa^\star} \end{aligned} \tag{36}$$

which leads to the COD tensor for an ellipse using (13)

$$\mathbf{B} = \mathbf{B}^{\mathscr{E}}(\vec{m}, \vec{n}, \eta) = \chi^{\mathscr{E}}\, \left(b\, \mathbf{\Lambda}^{\mathscr{E}}(\vec{m}, \vec{n}, a, b) \right)^{-1} = \frac{8}{3} \left(\int_{\varphi_{\kappa^\star}=0}^{2\pi} \hat{\mathbf{Q}}^\star_{nn} \left(\eta\, \cos\varphi_{\kappa^\star}\, \vec{l} + \sin\varphi_{\kappa^\star}\, \vec{m} \right) \mathrm{d}\varphi_{\kappa^\star} \right)^{-1} \quad (\mathscr{I} = \mathscr{E}) \tag{37}$$

Further simplifcations occur in the case of a ribbon-like crack. Indeed, since $\mathbf{S}^\dagger \underset{a\to\infty}{\to} \frac{\vec{m}\otimes\vec{m}}{b}$

$$b\, \mathbf{\Lambda}^{\mathscr{R}}(\vec{m}, \vec{n}, b) = \frac{1}{4} \int_{\varphi_{\kappa^\star}=0}^{2\pi} |\sin\varphi_{\kappa^\star}|\, \hat{\mathbf{Q}}^\star_{nn}(\vec{m})\, \mathrm{d}\varphi_{\kappa^\star} = \hat{\mathbf{Q}}^\star_{nn}(\vec{m}) \tag{38}$$

which entails with the help of (13)

$$\mathbf{B} = \mathbf{B}^{\mathscr{R}}(\vec{m}, \vec{n}) = \chi^{\mathscr{R}}\, \left(b\, \mathbf{\Lambda}^{\mathscr{R}}(\vec{m}, \vec{n}, b) \right)^{-1} = \frac{\pi}{4}\, \left(\hat{\mathbf{Q}}^\star_{nn}(\vec{m}) \right)^{-1} \quad (\mathscr{I} = \mathscr{R}) \tag{39}$$

for a ribbon.

For an open crack embedded in an isotropic matrix or aligned with the isotropy plane of a transversely isotropic matrix, closed-form expressions of the COD tensors $\mathbf{B}^{\mathscr{E}}$ and $\mathbf{B}^{\mathscr{R}}$ have been derived by various authors (Barthélémy et al., 2023; Barthélémy et al., 2021; Hoenig, 1978; Kachanov et al., 2003; Kachanov, 1992; Kachanov and Sevostianov, 2018; Kanaun and Levin, 2009; Sevostianov and Kachanov, 2002) and are recalled in Appendices (6.3.1) and (6.3.2).

2.5 Displacement and stress intensity factors

In order to introduce the displacement and stress intensity factors (DIF and SIF) a point $\vec{x}^\star$ belonging to the crack-plane is considered in the vicinity of the crack-tip, i.e. $\vec{x}^\star = \vec{x}^\star_0 + r\vec{v}$, where $\vec{x}^\star_0$ belongs to the crack-tip $\partial\mathscr{I}$, $\vec{v}$ is the outer unit normal to $\partial\mathscr{I}$ and $\vec{\tau} = \vec{n} \wedge \vec{v}$ is the unit tangent (see Fig. 3). For $r > 0$, the point $\vec{x}^\star$ is located in the (uncracked) solid; for $r < 0$, it is located inside the crack.

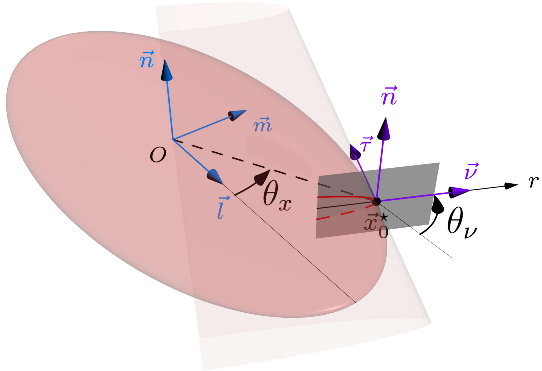

Fig. 3: Local frame and coordinates at crack border

The displacement intensity factor $\vec{N}$ and stress intensity factor $\vec{K}$ are two vectors that characterize at $\vec{x}^\star$ the asymptotic behavior when $r \to 0$ of the COD ($r < 0$) and the traction $\vec{t} = \boldsymbol{\sigma} \cdot \vec{n}$ ($r > 0$), respectively (Irwin, 1957; Kassir and Sih, 1968; Willis, 1968)

$$[\![\vec{u}]\!](\vec{x}_0^\star + r\vec{\nu}) \underset{r\to 0^-}{\sim} 8\sqrt{\frac{-r}{2\pi}}\,\vec{N} \quad \text{and} \quad \vec{t}(\vec{x}_0^\star + r\vec{\nu}) \underset{r\to 0^+}{\sim} \frac{\vec{K}}{\sqrt{2\pi r}} \tag{40}$$

Whereas the definition of the SIF $\vec{K}$ is rather classical in the literature, the factor appearing in the term introducing the DIF $\vec{N}$ in (40) is chosen by consistency with the local energy release rate provided in Barnett and Asaro (1972) and Rice (1989)

$$G = \vec{K} \cdot \vec{N} \tag{41}$$

This calibration confers to the DIF $\vec{N}$ the status of a vector *energetically conjugate* to the SIF $\vec{K}$, rather than of a mere relabelling of the asymptotic coefficient of the COD: any other scaling choice would introduce additional material, geometrical or simple constants in (41). Furthermore, the DIF will turn out to be the natural primary unknown for the transformation strategy developed in Section 3, since the transformation rules act directly on the COD tensor, and therefore on the DIF, whereas their counterpart on the SIF additionally involves the transformation of the COD tensor associated to a fictitious tangent ribbon-like crack (see Section 3.3).

It is emphasized that the above asymptotic behaviors of $[\![\vec{u}]\!]$ in $\sqrt{-r}$ and $\vec{t}$ in $1/\sqrt{r}$ in the vicinity of the crack border holds for *any anisotropy* of the matrix, as shown in the sequel devoted to the derivation of the expressions of $\vec{N}$ and $\vec{K}$. To begin with, it is convenient to introduce the associated point of the unit circle $\vec{y}_0^\star$ such that $\vec{x}_0^\star = \mathbf{S} \cdot \vec{y}_0^\star$. The outer normal to the crack at $\vec{x}^\star$ is classically expressed as follows (see Fig. 3)

$$\vec{\nu} = \frac{\mathbf{S}^\dagger \cdot \vec{y}_0^\star}{\|\mathbf{S}^\dagger \cdot \vec{y}_0^\star\|} \quad \text{therefore} \quad \vec{y}_0^\star \cdot \mathbf{S}^\dagger \cdot \vec{\nu} = \frac{\vec{y}_0^\star \cdot \mathbf{S}^\dagger \cdot \mathbf{S}^\dagger \cdot \vec{y}_0^\star}{\|\mathbf{S}^\dagger \cdot \vec{y}_0^\star\|} = \|\mathbf{S}^\dagger \cdot \vec{y}_0^\star\| \tag{42}$$

Plugging $\vec{x}^\star = \vec{x}_0^\star + r\vec{\nu}$ into (10), using the second identity in (42) and keeping only the dominant term in r, the first equation in (40) is retrieved

$$[\![\vec{u}]\!](\vec{x}_0^\star + r\vec{\nu}) \underset{r\to 0^-}{\sim} \sqrt{-2\,r\,\vec{\nu} \cdot \mathbf{S}^{2\dagger} \cdot \vec{x}_0^\star}\,\vec{\beta} = \sqrt{-2\,r\,\vec{\nu} \cdot \mathbf{S}^\dagger \cdot \vec{y}_0^\star}\,\vec{\beta} = \sqrt{-2\,r\,\|\mathbf{S}^\dagger \cdot \vec{y}_0^\star\|}\,\vec{\beta} = 8\sqrt{\frac{-r}{2\pi}}\,\vec{N}$$

where $\vec{N}$ is given by

$$\vec{N} = \frac{\sqrt{\pi}}{4}\sqrt{\|\mathbf{S}^\dagger \cdot \vec{y}_0^\star\|}\,\vec{\beta} \tag{43}$$

Then, in order to prove the second equation in (40) and to identify $\vec{K}$, the parameter $\vec{y}^\star = \mathbf{S}^\dagger\cdot(\vec{x}_0^\star + r\vec{v}) = \vec{y}_0^\star + r\,\mathbf{S}^\dagger\cdot\vec{v}$ is plugged into (27) and (32). Besides, only the terms likely to produce singularities when r tends to 0^+ are kept. In particular, the terms $\mathbf{\Sigma}\cdot\vec{n}$ and those involving the Heaviside function are bounded so they are neglected. Exploiting the π-periodicity of the integrand of (32) leads to

$$\vec{t}(\vec{x}^\star = \mathbf{S}\cdot\vec{y}^\star) \underset{r\to 0^+}{\sim} \left(\frac{1}{2}\int_{\varphi_{\kappa^\star}=0}^{\pi}\Big(\delta(\vec{\kappa}^\star\cdot\vec{y}^\star+1)+\delta(\vec{\kappa}^\star\cdot\vec{y}^\star-1)\Big)\,\hat{\mathbf{Q}}_{nn}^\star(\mathbf{S}^\dagger\cdot\vec{\kappa}^\star)\,\mathrm{d}\varphi_{\kappa^\star}\right)\cdot\vec{\beta} \tag{44}$$

where $\varphi_{\kappa^\star}$ is the polar angle of $\vec{\kappa}^\star$ with respect to the fixed unit vector $\vec{y}_0^\star$ (i.e. $\vec{\kappa}^\star = \cos\varphi_{\kappa^\star}\,\vec{y}_0^\star + \sin\varphi_{\kappa^\star}\,\vec{n}\wedge\vec{y}_0^\star$). Introducing the new integration variable $s = \cos\varphi_{\kappa^\star}$ ($\vec{\kappa}^\star = s\,\vec{y}_0^\star + \sqrt{1-s^2}\,\vec{n}\wedge\vec{y}_0^\star$), the above integral is transformed as follows

$$\vec{t}(\vec{x}^\star = \mathbf{S}\cdot\vec{y}^\star) \underset{r\to 0^+}{\sim} \left(\frac{1}{2}\int_{s=-1}^{1}\frac{\delta(s+r\,\vec{\kappa}^\star\cdot\mathbf{S}^\dagger\cdot\vec{v}+1)+\delta(s+r\,\vec{\kappa}^\star\cdot\mathbf{S}^\dagger\cdot\vec{v}-1)}{\sqrt{1-s^2}}\,\hat{\mathbf{Q}}_{nn}^\star(\mathbf{S}^\dagger\cdot\vec{\kappa}^\star)\,\mathrm{d}s\right)\cdot\vec{\beta} \tag{45}$$

The calculation of (45) requires to identify the values of s for which the arguments of the Dirac distribution δ vanish between -1 and 1 taking into account that r remains infinitesimal. Turning to the first occurence of the Dirac distribution, it is seen that $s + r\,\vec{\kappa}^\star\cdot\mathbf{S}^\dagger\cdot\vec{v}+1$ vanishes when s approaches -1 or $\vec{\kappa}^\star$ is in the vicinity of $-\vec{y}_0^\star$. Consequently $s \underset{r\to 0^+}{\sim} -1 + r\,\vec{y}_0^\star\cdot\mathbf{S}^\dagger\cdot\vec{v}$. Similarly, cancellation of the argument of the second Dirac distribution occurs for $s \underset{r\to 0^+}{\sim} 1 - r\,\vec{y}_0^\star\cdot\mathbf{S}^\dagger\cdot\vec{v}$. The dominant term in (45) as $r\to 0^+$ is therefore

$$\vec{t}(\vec{x}^\star = \mathbf{S}\cdot\vec{y}^\star) \underset{r\to 0^+}{\sim} \frac{\hat{\mathbf{Q}}_{nn}^\star(\mathbf{S}^\dagger\cdot\vec{y}_0^\star)}{\sqrt{2\,r\,\vec{y}_0^\star\cdot\mathbf{S}^\dagger\cdot\vec{v}}}\cdot\vec{\beta} \tag{46}$$

Finally, observing that $\hat{\mathbf{Q}}_{nn}^\star$ is positively homogeneous of degree 1, it results from (42) that

$$\hat{\mathbf{Q}}_{nn}^\star(\mathbf{S}^\dagger\cdot\vec{y}_0^\star) = \hat{\mathbf{Q}}_{nn}^\star(\|\mathbf{S}^\dagger\cdot\vec{y}_0^\star\|\,\vec{v}) = \|\mathbf{S}^\dagger\cdot\vec{y}_0^\star\|\,\hat{\mathbf{Q}}_{nn}^\star(\vec{v}) \quad\text{and}\quad \vec{t}(\vec{x}^\star = \mathbf{S}\cdot\vec{y}^\star) \underset{r\to 0^+}{\sim} \frac{\sqrt{\pi\,\|\mathbf{S}^\dagger\cdot\vec{y}_0^\star\|}\,\hat{\mathbf{Q}}_{nn}^\star(\vec{v})\cdot\vec{\beta}}{\sqrt{2\pi\,r}}$$

which confirms the form of the second equation in (40) where

$$\vec{K} = \sqrt{\pi\,\|\mathbf{S}^\dagger\cdot\vec{y}_0^\star\|}\,\hat{\mathbf{Q}}_{nn}^\star(\vec{v})\cdot\vec{\beta} \tag{47}$$

Eliminating $\vec{\beta}$ between (43) and (47) provides the following relationship between DIF and SIF vectors

$$\vec{K} = 4\,\hat{\mathbf{Q}}_{nn}^\star(\vec{v})\cdot\vec{N} \tag{48}$$

The relationship (48) recovers a result already proven in Kanaun (1981), Kunin (1983) or Kanaun and Levin (2009) in the more general framework of arbitrary crack shape by a reasoning which consists in inserting the asymptotical form (40) of $[\![\vec{u}]\!](\vec{x}_0^\star + r\vec{v})$ in the integral equation (20). Equivalent linear relationships between the SIF and the asymptotic coefficient of the COD have also been derived, by means of boundary integral equations, in Zhao et al. (1998) for a planar crack in the plane of isotropy of a TI matrix, and extended to coupled multi-field problems in Zhao et al. (2007) and Li et al. (2020). The present derivation (48) generalizes these relations to an arbitrary anisotropic matrix and an arbitrarily oriented elliptical or ribbon-like crack, the dependence on the local geometry being entirely carried by the kernel $\hat{\mathbf{Q}}_{nn}^\star(\vec{v})$. It is worth pointing out again here that the linear relationship (48) between $\vec{K}$ and $\vec{N}$ is *purely local*: it depends on neither the macroscopic loading nor the crack radii and not even on the crack shape according to Kanaun (1981), Kunin (1983) or Kanaun and Levin (2009) provided that $[\![\vec{u}]\!](\vec{x}_0^\star + r\vec{v})$ be of the form (40). It involves the tensor $\hat{\mathbf{Q}}_{nn}^\star(\vec{v})$ which is recognized in (39) as the inverse –up to a multiplicative constant– of the COD tensor $\mathbf{B}^{\mathscr{R}}(\vec{v},\vec{n})$ of a *fictitious* **open** ribbon-like crack of transverse direction $\vec{v}$ i.e. tangent to the border at the observation point

$$\vec{K} = \pi\, \left(\mathbf{B}^{\mathscr{R}}(\vec{v},\vec{n})\right)^{-1} \cdot \vec{N} \tag{49}$$

The local energy release rate G (41) can then be expressed as the quadratic forms

$$G = \pi\, \vec{N} \cdot \left(\mathbf{B}^{\mathscr{R}}(\vec{v},\vec{n})\right)^{-1} \cdot \vec{N} = \frac{1}{\pi} \vec{K} \cdot \mathbf{B}^{\mathscr{R}}(\vec{v},\vec{n}) \cdot \vec{K} \tag{50}$$

This highlights the relevance of a local 2D reasoning in the plane spanned by $\vec{v}$ and $\vec{n}$ as depicted in Fig. 3. Such a reasoning, assuming that local stress components result from a combination of plane strain and antiplane shear problems, is often taken as a starting point to analyze the DIF and SIF (see for example Kassir and Sih (1968), Budiansky and O'Connell (1976) and Hoenig (1978)).

The link between the DIF (respectively the SIF) and the macroscopic loading $\mathbf{\Sigma} \cdot \vec{n}$ is also obtained by eliminating $\vec{\beta}$ between (33) and (43) (respectively (47)), which yields

$$\vec{N} = \frac{\sqrt{\pi}}{4} \sqrt{\|\mathbf{S}^{\dagger} \cdot \vec{y}_0^{\star}\|}\, \mathbf{\Lambda}^{-1} \cdot \mathbf{\Sigma} \cdot \vec{n} \quad \text{and} \quad \vec{K} = \frac{\pi^{3/2}}{4} \sqrt{\|\mathbf{S}^{\dagger} \cdot \vec{y}_0^{\star}\|}\, \left(\mathbf{B}^{\mathscr{R}}(\vec{v},\vec{n})\right)^{-1} \cdot \mathbf{\Lambda}^{-1} \cdot \mathbf{\Sigma} \cdot \vec{n} \tag{51}$$

Note that in (51), $\mathbf{\Lambda}$ corresponds to the *actual* crack and is given by (36) and (38) for elliptical and ribbon-like cracks, respectively.

Thus for an elliptical crack with bounded radii, (51) can be rewritten in terms of (fictitious and actual) COD tensors thanks to (37), finally delivering

$$\vec{N}^{\mathscr{E}} = \frac{3\sqrt{\pi\, b}}{8} \sqrt{b\, \|\mathbf{S}^{\dagger} \cdot \vec{y}_0^{\star}\|}\, \mathbf{B}^{\mathscr{E}}(\vec{m},\vec{n},\eta) \cdot \mathbf{\Sigma} \cdot \vec{n} \quad \text{and} \quad \vec{K}^{\mathscr{E}} = \frac{3\,\pi^{3/2}\sqrt{b}}{8} \sqrt{b\, \|\mathbf{S}^{\dagger} \cdot \vec{y}_0^{\star}\|}\, \left(\mathbf{B}^{\mathscr{R}}(\vec{v},\vec{n})\right)^{-1} \cdot \mathbf{B}^{\mathscr{E}}(\vec{m},\vec{n},\eta) \cdot \mathbf{\Sigma} \cdot \vec{n} \tag{52}$$

where it is emphasized that $b\, \|\mathbf{S}^{\dagger} \cdot \vec{y}_0^{\star}\|$ is a dimensionless quantity. The local energy release rate (50) becomes

$$G^{\mathscr{E}} = \frac{9\,\pi^2\, b}{64} \left(b\, \|\mathbf{S}^{\dagger} \cdot \vec{y}_0^{\star}\|\right) \vec{n} \cdot \mathbf{\Sigma} \cdot \mathbf{B}^{\mathscr{E}}(\vec{m},\vec{n},\eta) \cdot \left(\mathbf{B}^{\mathscr{R}}(\vec{v},\vec{n})\right)^{-1} \cdot \mathbf{B}^{\mathscr{E}}(\vec{m},\vec{n},\eta) \cdot \mathbf{\Sigma} \cdot \vec{n} \tag{53}$$

For a ribbon-like crack thanks to (39) and noting that $\vec{y}_0^{\star} = \pm\vec{m}$, $\vec{v} = \pm\vec{m}$ and $\|\mathbf{S}^{\dagger} \cdot \vec{y}_0^{\star}\| = \frac{1}{b}$, DIF and SIF are given by

$$\vec{N}^{\mathscr{R}} = \sqrt{\frac{b}{\pi}}\, \mathbf{B}^{\mathscr{R}}(\vec{m},\vec{n}) \cdot \mathbf{\Sigma} \cdot \vec{n} \quad \text{and} \quad \vec{K}^{\mathscr{R}} = \sqrt{\pi\, b}\, \mathbf{\Sigma} \cdot \vec{n} \tag{54}$$

and the local energy release rate (50)

$$G^{\mathscr{R}} = b\, \vec{n} \cdot \mathbf{\Sigma} \cdot \mathbf{B}^{\mathscr{R}}(\vec{m},\vec{n}) \cdot \mathbf{\Sigma} \cdot \vec{n} \tag{55}$$

Quite remarkably, in the case of a ribbon-like crack embedded in an infinite elastic matrix, the SIF vector is proportional to the resolved stress $\mathbf{\Sigma} \cdot \vec{n}$ and does not depend on the matrix stiffness. This is no longer true for elliptical cracks as clearly put in evidence in (52). However the remarkable finding issued from the previous developments is that DIF or SIF vectors of an elliptical or ribbon-like crack write by means of only COD tensors, either the one attached to the actual crack or a combination of the latter and the one related to the tangent ribbon at the considered point of the crack front.

2.6 Extension to the case of a closed frictionless crack

A closed frictionless crack is characterized by a normal stress vector acting on the crack $\mathscr{I}$ and a purely tangential displacement discontinuity so that the last equation of (9) is replaced by

$$\vec{t} = \boldsymbol{\sigma} \cdot \vec{n} = t_n \vec{n} \quad \text{and} \quad [\![\vec{u}]\!] \cdot \vec{n} = 0 \qquad (\mathscr{I}) \tag{56}$$

where t_n is an arbitrary scalar (possibly restricted to negative values in case of unilateral conditions allowing opening and closing).

Beside strategies relying on the introduction of adequate 3D fictitious crack material within a flat ellipsoid (Deude et al., 2002; Dormieux and Kondo, 2009), the contribution of a closed frictionless crack may be simply addressed using the integral equation formalism presented in Section 2.3. In particular it is shown herein that the COD tensor of such a crack (denoted here with an overbar $\bar{\mathbf{B}}$) can easily be deduced from its open counterpart, i.e. the COD tensor of the open crack of the same geometry embedded in the same medium still denoted $\mathbf{B}$.

The reasoning starts by assuming that the displacement discontinuity still remains of the form (10) depending on the maximum COD $\vec{\beta}$ which must here satisfy $\vec{\beta} \cdot \vec{n} = 0$ according to (56). As $\vec{t}$ does not vanish anymore on the crack surface, (33) does not hold anymore but (27) applied at any point of $\mathscr{I}$ implies now

$$t_n \vec{n} = \boldsymbol{\Sigma} \cdot \vec{n} - \boldsymbol{\Lambda} \cdot \vec{\beta} \tag{57}$$

where the uniform tensor $\boldsymbol{\Lambda}$ is still given by (34) and the normal stress t_n is uniform over the crack surface. The condition $\vec{\beta} \cdot \vec{n} = 0$ finally yields

$$t_n = \frac{\vec{n} \cdot \boldsymbol{\Lambda}^{-1}}{\vec{n} \cdot \boldsymbol{\Lambda}^{-1} \cdot \vec{n}} \cdot \boldsymbol{\Sigma} \cdot \vec{n} \tag{58}$$

and

$$\vec{\beta} = \boldsymbol{\Lambda}^{-1} \cdot \left(\boldsymbol{\Sigma} \cdot \vec{n} - t_n \vec{n} \right) = \left(\boldsymbol{\Lambda}^{-1} - \frac{\vec{n} \cdot \boldsymbol{\Lambda}^{-1} \otimes \boldsymbol{\Lambda}^{-1} \cdot \vec{n}}{\vec{n} \cdot \boldsymbol{\Lambda}^{-1} \cdot \vec{n}} \right) \cdot \boldsymbol{\Sigma} \cdot \vec{n} \tag{59}$$

The normalized average COD is then given from (12)

$$\frac{\langle [\![\vec{u}]\!] \rangle_{\mathscr{I}}}{b} = \frac{\chi}{b} \left(\boldsymbol{\Lambda}^{-1} - \frac{\vec{n} \cdot \boldsymbol{\Lambda}^{-1} \otimes \boldsymbol{\Lambda}^{-1} \cdot \vec{n}}{\vec{n} \cdot \boldsymbol{\Lambda}^{-1} \cdot \vec{n}} \right) \cdot \boldsymbol{\Sigma} \cdot \vec{n} \tag{60}$$

Consistently with the general definition (14) of the COD tensor, a new COD tensor for the closed frictionless crack $\bar{\mathbf{B}}$ can be defined from (60) recalling that $\boldsymbol{\Lambda}^{-1}$ is related to the COD tensor of the corresponding open crack by (35)

$$\bar{\mathbf{B}} = \mathbf{B} - \frac{\vec{n} \cdot \mathbf{B} \otimes \mathbf{B} \cdot \vec{n}}{\vec{n} \cdot \mathbf{B} \cdot \vec{n}} \tag{61}$$

It is immediatly retrieved from (58), (59) and (61) that, whatever the anisotropy of the matrix, a remote uniaxial stress directed along the crack normal does not produce any crack opening displacement and the remote normal stress is fully transferred to the crack normal stress. The stress and strain fields are then indeed uniform in this case.

If $\mathbf{B}$ is diagonal in the crack axes i.e. of the form (120), for instance in the conditions of isotropic or transversely isotropic matrix of Appendix 6.3, the cracking modes are then uncoupled and the closed COD tensor $\bar{\mathbf{B}}$ is simply the projection of $\mathbf{B}$ onto the crack plane

$$\mathbf{B} = B_{ll}\, \vec{l} \otimes \vec{l} + B_{mm}\, \vec{m} \otimes \vec{m} + B_{nn}\, \vec{n} \otimes \vec{n} \Rightarrow \bar{\mathbf{B}} = B_{ll}\, \vec{l} \otimes \vec{l} + B_{mm}\, \vec{m} \otimes \vec{m} \tag{62}$$

In the general case of arbitrary anisotropy, $\mathbf{B}$ is a symmetric second-order tensor with possible non-zero off-diagonal terms inducing coupling between opening and shear modes. The closed counterpart $\bar{\mathbf{B}}$ writes from (61) as

$$\bar{\mathbf{B}} = \left(B_{ll} - \frac{B_{nl}^2}{B_{nn}} \right) \vec{l} \otimes \vec{l} + \left(B_{lm} - \frac{B_{nl}\, B_{mn}}{B_{nn}} \right) (\vec{l} \otimes \vec{m} + \vec{m} \otimes \vec{l}) + \left(B_{mm} - \frac{B_{mn}^2}{B_{nn}} \right) \vec{m} \otimes \vec{m} \tag{63}$$

Again as expected, a closed frictionless crack cannot exhibit any mode I so that the only possible couplings occur between shear modes in $\bar{\mathbf{B}}$. In addition it is shown on (63) that, in presence of initial couplings in open state (off-diagonal terms in $\mathbf{B}$), crack closure with frictionless condition implies a possible change of all (diagonal and off-diagonal) COD tensor components.

The subsequent calculation of DIF and SIF vectors may now stem from a careful adaptation of the results presented in Section 2.5. As already recalled in Section 2.5 invoking adequate references, the relationship (48) between $\vec{K}$ and $\vec{N}$ is very general and it has been shown in (49) that it involves the COD tensor of a local fictitious open ribbon-like crack tangent to the border at the observation point. The reasoning leading to the relationship (49) remains valid even in the case of a closed frictionless crack being understood that the fictitious tangent COD tensor is still that of an open crack and is still invertible so that (50) holds. What is changed in the case of a closed frictionless crack is the link between the local properties (COD, DIF, or SIF) and the remote loading $\mathbf{\Sigma}$ through the definition of the new COD tensor obtained from its open counterpart by (61). It follows that (64), (65), (66) and (67) are respectively modified as

$$\vec{N}^{\mathscr{E}} = \frac{3\sqrt{\pi\, b}}{8} \sqrt{b\, \|\mathbf{S}^{\dagger} \cdot \vec{y}_0^{\star}\|}\, \bar{\mathbf{B}}^{\mathscr{E}}(\vec{m}, \vec{n}, \eta) \cdot \mathbf{\Sigma} \cdot \vec{n} \quad \text{and} \quad \vec{K}^{\mathscr{E}} = \frac{3\, \pi^{3/2} \sqrt{b}}{8} \sqrt{b\, \|\mathbf{S}^{\dagger} \cdot \vec{y}_0^{\star}\|}\, \left(\mathbf{B}^{\mathscr{R}}(\vec{v}, \vec{n}) \right)^{-1} \cdot \bar{\mathbf{B}}^{\mathscr{E}}(\vec{m}, \vec{n}, \eta) \cdot \mathbf{\Sigma} \cdot \vec{n} \tag{64}$$

$$G^{\mathscr{E}} = \frac{9\, \pi^2\, b}{64} \left(b\, \|\mathbf{S}^{\dagger} \cdot \vec{y}_0^{\star}\| \right) \vec{n} \cdot \mathbf{\Sigma} \cdot \bar{\mathbf{B}}^{\mathscr{E}}(\vec{m}, \vec{n}, \eta) \cdot \left(\mathbf{B}^{\mathscr{R}}(\vec{v}, \vec{n}) \right)^{-1} \cdot \bar{\mathbf{B}}^{\mathscr{E}}(\vec{m}, \vec{n}, \eta) \cdot \mathbf{\Sigma} \cdot \vec{n} \tag{65}$$

$$\vec{N}^{\mathscr{R}} = \sqrt{\frac{b}{\pi}}\, \bar{\mathbf{B}}^{\mathscr{R}}(\vec{m}, \vec{n}) \cdot \mathbf{\Sigma} \cdot \vec{n} \quad \text{and} \quad \vec{K}^{\mathscr{R}} = \sqrt{\pi\, b}\, \left(\mathbf{B}^{\mathscr{R}}(\vec{m}, \vec{n}) \right)^{-1} \cdot \bar{\mathbf{B}}^{\mathscr{R}}(\vec{m}, \vec{n}) \cdot \mathbf{\Sigma} \cdot \vec{n} \tag{66}$$

$$G^{\mathscr{R}} = b\, \vec{n} \cdot \mathbf{\Sigma} \cdot \bar{\mathbf{B}}^{\mathscr{R}}(\vec{m}, \vec{n}) \cdot \mathbf{\Sigma} \cdot \vec{n} \tag{67}$$

To sum up the present section, the calculation of the COD tensor and subsequently the SIF vector of an open or closed frictionless crack embedded in an infinite matrix is reduced to the calculation of the integral (32), which specializes to (36) for an elliptical crack and (38) for a ribbon-like crack, being recalled that $\hat{\mathbf{Q}}_{nn}^{\star}$ is itself defined by an integral (24). Analytical evaluation of these integrals is possible in *a priori* a rather limited number of cases of material symmetries, such as cracks embedded in an isotropic matrix or a transversely isotropic matrix and aligned with the isotropy plane (Kanaun and Levin, 2009). Appendix 6.3 recalls the corresponding analytical expressions of the COD tensor. For more general cases of anisotropy, the COD tensors must be evaluated numerically by cubature (Kanaun and Levin, 2009). Note that an alternative numerical strategy relying on the application of the Cauchy residue theorem by Masson (2008) was proposed by Barthélémy (2009) to build the fourth-order crack compliance contribution tensor related to the COD tensor.

Linear transformations, as introduced by Pouya (2000) and exploited by Pouya and Zaoui (2006), Pouya (2007), Kachanov and Sevostianov (2018), Kushch and Sevostianov (2020), Sevostianov and Kushch (2020), Barthélémy (2020), Barthélémy et al. (2021) or Barthélémy et al. (2023), allow to widen considerably the class of material symmetries for which analytical expressions of the COD tensor and the SIF vector can be derived. In particular, the so-called *elliptical orthotropy* (EO), can be reached by transforming an isotropic matrix. Similarly, *transformed* *transversely isotropic* materials (TraTI) result from the linear transformation of a transversely isotropic (TI) matrix; the TraTI class contains not only a subset of orthotropy but also a subset of monoclinic symmetry. Linear transformations of the crack problem considered above are introduced in the next section.

3 Transformation of the crack problem

Linear transformations were introduced by Pouya (2000) within the framework of linear elasticity: from the solution to a well-posed problem of linear, elastic equilibrium, a variety of solutions to transformed problems can be produced by linear transformations. In particular, the known solution to the problem of a single crack embedded in a transversely isotropic (TI) matrix and aligned along the isotropy plane produces a new solution for a transformed crack embedded in the corresponding *transformed transversely isotropic* (TraTI) matrix. In particular DIF and SIF tensors can be calculated at any point of the boundary of the transformed crack.

The linear transformation involves two problems $\mathscr{P}$ and $\mathscr{P}^\sharp$ with the convention such that the symbol $^\sharp$ refers to the problem with known solution. In concrete terms, a linear relationship $\vec{x} \mapsto \vec{x}^\sharp$ is applied to the coordinates

$$\vec{x}^\sharp = \mathbf{P}^{-1} \cdot \vec{x} \qquad \Longleftrightarrow \qquad \vec{x} = \mathbf{P} \cdot \vec{x}^\sharp \tag{68}$$

where $\mathbf{P}$ denotes an invertible, second-order tensor.

As shown by Pouya and Zaoui (2006), the field solutions to $\mathscr{P}$ can be linearly related to those of $\mathscr{P}^\sharp$. Besides, in principle, the SIF and DIF vectors can then be retrieved from the asymptotic expansions (40) of $\vec{u}$ and $\boldsymbol{\sigma}$ near the tip of the crack $\mathscr{I}$. However, instead of resorting to these asymptotic expansions, it is chosen here to relate the (known) transformed COD tensor $\mathbf{B}^\sharp$ to the initial COD tensor $\mathbf{B}$ and consequently the SIF and DIF vectors $\vec{K}$ and $\vec{N}$ from their expressions as functions of $\mathbf{B}$, see (52) and (54). Such a derivation first requires to analyze the geometrical transformation of the crack as presented in Section 3.1 (with details in Appendix 6.5) and to recall that the relationship between the actual elastic stiffness $\boldsymbol{C}$ and its transformed counterpart $\boldsymbol{C}^\sharp$ is given by Pouya and Zaoui (2006) and Barthélémy (2020)

$$\boldsymbol{C} = (\mathbf{P} \overset{s}{\boxtimes} \mathbf{P}) : \boldsymbol{C}^\sharp : (\mathbf{P} \overset{s}{\boxtimes} \mathbf{P})^\intercal \tag{69}$$

3.1 Transformation of the crack

This section aims at examining the effect of a linear transformation on an elliptical or ribbon-like crack and concretely derive the relationships between the initial crack and its transformed counterpart. The main results are simply collected here whereas detailed proofs are provided in Appendix 6.5. It is first remarked that the present study of a transformed elliptical crack slightly differs from that in Barthélémy et al. (2021) and Barthélémy et al. (2023) in which the crack is seen as a flat ellipsoid.

Through the linear mapping (68), the initial crack $\mathscr{I}$ is transformed into $\mathscr{I}^\sharp$

$$\vec{x}^\sharp \in \mathscr{I}^\sharp \qquad \Longleftrightarrow \qquad \mathbf{P} \cdot \vec{x}^\sharp \in \mathscr{I} \tag{70}$$

The equation of the transformed crack relies then on the introduction of (68) in the ellipse parametrization (7) which yields the correspondence between the characteristic tensors $\mathbf{A}$ and $\mathbf{A}^\sharp$ respectively attached to $\mathscr{I}$ and $\mathscr{I}^\sharp$

$$\mathbf{A} = \mathbf{A}^\sharp \cdot \mathbf{P}^\intercal \qquad \Longleftrightarrow \qquad \mathbf{A}^\sharp = \mathbf{A} \cdot \mathbf{P}^{-\intercal} \tag{71}$$

The characteristic tensor $\mathbf{A}^\sharp$ of $\mathscr{I}^\sharp$ is associated with new radii $a^\sharp \geqslant b^\sharp$, major $\vec{l}^\sharp$ and minor $\vec{m}^\sharp$ directions and normal $\vec{n}^\sharp$. Since $\mathbf{P}$ is invertible, it preserves the rank of $\mathbf{A}$ so that the transformed crack remains elliptical (resp.

ribbon-like). The results fully describing the transformed crack are collected here, all the derivations being detailed in Appendix 6.5.

The normal $\vec{n}^\sharp$ to the transformed crack is given by

$$\vec{n}^\sharp = \frac{\mathbf{P}^\intercal \cdot \vec{n}}{\|\mathbf{P}^\intercal \cdot \vec{n}\|} \quad \Longleftrightarrow \quad \vec{n} = \frac{\mathbf{P}^{-\intercal} \cdot \vec{n}^\sharp}{\|\mathbf{P}^{-\intercal} \cdot \vec{n}^\sharp\|} \quad \text{and} \quad \|\mathbf{P}^\intercal \cdot \vec{n}\| = \frac{1}{\|\mathbf{P}^{-\intercal} \cdot \vec{n}^\sharp\|} \tag{72}$$

From the proof presented in Appendix 6.5, it comes that the radii $a^\sharp$ and $b^\sharp$ ($a^\sharp \geqslant b^\sharp$) read

$$a^\sharp = \frac{\sqrt{a^2\,\|\vec{g}\|^2 + b^2\,\|\vec{h}\|^2 + 2\,a\,b\,\|\vec{g}\wedge\vec{h}\|} + \sqrt{a^2\,\|\vec{g}\|^2 + b^2\,\|\vec{h}\|^2 - 2\,a\,b\,\|\vec{g}\wedge\vec{h}\|}}{2} \tag{73}$$

and

$$b^\sharp = \frac{\sqrt{a^2\,\|\vec{g}\|^2 + b^2\,\|\vec{h}\|^2 + 2\,a\,b\,\|\vec{g}\wedge\vec{h}\|} - \sqrt{a^2\,\|\vec{g}\|^2 + b^2\,\|\vec{h}\|^2 - 2\,a\,b\,\|\vec{g}\wedge\vec{h}\|}}{2} \tag{74}$$

where $\vec{g}$ and $\vec{h}$ are the images of the initial axes by the inverse transformation

$$\vec{g} = \mathbf{P}^{-1} \cdot \vec{l} \quad \text{and} \quad \vec{h} = \mathbf{P}^{-1} \cdot \vec{m} \tag{75}$$

and $\|\vec{g}\wedge\vec{h}\|$ is the area-stretch factor, equal to $\|\mathbf{P}^\intercal \cdot \vec{n}\|/|\det \mathbf{P}|$ by Nanson's formula (see Appendix 6.5.1).

The major $\vec{l}^\sharp$ and minor $\vec{m}^\sharp$ axes write in closed-form

$$\vec{l}^\sharp = \frac{\vec{w}}{\|\vec{w}\|} \quad \text{and} \quad \vec{m}^\sharp = \vec{n}^\sharp \wedge \vec{l}^\sharp \tag{76}$$

where $\vec{w}$ denotes the vector of largest norm between

$$\begin{aligned} \vec{w}_{\vec{l}} &= \left(a^2\,\|\vec{g}\|^2 - b^{\sharp 2}\right)\,\vec{g} + b^2\,(\vec{g}\cdot\vec{h})\,\vec{h} \\ \vec{w}_{\vec{m}} &= a^2\,(\vec{g}\cdot\vec{h})\,\vec{g} + \left(b^2\,\|\vec{h}\|^2 - b^{\sharp 2}\right)\,\vec{h} \end{aligned} \tag{77}$$

These expressions fully rely on the characteristics of the initial crack since $b^\sharp$ is given by (74). This choice guarantees a non-zero direction, except in the circular case $a^\sharp = b^\sharp$ for which the axes are arbitrary (see Appendix 6.5).

In the ribbon-like limit ($a, a^\sharp \to \infty$), the major axis aligns with $\vec{g}$ and the ratio $b^\sharp/b$ degenerates into

$$\vec{l}^\sharp \underset{a,a^\sharp\to\infty}{\sim} \frac{\vec{g}}{\|\vec{g}\|}\,, \quad \vec{m}^\sharp = \vec{n}^\sharp \wedge \vec{l}^\sharp \quad \text{and} \quad \frac{b^\sharp}{b} \underset{a,a^\sharp\to\infty}{\sim} \frac{\|\vec{g}\wedge\vec{h}\|}{\|\vec{g}\|} \tag{78}$$

3.2 Transformation of the crack opening displacement tensor

The starting point of the derivation is the transformation of the Green kernels in Fourier space. First, it is worth noting that $\vec{\xi}^\sharp = \mathbf{P}^\intercal \cdot \vec{\xi}$ in order to satisfy the consistency of the scalar product $\vec{x}\cdot\vec{\xi} = \vec{x}^\sharp \cdot \vec{\xi}^\sharp$. Then, after some algebra, the kernels $\hat{\boldsymbol{\Gamma}}$ and $\hat{\boldsymbol{Q}}$ defined in (22) are related to their transformed counterparts $\hat{\boldsymbol{\Gamma}}^\sharp$ and $\hat{\boldsymbol{Q}}^\sharp$ associated to the transformed stiffness $\boldsymbol{C}^\sharp$ (69) as

$$\begin{aligned} \hat{\boldsymbol{\Gamma}}(\vec{\xi}) &= (\mathbf{P} \overset{s}{\boxtimes} \mathbf{P})^{-\intercal} : \hat{\boldsymbol{\Gamma}}^\sharp(\mathbf{P}^\intercal\cdot\vec{\xi}) : (\mathbf{P} \overset{s}{\boxtimes} \mathbf{P})^{-1} \qquad (a) \\ \hat{\boldsymbol{Q}}(\vec{\xi}) &= (\mathbf{P} \overset{s}{\boxtimes} \mathbf{P}) : \hat{\boldsymbol{Q}}^\sharp(\mathbf{P}^\intercal\cdot\vec{\xi}) : (\mathbf{P} \overset{s}{\boxtimes} \mathbf{P})^\intercal \qquad (b) \end{aligned} \tag{79}$$

It follows that the reduced Fourier transforms $\hat{\mathbf{Q}}^{\star}_{nn}$ and $\hat{\mathbf{Q}}^{\sharp\star}_{nn}$ (see definition in (105) being understood that $\hat{\boldsymbol{Q}}$ and $\hat{\boldsymbol{Q}}^{\sharp}$ are reduced along and are left and right contracted by respectively $\vec{n}$ and $\vec{n}^{\sharp}$) can be related thanks to (72) after adequate calculations and change of integration variable

$$
\begin{aligned}
\hat{\mathbf{Q}}^{\star}_{nn}(\vec{\xi}^{\star}) &= \frac{1}{2\pi}\int_{\xi_n=-\infty}^{+\infty} \vec{n}\cdot\hat{\boldsymbol{Q}}(\vec{\xi}^{\star}+\xi_n\,\vec{n})\cdot\vec{n}\,\mathrm{d}\xi_n \\
&= \frac{1}{2\pi}\int_{\xi_n=-\infty}^{+\infty} \vec{n}\cdot(\mathbf{P}\overset{s}{\boxtimes}\mathbf{P}) : \hat{\boldsymbol{Q}}^{\sharp}\left(\mathbf{P}^{\intercal}\cdot\vec{\xi}^{\star}+\xi_n\,\mathbf{P}^{\intercal}\cdot\vec{n}\right) : (\mathbf{P}\overset{s}{\boxtimes}\mathbf{P})^{\intercal}\cdot\vec{n}\,\mathrm{d}\xi_n \\
&= \mathbf{P}\cdot\left(\frac{1}{2\pi}\int_{\xi_n=-\infty}^{+\infty}(\mathbf{P}^{\intercal}\cdot\vec{n})\cdot\hat{\boldsymbol{Q}}^{\sharp}\left(\mathbf{P}^{\intercal}\cdot\vec{\xi}^{\star}+\xi_n\,\mathbf{P}^{\intercal}\cdot\vec{n}\right)\cdot(\mathbf{P}^{\intercal}\cdot\vec{n})\,\mathrm{d}\xi_n\right)\cdot\mathbf{P}^{\intercal} \\
&= \|\mathbf{P}^{\intercal}\cdot\vec{n}\|^2\,\mathbf{P}\cdot\left(\frac{1}{2\pi}\int_{\xi_n=-\infty}^{+\infty}\vec{n}^{\sharp}\cdot\hat{\boldsymbol{Q}}^{\sharp}\left(\mathbf{P}^{\intercal}\cdot\vec{\xi}^{\star}+\xi_n\,\|\mathbf{P}^{\intercal}\cdot\vec{n}\|\,\vec{n}^{\sharp}\right)\cdot\vec{n}^{\sharp}\,\mathrm{d}\xi_n\right)\cdot\mathbf{P}^{\intercal} \\
&= \|\mathbf{P}^{\intercal}\cdot\vec{n}\|\,\mathbf{P}\cdot\left(\frac{1}{2\pi}\int_{\xi'=-\infty}^{+\infty}\vec{n}^{\sharp}\cdot\hat{\boldsymbol{Q}}^{\sharp}\left(\mathbf{P}^{\intercal}\cdot\vec{\xi}^{\star}+\xi'\,\vec{n}^{\sharp}\right)\cdot\vec{n}^{\sharp}\,\mathrm{d}\xi'\right)\cdot\mathbf{P}^{\intercal} \\
&= \|\mathbf{P}^{\intercal}\cdot\vec{n}\|\,\mathbf{P}\cdot\hat{\mathbf{Q}}^{\sharp\star}_{nn}(\mathbf{P}^{\intercal}\cdot\vec{\xi}^{\star})\cdot\mathbf{P}^{\intercal}
\end{aligned}
\tag{80}
$$

Before exploiting (80) in (34) to identify the relationship between the operator $\boldsymbol{\Lambda}$ and its counterpart $\boldsymbol{\Lambda}^{\sharp}$, it is worth recalling the following identity proven in Appendix 6.5.3

$$
\mathbf{P}^{\intercal}\cdot\mathbf{S}^{\dagger} = \mathbf{S}^{\sharp\dagger}\cdot\mathbf{R}^{\sharp\intercal}\cdot\mathbf{R}+\vec{n}^{\sharp}\otimes\vec{Y} \tag{81}
$$

where $\mathbf{R}^{\sharp\intercal}\cdot\mathbf{R}$ is a rotation sending $\vec{n}$ to $\vec{n}^{\sharp}$ and $\vec{n}^{\perp}$ to $\vec{n}^{\sharp\perp}$ and $\vec{Y}$ is an undefined vector. Using (34) together with (80) and (81) provides

$$
\begin{aligned}
\boldsymbol{\Lambda} &= \frac{1}{4}\int_{\vec{\kappa}^{\star}\in\vec{n}^{\perp},\|\vec{\kappa}^{\star}\|=1}\hat{\mathbf{Q}}^{\star}_{nn}(\mathbf{S}^{\dagger}\cdot\vec{\kappa}^{\star})\,\mathrm{d}\varphi_{\kappa^{\star}} \\
&= \|\mathbf{P}^{\intercal}\cdot\vec{n}\|\,\mathbf{P}\cdot\left(\frac{1}{4}\int_{\vec{\kappa}^{\star}\in\vec{n}^{\perp},\|\vec{\kappa}^{\star}\|=1}\hat{\mathbf{Q}}^{\sharp\star}_{nn}(\mathbf{P}^{\intercal}\cdot\mathbf{S}^{\dagger}\cdot\vec{\kappa}^{\star})\,\mathrm{d}\varphi_{\kappa^{\star}}\right)\cdot\mathbf{P}^{\intercal} \\
&= \|\mathbf{P}^{\intercal}\cdot\vec{n}\|\,\mathbf{P}\cdot\left(\frac{1}{4}\int_{\vec{\kappa}^{\sharp\star}\in\vec{n}^{\sharp\perp},\|\vec{\kappa}^{\sharp\star}\|=1}\hat{\mathbf{Q}}^{\sharp\star}_{nn}(\mathbf{S}^{\sharp\dagger}\cdot\vec{\kappa}^{\sharp\star})\,\mathrm{d}\varphi_{\kappa^{\sharp\star}}\right)\cdot\mathbf{P}^{\intercal} \\
&= \|\mathbf{P}^{\intercal}\cdot\vec{n}\|\,\mathbf{P}\cdot\boldsymbol{\Lambda}^{\sharp}\cdot\mathbf{P}^{\intercal} = \frac{1}{\|\mathbf{P}^{-\intercal}\cdot\vec{n}^{\sharp}\|}\,\mathbf{P}\cdot\boldsymbol{\Lambda}^{\sharp}\cdot\mathbf{P}^{\intercal}
\end{aligned}
\tag{82}
$$

where in the third equation, (81) is used to replace $\mathbf{P}^{\intercal}\cdot\mathbf{S}^{\dagger}\cdot\vec{\kappa}^{\star}$ by $\mathbf{S}^{\sharp\dagger}\cdot\mathbf{R}^{\sharp\intercal}\cdot\mathbf{R}\cdot\vec{\kappa}^{\star}+(\vec{Y}\cdot\vec{\kappa}^{\star})\vec{n}^{\sharp}$. This last term is removed by virtue of (107) and in the first term $\vec{\kappa}^{\sharp\star}=\mathbf{R}^{\sharp\intercal}\cdot\mathbf{R}\cdot\vec{\kappa}^{\star}$ describes the unit circle of the plane $\vec{n}^{\sharp\perp}$, since $\mathbf{R}^{\sharp\intercal}\cdot\mathbf{R}$ is a rotation mapping $\vec{n}^{\perp}$ to $\vec{n}^{\sharp\perp}$.

For elliptical cracks, the COD tensors $\mathbf{B}^{\mathscr{E}}(\vec{m},\vec{n},\eta)$ and $\mathbf{B}^{\mathscr{E}\sharp}(\vec{m}^{\sharp},\vec{n}^{\sharp},\eta^{\sharp})$ can be related by invoking (37), delivering

$$
\mathbf{B}^{\mathscr{E}}(\vec{m},\vec{n},\eta) = \frac{1}{\|\mathbf{P}^{\intercal}\cdot\vec{n}\|}\,\frac{b^{\sharp}}{b}\,\mathbf{P}^{-\intercal}\cdot\mathbf{B}^{\mathscr{E}\sharp}(\vec{m}^{\sharp},\vec{n}^{\sharp},\eta^{\sharp})\cdot\mathbf{P}^{-1} = \|\mathbf{P}^{-\intercal}\cdot\vec{n}^{\sharp}\|\,\frac{b^{\sharp}}{b}\,\mathbf{P}^{-\intercal}\cdot\mathbf{B}^{\mathscr{E}\sharp}(\vec{m}^{\sharp},\vec{n}^{\sharp},\eta^{\sharp})\cdot\mathbf{P}^{-1} \tag{83}
$$

where the dimensionless quantities $b^{\sharp}/b$ and $\eta^{\sharp}=b^{\sharp}/a^{\sharp}$ are given by expressions (146) and (147).

In the case of ribbon-like cracks, (39) and (78) providing $b^{\sharp}/b$ are used to transform (82) into

$$
\mathbf{B}^{\mathscr{R}}(\vec{m},\vec{n}) = \frac{1}{\|\mathbf{P}^{\intercal}\cdot\vec{n}\|}\,\frac{b^{\sharp}}{b}\,\mathbf{P}^{-\intercal}\cdot\mathbf{B}^{\mathscr{R}\sharp}(\vec{m}^{\sharp},\vec{n}^{\sharp})\cdot\mathbf{P}^{-1} = \frac{1}{\|\mathbf{P}^{-1}\cdot\vec{l}\|\,|\det\mathbf{P}|}\,\mathbf{P}^{-\intercal}\cdot\mathbf{B}^{\mathscr{R}\sharp}(\vec{m}^{\sharp},\vec{n}^{\sharp})\cdot\mathbf{P}^{-1} \tag{84}
$$

Note that, up to a different normalization of the COD tensors, the above results coincide with previous results presented in Barthélémy et al. (2021) and Barthélémy et al. (2023). The derivation proposed here is however more straightforward and more elegant.

3.3 Transformation of the displacement and stress intensity factors

In the present section, the above results are used to derive a strategy allowing to express the DIF and SIF vectors of cracks embedded in a transformed matrix before application to the TraTI case in Section 4.

The starting point is the initial problem $\mathscr{P}$ of an elliptical crack (possibly degenerated in a ribbon-like crack) embedded in an unbounded elastic matrix of stiffness $\boldsymbol{C}$. The expected outcomes of the analysis are the DIF and SIF vectors $\vec{N}$ and $\vec{K}$ of the crack embedded in the matrix of interest $\boldsymbol{C}$, together with the local energy release rate G which usually governs crack propagation. It is assumed that a linear transformation $\mathbf{P}$ has been identified, that transforms problem $\mathscr{P}$ into $\mathscr{P}^\sharp$, for which the COD tensor is known (for example, the transformed matrix $\boldsymbol{C}^\sharp$ is isotropic or transversely isotropic while the transformed crack $\mathscr{I}^\sharp$ is aligned with the isotropy plane, see Appendix 6.3).

Ideally, a direct relationship between initial and transformed DIF and SIF vectors should be derived, similarly to the relationship between initial and transformed COD derived in Section 3.2. However, the derivation of such relationships seems complex (if possible at all) and an alternative approach is presented here, based on the general results presented in Section 2.2. Indeed, for *any* stiffness tensor $\boldsymbol{C}$ and crack $\mathscr{I} \in \{\mathscr{E}, \mathscr{R}\}$, the DIF and SIF vectors can be expressed as function of the COD tensors, see (54) and (52). Note that for elliptical cracks, (52) involves the *true* COD tensor as well as the COD tensor of the fictitious tangent ribbon-like crack. From this observation, the proposed strategy becomes quite clear.

For a *ribbon-like crack*, first, the SIF vector $\vec{K}^{\mathscr{R}}$ is readily found from (54). The COD tensor $\mathbf{B}^{\mathscr{R}\sharp}$ of the *transformed* ribbon being known, the COD tensor of the *initial* ribbon $\mathbf{B}^{\mathscr{R}}$ is obtained from (84). The DIF vector $\vec{N}^{\mathscr{R}}$ of the *initial* problem then results from (54). The local energy release rate $G^{\mathscr{R}}$ finally follows from (41) or (55).

For an *elliptical crack*, the strategy is more involved and detailed below. The initial crack is defined by the tensor $\mathbf{A}$ and its decomposition (99). The initial stiffness tensor $\boldsymbol{C}$ and linear transformation $\mathbf{P}$ are also given.

1. Use (72) to find the normal $\vec{n}^\sharp$ to the transformed crack.
2. Find the transformed axes $\vec{l}^\sharp$ and $\vec{m}^\sharp$ from (76), together with the transformed radii $a^\sharp$, $b^\sharp$ and aspect ratio $\eta^\sharp = b^\sharp/a^\sharp$ from (73), (74) and (147).
3. Identify the transformed stiffness tensor $\boldsymbol{C}^\sharp$ from (69).
4. Calculate the transformed COD tensor $\mathbf{B}^{\mathscr{E}\sharp}(\vec{m}^\sharp, \vec{n}^\sharp, \eta^\sharp)$. If the transformed matrix has simple symmetries, use Appendix 6.3.
5. Use (83) to evaluate the initial COD tensor $\mathbf{B}^{\mathscr{E}}(\vec{m}, \vec{n}, \eta)$.
6. Choose a point $\vec{x}_0^\star \in \partial\mathscr{E}$ at which the DIF and SIF vectors are to be evaluated. Use for example the parametrizations proposed in Section 6.4 where $\vec{y}_0^\star$ and $\vec{x}_0^\star$ are expressed as in (134).
7. Find the DIF from (52) and (136)

$$\vec{N}^{\mathscr{E}} = \frac{3\sqrt{\pi\, b}}{8}\sqrt{b\,\|\mathbf{S}^\dagger \cdot \vec{y}_0^\star\|}\,\mathbf{B}^{\mathscr{E}}(\vec{m}, \vec{n}, \eta) \cdot \boldsymbol{\Sigma} \cdot \vec{n} \tag{85}$$

8. Use (135) to find the initial tangent frame $(\vec{\nu}, \vec{\tau})$.
9. Compute the transformed tangent frame $(\vec{\nu}^\sharp, \vec{\tau}^\sharp)$ from the following identities

$$\vec{\tau}^\sharp = \frac{\mathbf{P}^{-1} \cdot \vec{\tau}}{\|\mathbf{P}^{-1} \cdot \vec{\tau}\|} \quad \text{and} \quad \vec{\nu}^\sharp = \vec{\tau}^\sharp \wedge \vec{n}^\sharp \tag{86}$$

10. Calculate the COD tensor of the transformed, fictitious, tangent ribbon-like crack $\mathbf{B}^{\mathcal{R}\sharp}(\vec{v}^\sharp, \vec{n}^\sharp)$. If possible, use Appendix 6.3. Beware that the transverse vector is $\vec{v}^\sharp$ and not $\vec{m}^\sharp$.
11. Calculate $\mathbf{B}^{\mathcal{R}}(\vec{v}, \vec{n})$ from equation (84). Beware that the longitudinal vector of the fictitious ribbon is $\vec{\tau}$ and not $\vec{l}$

$$\mathbf{B}^{\mathcal{R}}(\vec{v}, \vec{n}) = \frac{1}{\|\mathbf{P}^{-1} \cdot \vec{\tau}\| \, |\det \mathbf{P}|} \mathbf{P}^{-\intercal} \cdot \mathbf{B}^{\mathcal{R}\sharp}(\vec{v}^\sharp, \vec{n}^\sharp) \cdot \mathbf{P}^{-1} \tag{87}$$

12. Use (52) and (136) to evaluate the SIF vector $\vec{K}$

$$\vec{K}^{\mathcal{E}} = \frac{3\,\pi^{3/2}\sqrt{b}}{8} \sqrt{b\,\|\mathbf{S}^\dagger \cdot \vec{y}_0^\star\|} \, \left(\mathbf{B}^{\mathcal{R}}(\vec{v}, \vec{n})\right)^{-1} \cdot \mathbf{B}^{\mathcal{E}}(\vec{m}, \vec{n}, \eta) \cdot \mathbf{\Sigma} \cdot \vec{n} \tag{88}$$

13. The local energy release rate $G^{\mathcal{E}}$ then follows directly from (41) as $G^{\mathcal{E}} = \vec{K}^{\mathcal{E}} \cdot \vec{N}^{\mathcal{E}}$, or equivalently from the quadratic form (53).

The SIF vector can classically be decomposed in modes

$$K_I = |\vec{K}^{\mathcal{E}} \cdot \vec{n}| \,, \quad K_{II} = |\vec{K}^{\mathcal{E}} \cdot \vec{v}| \,, \quad K_{III} = |\vec{K}^{\mathcal{E}} \cdot \vec{\tau}| \tag{89}$$

The strategy above extends to a closed frictionless crack within the same framework. Following Section 2.6, it suffices to replace the COD tensor of the actual crack by its closed counterpart $\bar{\mathbf{B}}$ defined in (61), the fictitious tangent ribbon-like crack remaining open. The DIF, SIF and energy release rate are then obtained from (64) and (65) for an elliptical crack, and from (66) and (67) for a ribbon-like crack, instead of their open-crack analogues.

4 Application to a transformed transversely isotropic material

In this section a short example is proposed. In this application, the stiffness tensor $\boldsymbol{C}$ that stems from a TI tensor $\boldsymbol{C}^\sharp$ of axis $\vec{e}_3$ and parameters E, H, ν_1, ν_2 and Γ (see (126)) and a transformation tensor $\mathbf{P}$ depending on three parameters, a ratio $\varpi > 0$ and two angles θ and ϕ, of the form

$$\mathbf{P} = \varpi\,\vec{e}_1 \otimes \vec{e}_1 + \vec{e}_2 \otimes \vec{e}_2 + \vec{e}_r(\theta, \phi) \otimes \vec{e}_3 \quad \text{with} \quad \vec{e}_r(\theta, \phi) = \cos\theta\,\vec{e}_3 + \sin\theta\,(\cos\phi\,\vec{e}_1 + \sin\phi\,\vec{e}_2) \tag{90}$$

where the angles $\theta \in [0, \pi/2[$ and $\phi \in [0, 2\pi]$ induce a monoclinic material symmetry by inclination of the axis $\vec{e}_3$ towards $\vec{e}_r(\theta, \phi)$ and ϖ allows to break the isotropy in the plane Span $(\vec{e}_1, \vec{e}_2)$. The effect of the latter parameter can be observed on the Kelvin-Mandel representation of the transformed compliance tensor (127) for $\theta = 0$

$$\mathrm{Mat}\,(\boldsymbol{S}(\theta = 0)) = \begin{pmatrix} \frac{1}{E\varpi^4} & \frac{-\nu_1}{E\varpi^2} & \frac{-\nu_2}{E\varpi^2} & 0 & 0 & 0 \\ \frac{-\nu_1}{E\varpi^2} & \frac{1}{E} & \frac{-\nu_2}{E} & 0 & 0 & 0 \\ \frac{-\nu_2}{E\varpi^2} & \frac{-\nu_2}{E} & \frac{1}{EH} & 0 & 0 & 0 \\ 0 & 0 & 0 & \frac{1+\nu_1}{E\Gamma} & 0 & 0 \\ 0 & 0 & 0 & 0 & \frac{1+\nu_1}{E\Gamma\varpi^2} & 0 \\ 0 & 0 & 0 & 0 & 0 & \frac{1+\nu_1}{E\varpi^2} \end{pmatrix} \tag{91}$$

The ellipse is chosen in such a way that $\vec{e}_1$ is the major and $\vec{e}_2$ the minor axes, which implies that the transformation of the type (90) leaves the orientations of axes unchanged but applies a homothety on the radius a, in other words

$$\mathbf{A} = b\left(\frac{\vec{e}_1 \otimes \vec{e}_1}{\eta} + \vec{e}_2 \otimes \vec{e}_2\right) \quad \text{and} \quad \mathbf{A}^\sharp = \mathbf{A} \cdot \mathbf{P}^{-\intercal} = b\left(\frac{\vec{e}_1 \otimes \vec{e}_1}{\eta\,\varpi} + \vec{e}_2 \otimes \vec{e}_2\right) \tag{92}$$

It follows that the aspect ratio $\eta^\sharp$ is $\min\left(\eta\,\varpi, \frac{1}{\eta\,\varpi}\right)$ and the orientations of major and minor axes are possibly inverted between the two ellipses depending on the magnitude of $\eta\,\varpi$.

Application of the strategy proposed in Section 3.3 delivers the local stress and displacement intensity factors $\vec{K}$ and $\vec{N}$, from which the local energy release rate G (41) can be evaluated.

As regards remote conditions and numerical values, an elliptical crack of aspect ratio $\eta = 1/4$ is considered, subjected to a uniform remote traction $\mathbf{\Sigma} = \Sigma_{33}\vec{e}_3 \otimes \vec{e}_3$. The initial TI matrix, from which the actual TraTI matrix derives, is defined by the following parameters

$$H = 2, \quad \nu_1 = 0.4, \quad \nu_2 = 0.3 \quad \text{and} \quad \Gamma = 3,$$

with various values of θ, ϕ and ϖ for the transformation $\mathbf{P}$ (90). As the energy release rate G is always normalized in the sequel, the modulus E doesn't play any role. It is however emphasized that the normalization value for G is systematically unique, taken from the analytical derivation, for different methods used in the same figure so that absolute and not only relative values remain comparable: practically, for each (ϕ, ϖ) pair, the local energy release rate is normalized by the maximum local value of the present closed-form solution. This maximum occurs for $\theta = \pi/4$ in the following results.

The closed-form solution is first assessed in 4.1 against two independent numerical methods, a direct finite element simulation and a semi-analytical evaluation with the `Echoes` library (Barthélémy, 2026), the former being limited to a moderate stiffness contrast for the reason explained therein. It is then exploited in 4.2 to study the influence of the transformation on the local energy release rate over a wide range of contrasts, for which a direct numerical resolution would be impractical.

4.1 Numerical and semi-analytical validation

The closed-form distributions are first verified by a direct finite element (FE) simulation. The infinite medium is truncated by a sphere of radius $R = 5\,a$, meshed with tetrahedra refined in a torus around the crack front (element size $b/12$ at the tip) with `Gmsh` (Geuzaine and Remacle, 2009), the elasticity problem being solved with cubic (P_3) Lagrange elements (of the order of 7.3×10^5 degrees of freedom) in the `FEniCSx/DOLFINx` environment (Baratta et al., 2023).

Truncating the medium to a finite sphere would, on its own, bias the crack opening by a term of order $O\big((a/R)^3\big)$. This bias is attenuated by the finite-distance correction of Adessina et al. (2017) and Du et al. (2020), revisited here for a crack. Far from the crack, the opened crack radiates as an elastic dipole, so the displacement prescribed on the outer boundary superposes the remote affine field and this dipole field,

$$\vec{u}(\vec{x}) \underset{\|\vec{x}\|\to\infty}{\approx} (\boldsymbol{S} : \mathbf{\Sigma}) \cdot \vec{x} - b\, S^{\mathscr{E}} \left(\boldsymbol{grad}\,\mathbf{G}(\vec{x}) : \boldsymbol{C} \cdot \vec{n}\right) \cdot \vec{U}, \qquad S^{\mathscr{E}} = \pi\, a\, b, \quad \vec{U} = \frac{\langle [\![\vec{u}]\!] \rangle}{b}, \tag{93}$$

where $\boldsymbol{grad}\,\mathbf{G}$ is the gradient of the Green tensor of the actual TraTI medium (Pouya, 2007) and $\vec{U}$ is the *a priori* unknown normalized average opening. Because the opening of a planar crack is governed solely by the traction $\vec{t} = \mathbf{\Sigma} \cdot \vec{n}$, the dipole amplitude is identified from *three* traction problems (prescribing $\vec{u} = (\boldsymbol{S} : \mathbf{\Sigma}^{(i)}) \cdot \vec{x}$ on the boundary, with $\mathbf{\Sigma}^{(i)} \cdot \vec{n} = \vec{e}_i$), which yield the columns of an apparent COD tensor $\mathbf{B}_t$, and *three* dipole problems (prescribing (93) for $\vec{U} = \vec{e}_m$), which yield a dipole-response tensor $\mathbf{B}_U$, in place of the 2×6 elementary problems required for a general ellipsoidal inhomogeneity. Enforcing self-consistency $\vec{U} = \mathbf{B}_t \cdot \vec{t} + \mathbf{B}_U \cdot \vec{U}$ then yields the infinite-medium COD tensor

$$\mathbf{B}_\infty = \big(\mathbf{1} - \mathbf{B}_U\big)^{-1} \cdot \mathbf{B}_t, \tag{94}$$

directly comparable, term by term, with the closed-form. The six problems share a single matrix factorization, and $\mathbf{B}_\infty$ is found identical for $R = 5\,a$, $10\,a$ and $30\,a$. The solution corresponding to a given prescribed $\mathbf{\Sigma}$

(e.g. $\mathbf{\Sigma} = \Sigma_{33}\vec{e}_3 \otimes \vec{e}_3$) is eventually provided by the addition of both (homogeneous traction and dipole) problems ensuring the boundary condition (93) together with the consistency rule $\vec{U} = \mathbf{B}_\infty \cdot \mathbf{\Sigma} \cdot \vec{n}$.

Two independent estimates of G are then extracted at each azimuth θ_y of the front. The first is an energy based domain integral (G-θ method) (Destuynder and Djaoua, 1981; Li et al., 1985; Shih et al., 1986): a virtual crack-advance field $\vec{\theta} = q\,\vec{v}_0$, where $\vec{v}_0$ is the in-plane outward normal to the front at θ_y and q a hat function supported on a tube of radii $r_1 < r_2$ around the front point, gives

$$G(\theta_y) \int_{\mathscr{F}} q\,(\vec{v}_0 \cdot \vec{v})\,\mathrm{d}s = \int_\Omega \left[\boldsymbol{\sigma} : \left(\mathbf{grad}\,\vec{u} \cdot \mathbf{grad}\,\vec{\theta}\right) - \frac{1}{2}(\boldsymbol{\sigma} : \boldsymbol{\varepsilon})\,\mathrm{div}\,\vec{\theta}\right] \mathrm{d}\Omega, \tag{95}$$

where $\mathscr{F}$ is the crack front, the right-hand side is the domain integral of the Eshelby energy-momentum tensor contracted with $\mathbf{grad}\,\vec{\theta}$ (it reduces to the shell $r_1 < \|\vec{x} - \vec{x}_0\| < r_2$ where $\mathbf{grad}\,\vec{\theta} \neq 0$), and the left-hand side normalizes the local advance, with no contour to choose. The second is a modal estimate $G = \pi\,\vec{N} \cdot \left(\mathbf{B}^{\mathscr{R}}(\vec{v},\vec{n})\right)^{-1} \cdot \vec{N}$ that combines the FE crack opening ($\vec{N}$ is estimated by least-square method along a radial leading to the considered front point) with the closed-form ribbon relation between $\vec{K}$ and $\vec{N}$ established above. As shown in Fig. 4, both reproduce the closed-form solution to about 3% on average. The residual deviation is not the same for $\varpi = 3$ and $\varpi = 1/3$, even though both share the contrast $\varpi^4 = 81$: the modal estimate departs most for $\varpi = 3$ (about 5%, against some 2 to 3% for $\varpi = 1$ and $\varpi = 1/3$), the best agreement being reached for the unstretched case $\varpi = 1$. This asymmetry shows that the residual discrepancy is controlled by the orientation of the stretched direction relative to the crack, and not by the contrast magnitude alone.

The stiffness contrast of the transformed material scales as ϖ^4. The strongly stretched transformations ($\varpi = 10$ or $\varpi = 1/10$, contrast 10^4), as considered in Section 4.2, render the matrix nearly inextensible along the stretched axis and make low order elements *lock*, underestimating the crack opening regardless of the mesh size. The direct FE validation is therefore restricted to the moderate contrast $\varpi \in \{3, 1, 1/3\}$ (contrast $\varpi^4 \leq 81$). However, such a contrast already has a slightly noticeable effect on numerical FE calculations, as seen in Fig. 4. The severely contrasted configurations, where a direct FE computation becomes impractical, are precisely those for which the present closed-form solution is the most valuable; they are the ones explored in 4.2 and are cross-checked semi-analytically as follows.

For an arbitrary anisotropy, the COD tensors of the *actual* medium can be obtained, without any transformation, from the crack compliance computation of Barthélémy (2009) implemented in the `Echoes` library (Barthélémy, 2026). The average COD tensor $\mathbf{B}^{\mathscr{E}}$ of the elliptical crack and the COD tensor $\mathbf{B}^{\mathscr{R}}(\vec{v},\vec{n})$ of the fictitious tangent ribbon both follow from the corresponding crack-compliance (Hill) tensors $\boldsymbol{H}^{\mathscr{E}}$ and $\boldsymbol{H}^{\mathscr{R}}$ of the actual medium, evaluated as the flat-inclusion limits of Barthélémy (2009) (normalized respectively by the major semi-axis and by the in-plane half-width). As the COD is normalized here by the minor semi-axis b, and not by a as in Barthélémy et al. (2023), the conversion reads

$$\vec{n} \overset{s}{\otimes} \mathbf{B}^{\mathscr{E}} \overset{s}{\otimes} \vec{n} = \frac{4}{3\eta}\,\boldsymbol{H}^{\mathscr{E}} \qquad \text{and} \qquad \vec{n} \overset{s}{\otimes} \mathbf{B}^{\mathscr{R}} \overset{s}{\otimes} \vec{n} = \frac{\pi}{2}\,\boldsymbol{H}^{\mathscr{R}}, \tag{96}$$

the two prefactors involving the area coefficients $\chi^{\mathscr{E}} = 2/3$ and $\chi^{\mathscr{R}} = \pi/4$ of (13). Feeding the resulting $\mathbf{B}^{\mathscr{E}}$ and $\mathbf{B}^{\mathscr{R}}$ into the local relations of Section 3.3 yields a semi-analytical estimate of G valid at *any* contrast. As reported in Fig. 4 and Fig. 5, it reproduces the closed-form solution to better than 0.25% at every azimuth and contrast, including the strongly stretched cases out of reach of the FE computation; the average COD tensor agrees to four significant digits, for instance $B_{33} = 2.168$ for $\theta = \pi/4$, $\phi = 0$ and $\varpi = 3$.

4.2 Parametric study of the local energy release rate

Fig. 5 displays both the closed-form energy release rate and the semi-analytical counterpart from `Echoes` for a high contrast between moduli: here $\varpi \in \{10, 1, 1/10\}$ (contrast 10^4)

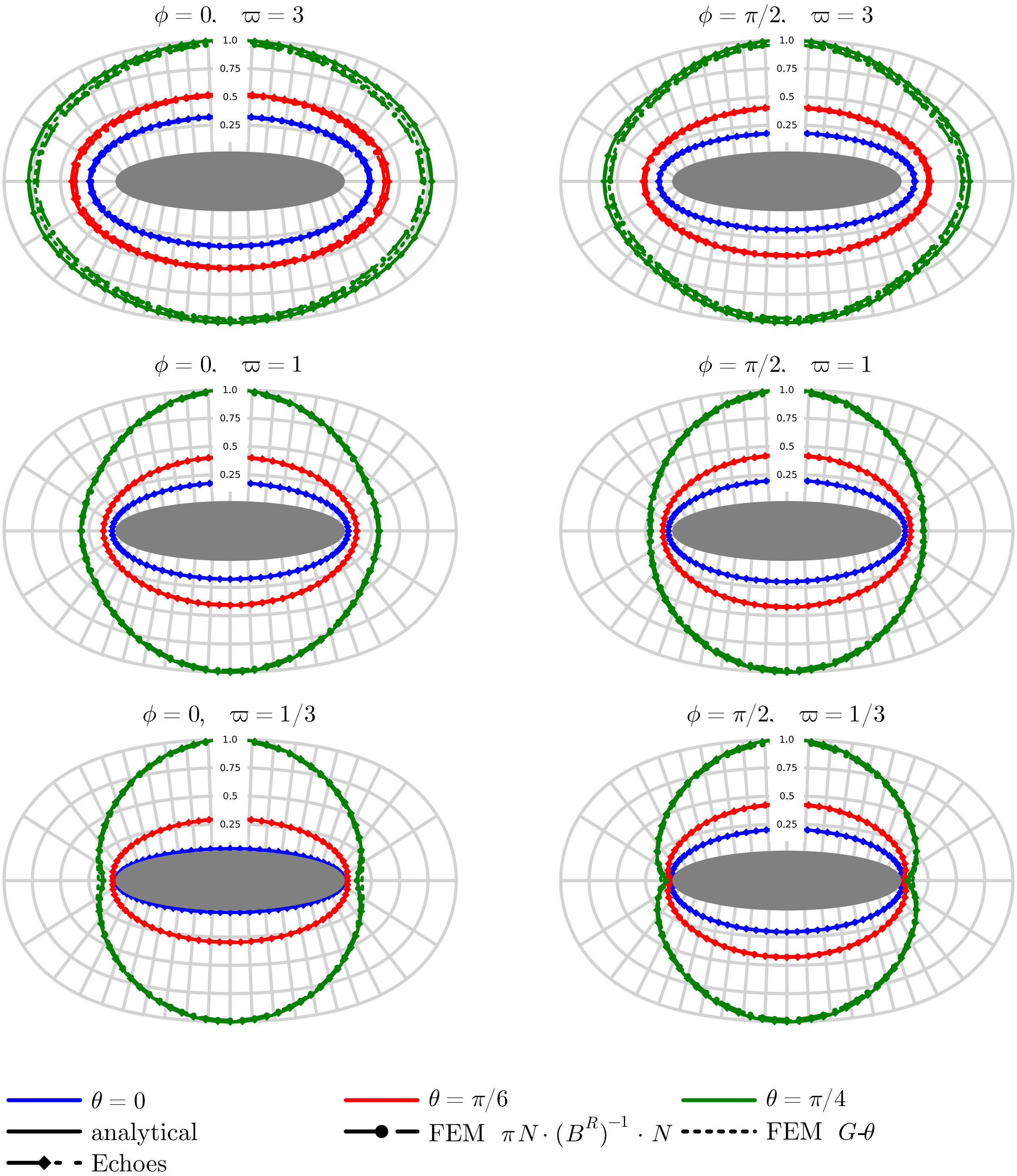

Fig. 4: Finite element and semi-analytical validation of the normalized local energy release rate at moderate stiffness contrast ($\varpi \in \{3, 1, 1/3\}$, contrast $\varpi^4 \leq 81$), ellipse aspect ratio $\eta = 1/4$ and matrix properties $H = 2$, $\nu_1 = 0.4$, $\nu_2 = 0.3$, $\Gamma = 3$. The closed-form solution (solid) is superimposed with two independent finite element estimates sharing the same analytical normalization, the modal $G_{\mathbf{B}^{\mathscr{R}}} = \pi\vec{N} \cdot (\mathbf{B}^{\mathscr{R}})^{-1} \cdot \vec{N}$ (dashed, circles) and the domain integral G-θ (dotted), together with the semi-analytical `Echoes` evaluation (dash-dotted, diamonds). The finite element estimates agree with the closed-form to about 3% on average and the `Echoes` evaluation to better than 0.25%.

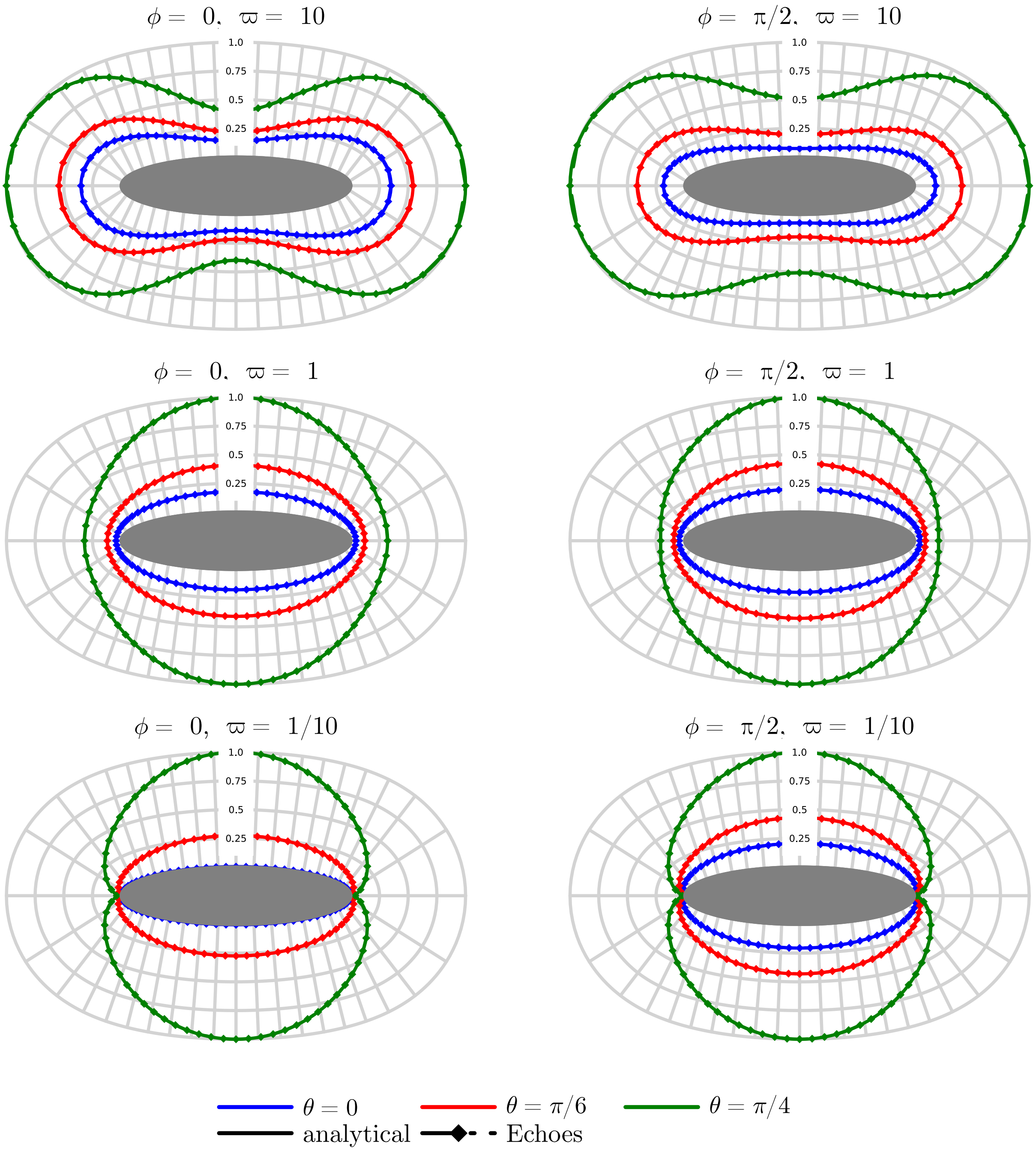

Fig. 5: Normalized local energy release rate around an elliptical crack (shaded areas in the figure) embedded in a monoclinic TraTI matrix. The ellipse aspect ratio is $\eta = 1/4$ and the matrix properties are $H = 2$, $\nu_1 = 0.4$, $\nu_2 = 0.3$, $\Gamma = 3$

For $\varpi = 1$ and $\theta = 0$, $\mathbf{P}$ reduces to the identity, and the crack is embedded in a TI matrix. In that case, it is observed that the local energy release rate is maximum on the minor axis. Upon propagation, the aspect ratio of the crack is therefore expected to *increase* (the crack becomes a circle). This effect was recently observed numerically by Villani et al. (2023).

The left and right columns correspond to two extreme cases: for $\phi = 0$, $\vec{e}_r$ leans towards the *major* axis of the crack, while for $\phi = \pi/2$, it leans towards its *minor* axis. In both cases, it is observed that the maximum of the local energy release rate always occurs at the *same* location: whether the crack tends to circularize of flatten depends only on the value of ϖ: for $\varpi = 0.1$ and $\varpi = 1$, the minor axis of the crack increases, while for $\varpi = 10$, the major axis increases due to very high stiffness along axis $\vec{e}_1$.

These strongly contrasted configurations are out of reach of a direct FE computation (Section 4.1), but the semi-analytical `Echoes` evaluation, overlaid in Fig. 5, again confirms the closed-form distributions at every contrast.

5 Conclusion

The present paper has derived general analytical expressions for the crack opening displacement (COD) tensor, displacement intensity factor (DIF) and stress intensity factor (SIF) vectors for elliptical and ribbon-like cracks embedded in an infinite matrix of arbitrary anisotropy. The framework, based on the integral equation approach of Kunin (1983) and Kanaun and Levin (2009), provides closed-form relationships between these quantities and the material properties of the matrix. It has also been extended to the case of a closed frictionless crack, for which the COD tensor reduces to a simple projection of the open crack COD tensor that removes the normal component.

The method of linear transformation of elastic boundary value problems has then been applied to derive transformation rules for the COD tensor, DIF and SIF, connecting a problem in an arbitrary matrix to a reference problem – isotropic or TI – for which analytical solutions are available. In the specific case of a TraTI matrix, which encompasses a broad range of anisotropies including orthotropic and monoclinic symmetries, the transformation connects the original problem to that of a crack aligned with the isotropy plane of a TI matrix, for which closed-form COD tensors are recalled in the appendices. The resulting analytical procedure, more direct than those of Barthélémy et al. (2021) and Barthélémy et al. (2023), yields fully closed-form DIF and SIF vectors for both elliptical and ribbon-like cracks.

The numerical application to an elliptical crack embedded in a monoclinic TraTI matrix illustrates the sensitivity of the local energy release rate distribution along the crack front to the transformation parameters. In particular, whether the crack tends to circularize or flatten upon propagation is governed by the in-plane anisotropy of the transformation. These results open perspectives for the analytical prediction of crack propagation paths in anisotropic media and for the implementation of homogenization schemes for cracked TraTI materials.

6 Appendices

6.1 On the polar decomposition of a tensor

In the present appendix, it is shown that for any second-order tensor $\mathbf{A}$ or rank 2, there exists a *symmetric*, *diagonal* and *positive*, second-order tensor $\mathbf{S}$ of rank 2 and a rotation tensor $\mathbf{R}$ such that $\mathbf{A} = \mathbf{R} \cdot \mathbf{S}$. This classical result is known as the *polar decomposition* when $\mathbf{A}$ is invertible and extended here to tensors of rank 2.

The kernel of $\mathbf{A}$ is spanned by the unit-vector $\vec{n}$. The tensor $\mathbf{A}^\intercal \cdot \mathbf{A}$ is symmetric and positive: it can therefore be diagonalized in an orthonormal basis. Since $\vec{n}$ belongs to the kernel of $\mathbf{A}^\intercal \cdot \mathbf{A}$, it is an eigenvector of $\mathbf{A}^\intercal \cdot \mathbf{A}$. Then, two other unit eigenvectors, namely $\vec{l}$ and $\vec{m}$, can be found, such that $\vec{n} = \vec{l} \wedge \vec{m}$ and

$$\mathbf{A}^\intercal \cdot \mathbf{A} = a^2\, \vec{l} \otimes \vec{l} + b^2\, \vec{m} \otimes \vec{m}, \tag{97}$$

where a^2 and b^2 are the associated non-null eigenvalues (note that these eigenvalues are positive since $\mathbf{A}^\intercal \cdot \mathbf{A}$ is a positive tensor). With no loss of generality, it can be assumed that $a, b \geqslant 0$. Recalling that $\mathbf{A} \cdot \vec{l} \neq \vec{0}$ and $\mathbf{A} \cdot \vec{m} \neq \vec{0}$ by construction (since $\operatorname{Ker}\mathbf{A} = \operatorname{Span}\vec{n}$), the following unit vectors are then defined

$$\vec{U} = \frac{\mathbf{A} \cdot \vec{l}}{\|\mathbf{A} \cdot \vec{l}\|} \quad \text{and} \quad \vec{V} = \frac{\mathbf{A} \cdot \vec{m}}{\|\mathbf{A} \cdot \vec{m}\|}, \quad (\|\vec{U}\| = \|\vec{V}\| = 1)$$

Note that $\vec{U}$ and $\vec{V}$ are orthogonal vectors, since from (97)

$$\vec{U} \cdot \vec{V} = \frac{(\mathbf{A} \cdot \vec{l})}{\|\mathbf{A} \cdot \vec{l}\|} \cdot \frac{(\mathbf{A} \cdot \vec{m})}{\|\mathbf{A} \cdot \vec{m}\|} = \frac{\vec{l} \cdot (\mathbf{A}^\intercal \cdot \mathbf{A}) \cdot \vec{m}}{\|\mathbf{A} \cdot \vec{l}\|\|\mathbf{A} \cdot \vec{m}\|} = 0$$

and, the three vectors $\vec{U}$, $\vec{V}$ and $\vec{W} = \vec{U} \wedge \vec{V}$, in that order, form a right-handed orthonormal frame. Since $\mathbf{A} \cdot \vec{n} = \vec{0}$, the following expression holds

$$\mathbf{A} = (\mathbf{A} \cdot \vec{l}) \otimes \vec{l} + (\mathbf{A} \cdot \vec{m}) \otimes \vec{m} + (\mathbf{A} \cdot \vec{n}) \otimes \vec{n} = \|\mathbf{A} \cdot \vec{l}\| \vec{U} \otimes \vec{l} + \|\mathbf{A} \cdot \vec{m}\| \vec{V} \otimes \vec{m}$$

Comparison with (97) necessarily delivers

$$a^2 = \|\mathbf{A} \cdot \vec{l}\|^2 \quad \text{and} \quad b^2 = \|\mathbf{A} \cdot \vec{m}\|^2 \quad \text{therefore} \quad a = \|\mathbf{A} \cdot \vec{l}\| \quad \text{and} \quad b = \|\mathbf{A} \cdot \vec{m}\|$$

and it has been shown that $\mathbf{A}$ writes by means of two orthonormal vectors $\vec{U}$ and $\vec{V}$ spanning the image of $\mathbf{A}$ ($\operatorname{Im}\mathbf{A} = \operatorname{Span}(\vec{U}, \vec{V})$) such that

$$\mathbf{A} = a\, \vec{U} \otimes \vec{l} + b\, \vec{V} \otimes \vec{m} \tag{98}$$

The orthogonal to $\operatorname{Im}\mathbf{A}$ is then a line spanned by the unit vector $\vec{W}$ and

$$\mathbf{A} = \mathbf{R} \cdot \mathbf{S} \quad \text{with} \quad \begin{cases} \mathbf{R} = \vec{U} \otimes \vec{l} + \vec{V} \otimes \vec{m} + \vec{W} \otimes \vec{n} \\ \mathbf{S} = a\, \vec{l} \otimes \vec{l} + b\, \vec{m} \otimes \vec{m} \end{cases} \tag{99}$$

where $\mathbf{R}$ is a rotation tensor since it maps the right-handed orthonormal frame $(\vec{l}, \vec{m}, \vec{n})$ onto the right-handed orthonormal frame $(\vec{U}, \vec{V}, \vec{W})$. Note that the Moore-Penrose inverse of $\mathbf{S}$ and $\mathbf{A}$ are simply

$$\mathbf{S}^\dagger = \frac{\vec{l} \otimes \vec{l}}{a} + \frac{\vec{m} \otimes \vec{m}}{b} \quad \text{and} \quad \mathbf{A}^\dagger = \mathbf{S}^\dagger \cdot \mathbf{R}^\intercal = \frac{\vec{l} \otimes \vec{U}}{a} + \frac{\vec{m} \otimes \vec{V}}{b} \tag{100}$$

As explained in Section 2.1, the case of rank-one tensors should be addressed with care since now $\mathbf{A}$ does not contain anymore all required information for geometrical characterization of the crack since $\vec{n}$ and the direction of invariance $\vec{l}$ both belong to its kernel. It is actually necessary to consider that a ribbon is a degenerated ellipse for which $a \to +\infty$ and explicitly provide the information about the direction of $\vec{l}$ or $\vec{n}$ in addition to $\mathbf{A}$.

6.2 Useful results of Fourier transforms

Let ϕ be a tensor function defined on $\mathbb{R}^d$ ($d = 1, 2, 3$). Its Fourier transform and its reciprocal are defined by

$$\hat{\phi}(\vec{\xi}) = \int_{\vec{x}\in\mathbb{R}^d} \mathrm{e}^{-i\,\vec{\xi}\cdot\vec{x}}\ \phi(\vec{x})\,\mathrm{d}\Omega_x \quad ; \quad \phi(\vec{x}) = \frac{1}{(2\pi)^d}\int_{\vec{\xi}\in\mathbb{R}^d} \mathrm{e}^{i\,\vec{\xi}\cdot\vec{x}}\ \hat{\phi}(\vec{\xi})\,\mathrm{d}\Omega_\xi \tag{101}$$

where $\vec{\xi}\cdot\vec{x}$ denotes the usual inner product of $\mathbb{R}^d$.

The Dirac distribution of $\mathbb{R}^d$ is classically defined as an operator acting as ((Gel'fand and Shilov, 1964), (Schwartz, 1966))

$$\int_{\vec{x}\in\mathbb{R}^d} \delta(\vec{x})\phi(\vec{x})\,\mathrm{d}\Omega_x = \phi(\vec{0}_{\mathbb{R}^d}) \tag{102}$$

and satisfies $\delta(\mathbf{P}\cdot\vec{x}) = \delta(\vec{x})/|\det\mathbf{P}|$ for any invertible second-order tensor $\mathbf{P}$ (in particular $\delta(\lambda\vec{x}) = \delta(\vec{x})/|\lambda|^d$ for any $\lambda \neq 0$) as well as

$$\hat{\delta}(\vec{\xi}) = \int_{\vec{x}\in\mathbb{R}^d} \mathrm{e}^{-i\,\vec{\xi}\cdot\vec{x}}\ \delta(\vec{x})\,\mathrm{d}\Omega_x = 1 \quad ; \quad \delta(\vec{x}) = \frac{1}{(2\pi)^d}\int_{\vec{\xi}\in\mathbb{R}^d} \mathrm{e}^{i\,\vec{\xi}\cdot\vec{x}}\ \mathrm{d}\Omega_\xi \tag{103}$$

Note that the last integral of (103) must actually be considered in the sense of distributions. In addition the same notation δ is adopted for all Dirac distributions whatever the dimension d since the information of the space is given by the nature of the variable. The Dirac distribution of $\mathbb{R}^d$ can be seen as a product of Dirac distributions over each component $\delta(\vec{x}) = \delta(x_1)\cdots\delta(x_d)$. Besides, the Heaviside function H[4], which satisfies $\mathrm{H}' = \delta$ in the sense of distributions, can also be expressed by integration of the right term of (103) with $d = 1$ recalling that $\int_{t=0}^{+\infty}\frac{\sin(t)}{t}\mathrm{d}t = \frac{\pi}{2}$

$$\hat{\mathrm{H}}(\xi) = \pi\ \delta(\xi) - \frac{i}{\xi} \quad ; \quad \mathrm{H}(x) = \frac{1}{2\pi}\int_{\vec{x}\in\mathbb{R}} \frac{\mathrm{e}^{i\,\xi\,x}}{i\,\xi}\mathrm{d}\xi + \frac{1}{2} = \frac{1}{2\pi}\int_{\vec{x}\in\mathbb{R}} \frac{\sin(\xi\,x)}{\xi}\mathrm{d}\xi + \frac{1}{2} \tag{104}$$

It is also useful to introduce the notion of dimension reduction of a Fourier transform along a line directed by a unit vector $\vec{n}$ i.e. Span$(\vec{n})$. The Fourier transform of ϕ on $\vec{n}^\perp$ is defined by means of its Fourier transform on all $\mathbb{R}^d$ by

$$\hat{\phi}^\star(\vec{\xi}^\star) = \frac{1}{2\pi}\int_{\xi_n=-\infty}^{+\infty} \hat{\phi}(\vec{\xi}^\star + \xi_n\,\vec{n})\,\mathrm{d}\xi_n \tag{105}$$

The function $\hat{\phi}^\star(\vec{\xi}^\star)$ can indeed be interpreted as the Fourier transform of the restriction of ϕ to $\vec{n}^\perp$. Indeed, invoking the reciprocal Fourier transform in (101) restricted to $\vec{n}^\perp$ and assuming that Fubini theorem applies to decompose the integration over $\mathbb{R}^d$ as an integration over the line Span $\vec{n}$ and over $\vec{n}^\perp$ of dimension $d-1$, it comes that

$$\begin{aligned}\phi(\vec{x}^\star) &= \frac{1}{(2\pi)^d}\int_{\vec{\xi}\in\mathbb{R}^d} \mathrm{e}^{i\,\vec{\xi}^\star\cdot\vec{x}^\star}\ \hat{\phi}(\vec{\xi}^\star + \xi_n\,\vec{n})\,\mathrm{d}\Omega_\xi \\ &= \frac{1}{(2\pi)^{d-1}}\int_{\vec{\xi}^\star\in\vec{n}^\perp} \mathrm{e}^{i\,\vec{\xi}^\star\cdot\vec{x}^\star}\left(\frac{1}{2\pi}\int_{\xi_n=-\infty}^{+\infty}\hat{\phi}(\vec{\xi}^\star + \xi_n\,\vec{n})\,\mathrm{d}\xi_n\right)\mathrm{d}\Omega_{\xi^\star} \\ &= \frac{1}{(2\pi)^{d-1}}\int_{\vec{\xi}^\star\in\vec{n}^\perp} \mathrm{e}^{i\,\vec{\xi}^\star\cdot\vec{x}^\star}\ \hat{\phi}^\star(\vec{\xi}^\star)\,\mathrm{d}\Omega_{\xi^\star}\end{aligned} \tag{106}$$

The function $\hat{\phi}^\star$ has the following properties

[4] $\mathrm{H}(x) = 1$ if $x \geqslant 0$ and $\mathrm{H}(x) = 0$ if $x < 0$

- $\hat{\phi}^\star$ can be seen as a function over all $\mathbb{R}^d$ but it is insensitive to any component along $\vec{n}$ of its variable by simple change of variable of integration $\xi_n \to \xi_n + \lambda$ in (105)

$$\forall \lambda \in \mathbb{R}, \quad \hat{\phi}^\star(\vec{\xi}^\star + \lambda\,\vec{n}) = \hat{\phi}^\star(\vec{\xi}^\star) \tag{107}$$

- if $\hat{\phi}$ is positively homogeneous of degree ω then $\hat{\phi}^\star$ is positively homogeneous of degree $\omega + 1$ which is also proven by a change of variable of integration in (105)

$$\begin{aligned}\forall \lambda \in \mathbb{R} \setminus \{0\}, \quad \hat{\phi}^\star(\lambda\,\vec{\xi}^\star) &= \frac{1}{2\pi}\int_{\xi_n=-\infty}^{+\infty} \hat{\phi}(\lambda\,\vec{\xi}^\star + \xi_n\,\vec{n})\,\mathrm{d}\xi_n \\ &= |\lambda|^\omega \frac{1}{2\pi}\int_{\xi_n=-\infty}^{+\infty} \hat{\phi}\left(\vec{\xi}^\star + \frac{\xi_n}{\lambda}\,\vec{n}\right)\,\mathrm{d}\xi_n \\ &= |\lambda|^{\omega+1} \frac{1}{2\pi}\int_{\xi_n=-\infty}^{+\infty} \hat{\phi}\left(\vec{\xi}^\star + \xi_n\,\vec{n}\right)\,\mathrm{d}\xi_n \\ &= |\lambda|^{\omega+1}\,\hat{\phi}^\star(\vec{\xi}^\star)\end{aligned} \tag{108}$$

  In particular, if $\hat{\phi}$ is insensitive to the norm of its variable ($\omega = 0$) then $\hat{\phi}^\star$ is positively homogeneous of degree 1.

Besides the following results are recalled since they are needed in the paper

$$\forall \vec{\xi} \in \mathbb{R}^2, \quad \int_{\vec{x}\in\mathbb{R}^2, \|\vec{x}\|\leqslant 1} \mathrm{e}^{-i\,\vec{\xi}\cdot\vec{x}}\,\sqrt{1-\|\vec{x}\|^2}\,\mathrm{d}S_{\vec{x}} = 2\pi\,\frac{j_1(\|\vec{\xi}\|)}{\|\vec{\xi}\|} \quad \text{with} \quad j_1(\xi) = \frac{\sin\xi - \xi\,\cos\xi}{\xi^2} \tag{109}$$

$$\forall x \in \mathbb{R}, \quad \frac{1}{2\pi}\int_{\xi=-\infty}^{+\infty} \mathrm{e}^{i\,\xi\,x}\,\xi\,j_1(\xi)\,\mathrm{d}\xi = \frac{1}{2}\Big(\mathrm{H}(x+1) - \mathrm{H}(x-1) - \delta(x+1) - \delta(x-1)\Big) \tag{110}$$

where j_1 is the spherical Bessel function of the first kind and first order (Abramowitz and Stegun, 1972).

The proof of (109) relies on an integration in cartesian coordinates $\vec{x} \equiv (x, y)$ such that $\vec{\xi}$ is oriented along the direction of the first coordinate x. The notation $\xi = \|\vec{\xi}\|$ is introduced for convenience. By symmetry it comes that

$$\int_{\vec{x}\in\mathbb{R}^2, \|\vec{x}\|\leqslant 1} \mathrm{e}^{-i\,\vec{\xi}\cdot\vec{x}}\,\sqrt{1-\|\vec{x}\|^2}\,\mathrm{d}S_{\vec{x}} = 4\int_{x=0}^{1}\int_{y=0}^{\sqrt{1-x^2}} \cos(\xi x)\sqrt{1-x^2-y^2}\,\mathrm{d}y\,\mathrm{d}x \tag{111}$$

Adopting the change of variable $y = s\sqrt{1-x^2}$ and noting that $\int_{s=0}^{1}\sqrt{1-s^2}\mathrm{d}s = \frac{\pi}{4}$, (111) becomes

$$\begin{aligned}\int_{\vec{x}\in\mathbb{R}^2, \|\vec{x}\|\leqslant 1} \mathrm{e}^{-i\,\vec{\xi}\cdot\vec{x}}\,\sqrt{1-\|\vec{x}\|^2}\,\mathrm{d}S_{\vec{x}} &= 4\int_{x=0}^{1}\int_{s=0}^{1} \cos(\xi x)(1-x^2)\sqrt{1-s^2}\,\mathrm{d}s\,\mathrm{d}x \\ &= \pi\int_{x=0}^{1} \cos(\xi x)(1-x^2)\,\mathrm{d}x\end{aligned} \tag{112}$$

The end of the proof is simply obtained by integrating twice by parts.

The proof of (110) simply consists in identifying inverse Fourier transforms of Dirac (103) and Heaviside (104) in

$$\begin{aligned}\frac{1}{2\pi}\int_{\xi=-\infty}^{+\infty} \mathrm{e}^{i\,\xi\,x}\,\xi\,j_1(\xi)\,\mathrm{d}\xi &= \frac{1}{2\pi}\int_{\xi=-\infty}^{+\infty} \mathrm{e}^{i\,\xi\,x}\,\frac{\sin\xi - \xi\,\cos\xi}{\xi}\,\mathrm{d}\xi \\ &= \frac{1}{2\pi}\int_{\xi=-\infty}^{+\infty} \frac{1}{2}\left(\frac{\mathrm{e}^{i\,\xi\,(x+1)} - \mathrm{e}^{i\,\xi\,(x-1)}}{i\,\xi} - \mathrm{e}^{i\,\xi\,(x+1)} - \mathrm{e}^{i\,\xi\,(x-1)}\right)\mathrm{d}\xi\end{aligned} \tag{113}$$

6.3 COD tensors

The present Appendix gathers analytical expressions of the COD tensor of an elliptical crack in an isotropic matrix or a transversely isotropic matrix of isotropy plane aligned with the crack. The following expressions are rewritten from those proposed in the literature by using the quantities $\mathscr{C}_\eta$ and $\mathscr{S}_\eta$ introduced in 116 in order to make the limits for circular or ribbon shapes more straightforward. Note that the COD tensors reported in this section are consistent with the definition (14) based on the normalization of the average COD by the second radius b for easier correspondence between elliptical and ribbon-like cracks.

6.3.1 COD tensors in an isotropic matrix

For details about the derivations of formulas, see Kachanov (1992), Sevostianov and Kachanov (2002), Kachanov and Sevostianov (2018) or Barthélémy et al. (2021) (it is worth recalling however that the length normalization of the COD tensor has been changed between this last reference and the present paper). Young's modulus and Poisson's ratio of the matrix are respectively denoted by E and ν.

- Elliptical crack

$$\mathbf{B}^{\mathscr{E},\mathrm{ISO}}(\eta) = \frac{8\,(1-\nu^2)}{3\,E}\left(\frac{\vec{l}\otimes\vec{l}}{(1-\nu)\,\mathscr{C}_\eta + \eta^2\,\mathscr{S}_\eta} + \frac{\vec{m}\otimes\vec{m}}{(1-\nu)\,\eta^2\,\mathscr{S}_\eta + \mathscr{C}_\eta} + \frac{\vec{n}\otimes\vec{n}}{\mathscr{E}_\eta}\right) \tag{114}$$

  where $\mathscr{C}_\eta$ and $\mathscr{S}_\eta$ are built by means of the complete elliptical integrals of first $\mathscr{K}_\eta$ and second $\mathscr{E}_\eta$ kind (Abramowitz and Stegun, 1972)

$$\mathscr{K}_\eta = \int_{\phi=0}^{\frac{\pi}{2}} \frac{\mathrm{d}\phi}{\sqrt{\cos^2\phi + \eta^2\,\sin^2\phi}}\ ; \quad \mathscr{E}_\eta = \int_{\phi=0}^{\frac{\pi}{2}} \sqrt{\cos^2\phi + \eta^2\,\sin^2\phi}\,\mathrm{d}\phi \tag{115}$$

  as

$$\mathscr{C}_\eta = \frac{\mathscr{E}_\eta - \eta^2\,\mathscr{K}_\eta}{1-\eta^2} = \int_{\phi=0}^{\frac{\pi}{2}} \frac{\cos^2\phi\,\mathrm{d}\phi}{\sqrt{\cos^2\phi + \eta^2\,\sin^2\phi}}\ ; \quad \mathscr{S}_\eta = \frac{\mathscr{K}_\eta - \mathscr{E}_\eta}{1-\eta^2} = \int_{\phi=0}^{\frac{\pi}{2}} \frac{\sin^2\phi\,\mathrm{d}\phi}{\sqrt{\cos^2\phi + \eta^2\,\sin^2\phi}} \tag{116}$$

  Note the useful limits for circular and ribbon cases

$$\begin{aligned}
&\lim_{\eta\to1}\mathscr{K}_\eta = \lim_{\eta\to1}\mathscr{E}_\eta = \frac{\pi}{2}\ ; \quad \lim_{\eta\to1}\mathscr{C}_\eta = \lim_{\eta\to1}\mathscr{S}_\eta = \frac{\pi}{4} && (a)\\
&\lim_{\eta\to0}\mathscr{E}_\eta = 1\ ; \quad \lim_{\eta\to0}\mathscr{C}_\eta = 1\ ; \quad \lim_{\eta\to0}\eta^2\,\mathscr{S}_\eta = 0 && (b)
\end{aligned} \tag{117}$$

- Circular crack

$$\mathbf{B}^{\mathscr{E},\mathrm{ISO}}(\eta=1) = \frac{16\,(1-\nu^2)}{3\pi\,E}\left(\frac{2\,(\vec{l}\otimes\vec{l}+\vec{m}\otimes\vec{m})}{2-\nu} + \vec{n}\otimes\vec{n}\right) \tag{118}$$

- Ribbon-like crack

$$\mathbf{B}^{\mathscr{R},\mathrm{ISO}} = \frac{3\pi}{8}\lim_{\eta\to0}\mathbf{B}^{\mathscr{E},\mathrm{ISO}}(\eta) = \frac{\pi\,(1-\nu^2)}{E}\left(\frac{\vec{l}\otimes\vec{l}}{1-\nu} + \vec{m}\otimes\vec{m} + \vec{n}\otimes\vec{n}\right) \tag{119}$$

6.3.2 COD tensors in a transversely isotropic matrix of isotropy plane aligned with the crack

In this paragraph, the matrix obeys a TI behavior of axis $\vec{e}_3$ (for convenience of writing the components C_{ijkl} in the following expressions) and the unit normal to the crack is assumed to be oriented along the same axis $\vec{n} = \vec{e}_3$, which means that $\vec{l}$ and $\vec{m}$ form a rotated orthonormal basis of the plane spanned by $\vec{e}_1$ and $\vec{e}_2$. The elliptical or ribbon-like shape of the crack and the orientation of $\boldsymbol{C}$ are then such that the COD tensor is expected of the form

$$\mathbf{B} = B_{ll}\, \vec{l} \otimes \vec{l} + B_{mm}\, \vec{m} \otimes \vec{m} + B_{nn}\, \vec{n} \otimes \vec{n} \tag{120}$$

- Elliptical crack

  The following expressions result from the derivation proposed in Barthélémy et al. (2023) but other expressions (consistent but written under other forms) can be found in Hoenig (1978) and Kanaun and Levin (2009).

$$\begin{aligned}
B_{ll}^{\mathscr{E},\mathrm{TI}}(\eta) &= \frac{1}{3\,(R_{2323}\,\mathscr{C}_\eta + R_{3131}\,\eta^2\,\mathscr{S}_\eta)\,C_{2323}^2} && (a)\\
B_{mm}^{\mathscr{E},\mathrm{TI}}(\eta) &= \frac{1}{3\,(R_{2323}\,\eta^2\,\mathscr{S}_\eta + R_{3131}\,\mathscr{C}_\eta)\,C_{2323}^2} && (b)\\
B_{nn}^{\mathscr{E},\mathrm{TI}}(\eta) &= \frac{4}{3\left(R_{1111}\,C_{1133}^2 + 2\,R_{1133}\,C_{1133}\,C_{3333} + R_{3333}\,C_{3333}^2\right)\mathscr{E}_\eta} && (c)
\end{aligned} \tag{121}$$

  with

$$\begin{aligned}
R_{1111} &= -\frac{1}{\sigma_\gamma}\left(\frac{1}{C_{2323}} + \frac{1}{\sqrt{C_{1111}\,C_{3333}}}\right) && (a)\\
R_{1133} &= \frac{1}{\sigma_\gamma}\,\frac{C_{1133} + C_{2323}}{C_{2323}\,C_{3333}} && (b)\\
R_{3333} &= \frac{1}{\sigma_\gamma}\left(\sqrt{\frac{C_{1111}}{C_{3333}}} - \frac{C_{1133}\,(C_{1133} + 2\,C_{2323})}{C_{2323}\,C_{3333}}\right)\frac{1}{C_{3333}} && (c)\\
R_{2323} &= \frac{1}{4\sqrt{2}}\sqrt{\frac{C_{1111} - C_{1122}}{C_{2323}^3}} && (d)\\
R_{3131} &= \frac{1}{4\,\sigma_\gamma}\,\frac{C_{1111}\,C_{3333} - C_{1133}^2}{C_{2323}^2\,C_{3333}} && (e)
\end{aligned} \tag{122}$$

  and

$$\sigma_\gamma = \sqrt{\frac{C_{1111}\,C_{3333} - C_{1133}^2 - 2\,C_{1133}\,C_{2323}}{C_{2323}\,C_{3333}} + 2\sqrt{\frac{C_{1111}}{C_{3333}}}} \tag{123}$$

  Note that the components R_{ijkl}, finding their origin in the solution derived in Barthélémy et al. (2023), depend only on the matrix moduli but do not satisfy TI symmetry, in particular $R_{2323} \neq R_{3131}$.

- Circular crack

$$
\begin{aligned}
B_{ll}^{\mathscr{E},\mathrm{TI}}(\eta=1) &= \frac{4}{3\pi\,(R_{2323}+R_{3131})\,C_{2323}^2} && (a)\\
B_{mm}^{\mathscr{E},\mathrm{TI}}(\eta=1) &= \frac{4}{3\pi\,(R_{2323}+R_{3131})\,C_{2323}^2} && (b)\\
B_{nn}^{\mathscr{E},\mathrm{TI}}(\eta=1) &= \frac{8}{3\pi\left(R_{1111}\,C_{1133}^2+2\,R_{1133}\,C_{1133}\,C_{3333}+R_{3333}\,C_{3333}^2\right)} && (c)
\end{aligned}
\tag{124}
$$

- Ribbon-like crack

$$
\begin{aligned}
B_{ll}^{\mathscr{R},\mathrm{TI}} &= \frac{\pi}{8\,R_{2323}\,C_{2323}^2} && (a)\\
B_{mm}^{\mathscr{R},\mathrm{TI}} &= \frac{\pi}{8\,R_{3131}\,C_{2323}^2} && (b)\\
B_{nn}^{\mathscr{R},\mathrm{TI}} &= \frac{\pi}{2\left(R_{1111}\,C_{1133}^2+2\,R_{1133}\,C_{1133}\,C_{3333}+R_{3333}\,C_{3333}^2\right)} && (c)
\end{aligned}
\tag{125}
$$

Alternatively the TI matrix can be written in terms of engineering parameters defined on components of the compliance tensor $\boldsymbol{S}=\boldsymbol{C}^{-1}$. By consistency with Hoenig (1978), these parameters are chosen as E, ν_1, ν_2, H and Γ such that

$$
E=\frac{1}{S_{1111}}\ ;\quad \nu_1=-S_{1122}\,E\ ;\quad \nu_2=-S_{1133}\,E\ ;\quad H=\frac{1}{S_{3333}\,E}\ ;\quad \Gamma=\frac{1}{S_{2323}}\,\frac{1+\nu_1}{2\,E}
\tag{126}
$$

with a Kelvin-Mandel representation of the form

$$
\mathrm{Mat}(\boldsymbol{S})=\begin{pmatrix}
\frac{1}{E} & \frac{-\nu_1}{E} & \frac{-\nu_2}{E} & 0 & 0 & 0\\
\frac{-\nu_1}{E} & \frac{1}{E} & \frac{-\nu_2}{E} & 0 & 0 & 0\\
\frac{-\nu_2}{E} & \frac{-\nu_2}{E} & \frac{1}{EH} & 0 & 0 & 0\\
0 & 0 & 0 & \frac{1+\nu_1}{E\Gamma} & 0 & 0\\
0 & 0 & 0 & 0 & \frac{1+\nu_1}{E\Gamma} & 0\\
0 & 0 & 0 & 0 & 0 & \frac{1+\nu_1}{E}
\end{pmatrix}
\tag{127}
$$

Setting $A=1-\nu_1-2\,H\,\nu_2^2$, it follows that the TI components C_{ijkl} write

$$
\begin{aligned}
C_{1111} &= \frac{E\,(1-H\,\nu_2^2)}{A\,(1+\nu_1)}\ ;\quad C_{1122}=\frac{E\,(\nu_1+H\,\nu_2^2)}{A\,(1+\nu_1)}\\
C_{1133} &= \frac{E\,H\,\nu_2}{A}\ ;\quad C_{3333}=\frac{E\,H\,(1-\nu_1)}{A}\ ;\quad C_{2323}=\frac{E\,\Gamma}{2\,(1+\nu_1)}
\end{aligned}
\tag{128}
$$

σ_γ (123) becomes

$$
\sigma_\gamma=\sqrt{2}\sqrt{\frac{1-\Gamma\,\nu_2}{\Gamma\,(1-\nu_1)}+\sqrt{\frac{1-H\,\nu_2^2}{H\,(1-\nu_1^2)}}}
\tag{129}
$$

and the components R_{ijkl} (122) write

$$
\begin{aligned}
R_{1111} &= -\frac{A}{E\,\sigma_\gamma\,H\,(1-\nu_1)}\left(\sqrt{\frac{H\,(1-\nu_1^2)}{1-H\,\nu_2^2}}+\frac{2\,H\,(1-\nu_1^2)}{A\,\Gamma}\right) && (a)\\
R_{1133} &= \frac{A}{E\,\sigma_\gamma\,H\,(1-\nu_1)}\left(1+\frac{2\,H\,\nu_2\,(1+\nu_1)}{A\,\Gamma}\right) && (b)\\
R_{3333} &= \frac{A}{E\,\sigma_\gamma\,H\,(1-\nu_1)}\left(\sqrt{\frac{1-H\,\nu_2^2}{H\,(1-\nu_1^2)}}-\frac{2\,\nu_2}{1-\nu_1}\left(1+\frac{H\,\nu_2\,(1+\nu_1)}{A\,\Gamma}\right)\right) && (c)\\
R_{2323} &= \frac{1+\nu_1}{2\,E\,\Gamma^{\frac{3}{2}}} && (d)\\
R_{3131} &= \frac{1+\nu_1}{E\,\sigma_\gamma\,\Gamma^2\,(1-\nu_1)} && (e)
\end{aligned}
\tag{130}
$$

Inserting (128), (129) and (130) in (121), (124) and (125), the COD tensors can now be rewritten in terms of engineering parameters.

- Elliptical crack

$$
\mathbf{B}^{\mathscr{E},\mathrm{TI}}(\eta) = \frac{4\,\sigma_\gamma\,(1-\nu_1^2)}{3\,E}\left(\frac{\vec{l}\otimes\vec{l}}{\frac{\sigma_\gamma}{2}\sqrt{\Gamma}\,(1-\nu_1)\,\mathscr{C}_\eta+\eta^2\,\mathscr{S}_\eta}+\frac{\vec{m}\otimes\vec{m}}{\frac{\sigma_\gamma}{2}\sqrt{\Gamma}\,(1-\nu_1)\,\eta^2\,\mathscr{S}_\eta+\mathscr{C}_\eta}+\sqrt{\frac{1-H\,\nu_2^2}{H\,(1-\nu_1^2)}}\,\frac{\vec{n}\otimes\vec{n}}{\mathscr{E}_\eta}\right)
\tag{131}
$$

- Circular crack

$$
\mathbf{B}^{\mathscr{E},\mathrm{TI}}(\eta=1) = \frac{8\,\sigma_\gamma\,(1-\nu_1^2)}{3\pi\,E}\left(\frac{2\,\vec{l}\otimes\vec{l}}{\frac{\sigma_\gamma}{2}\sqrt{\Gamma}\,(1-\nu_1)+1}+\frac{2\,\vec{m}\otimes\vec{m}}{\frac{\sigma_\gamma}{2}\sqrt{\Gamma}\,(1-\nu_1)+1}+\sqrt{\frac{1-H\,\nu_2^2}{H\,(1-\nu_1^2)}}\,\vec{n}\otimes\vec{n}\right)
\tag{132}
$$

- Ribbon-like crack

$$
\mathbf{B}^{\mathscr{R},\mathrm{TI}} = \frac{3\pi}{8}\lim_{\eta\to 0}\mathbf{B}^{\mathscr{E},\mathrm{TI}}(\eta) = \frac{\pi\,(1-\nu_1^2)}{E}\left(\frac{\vec{l}\otimes\vec{l}}{\sqrt{\Gamma}\,(1-\nu_1)}+\frac{\sigma_\gamma\,\vec{m}\otimes\vec{m}}{2}+\sqrt{\frac{1-H\,\nu_2^2}{H\,(1-\nu_1^2)}}\,\frac{\sigma_\gamma\,\vec{n}\otimes\vec{n}}{2}\right)
\tag{133}
$$

Note that the formulas for the isotropic case can be retrieved from those of the TI one by setting $\nu_1 = \nu_2 = \nu$, $H = \Gamma = 1$, $\sigma_\gamma = 2$ and $A = (1+\nu)(1-2\nu)$.

6.4 Alternative expressions of the SIF and DIF vectors

Adopting the polar angle θ_y of $\vec{y}_0^\star$ or alternatively the polar angle θ_x of $\vec{x}_0^\star$ (see Fig. 3), the following parametrizations are obtained

$$
\vec{y}_0^\star = \cos\theta_y\,\vec{l}+\sin\theta_y\,\vec{m} \quad ; \quad \vec{x}_0^\star = a\cos\theta_y\,\vec{l}+b\sin\theta_y\,\vec{m} = \frac{\cos\theta_x\,\vec{l}+\sin\theta_x\,\vec{m}}{\sqrt{\frac{\cos^2\theta_x}{a^2}+\frac{\sin^2\theta_x}{b^2}}}
\tag{134}
$$

The normal $\vec{\nu}$ at $\vec{x}_0^\star$ directed from the crack to the matrix and the tangential unit vector $\vec{\tau}$ such that $(\vec{\nu}, \vec{\tau}, \vec{n})$ form a right-handed orthonormal basis (see Fig. 3) are given by

$$\vec{\nu} = \frac{\mathbf{S}^\dagger \cdot \vec{y}_0^\star}{\|\mathbf{S}^\dagger \cdot \vec{y}_0^\star\|} = \frac{\frac{\cos\theta_y}{a}\,\vec{l} + \frac{\sin\theta_y}{b}\,\vec{m}}{\sqrt{\frac{\cos^2\theta_y}{a^2} + \frac{\sin^2\theta_y}{b^2}}} = \cos\theta_\nu\,\vec{l} + \sin\theta_\nu\,\vec{m} \qquad (a)$$

$$\vec{\tau} = \frac{-\frac{\sin\theta_y}{b}\,\vec{l} + \frac{\cos\theta_y}{a}\,\vec{m}}{\sqrt{\frac{\cos^2\theta_y}{a^2} + \frac{\sin^2\theta_y}{b^2}}} = -\sin\theta_\nu\,\vec{l} + \cos\theta_\nu\,\vec{m} \qquad (b) \tag{135}$$

Several equivalent expressions of the dimensionless quantity $b\,\|\mathbf{S}^\dagger \cdot \vec{y}_0^\star\|$ can be established

$$b\,\|\mathbf{S}^\dagger \cdot \vec{y}_0^\star\| = \sqrt{\eta^2\,\cos^2\theta_y + \sin^2\theta_y} = \sqrt{\frac{\eta^4\,\cos^2\theta_x + \sin^2\theta_x}{\eta^2\,\cos^2\theta_x + \sin^2\theta_x}} = \frac{\eta}{\sqrt{\cos^2\theta_\nu + \eta^2\,\sin^2\theta_\nu}} \tag{136}$$

Upon combination of equations (43), (47) and (136), the following equivalent expressions of $\vec{N}$ and $\vec{K}$ are found

$$\vec{N} = \frac{1}{4}\sqrt{\frac{\pi}{b}}\,\sqrt[4]{\eta^2\,\cos^2\theta_y + \sin^2\theta_y}\,\vec{\beta} = \frac{1}{4}\sqrt{\frac{\pi}{b}}\,\sqrt[4]{\frac{\eta^4\,\cos^2\theta_x + \sin^2\theta_x}{\eta^2\,\cos^2\theta_x + \sin^2\theta_x}}\,\vec{\beta}$$

and

$$\vec{K} = \sqrt{\frac{\pi}{b}}\,\sqrt[4]{\eta^2\,\cos^2\theta_y + \sin^2\theta_y}\,\hat{\mathbf{Q}}^\star_{nn}(\vec{\nu}) \cdot \vec{\beta} = \sqrt{\frac{\pi}{b}}\,\sqrt[4]{\frac{\eta^4\,\cos^2\theta_x + \sin^2\theta_x}{\eta^2\,\cos^2\theta_x + \sin^2\theta_x}}\,\hat{\mathbf{Q}}^\star_{nn}(\vec{\nu}) \cdot \vec{\beta}$$

6.5 Supplementary results for the transformation of a crack

6.5.1 Identification of the transformed ellipse

This appendix gathers the detailed derivations of the geometrical features of the transformed crack for which results are reported in Section 3.1. As obviously seen from (71), $\mathbf{A}$ and $\mathbf{A}^\sharp$ share the same image so that the parametrization of $\mathscr{I}^\sharp$ is consistently deduced from (7) by

$$\mathscr{I}^\sharp = \left\{ \vec{x}^\sharp = \mathbf{P}^{-1} \cdot \mathbf{A}^\intercal \cdot \vec{y} = \mathbf{A}^{\sharp\intercal} \cdot \vec{y}, \quad \vec{y} \in \left(\operatorname{Ker}\mathbf{A}^\intercal\right)^\perp = \operatorname{Im}\mathbf{A} = \operatorname{Im}\mathbf{A}^\sharp = \vec{W}^\perp, \quad \|\vec{y}\| \leqslant 1 \right\} \tag{137}$$

As $\mathbf{P}$ is invertible, the ranks of $\mathbf{A}$ and $\mathbf{A}^\sharp$ are equal so that these tensors define cracks of similar (both either elliptical or ribbon-like) nature. Moreover, as seen in Section 2.1, the normal of an elliptical crack (rank-two $\mathbf{A}$) is defined as the unit vector (up to a multiplication by -1) spanning the kernel of the characteristic tensor ($\operatorname{Ker}\mathbf{A} = \operatorname{Span}(\vec{n})$). It follows then from (71) that the normal $\vec{n}^\sharp$ associated to $\mathbf{A}^\sharp$, i.e. the direction of $\operatorname{Ker}\mathbf{A}^\sharp$, is necessarily oriented along $\mathbf{P}^\intercal \cdot \vec{n}$, which yields (72). Note that, since $\mathbf{P}^\intercal \cdot (\mathbf{A}^\intercal \cdot \mathbf{A})^\dagger \cdot \mathbf{P} \neq (\mathbf{P}^{-1} \cdot \mathbf{A}^\intercal \cdot \mathbf{A} \cdot \mathbf{P}^{-\intercal})^\dagger$ in general for arbitrary non-singular $\mathbf{P}$ and rank-two $\mathbf{A}$, it would have been wrong to abruptly introduce (68) in the quadratic form of (1) to deduce $\mathbf{A}^\sharp$. Indeed these quadratic forms coincide only if they apply on vectors $\vec{x}^\sharp$ such that $\vec{x}^\sharp \cdot \vec{n}^\sharp = 0$. That is why a reasoning based on the parametrization (7) may be clearer. However, the quadratic definition (1) of the crack in problem $\mathscr{P}$ can eventually be transposed here to the crack of problem $\mathscr{P}^\sharp$

$$\vec{x}^\sharp \in \mathscr{I}^\sharp \quad \Longleftrightarrow \quad \vec{x}^\sharp \cdot \vec{n}^\sharp = 0 \quad \text{and} \quad \vec{x}^\sharp \cdot (\mathbf{A}^{\sharp\intercal} \cdot \mathbf{A}^\sharp)^\dagger \cdot \vec{x}^\sharp \leqslant 1 \tag{138}$$

The features of the transformed crack in terms of radii and orientation are derived from the diagonalization of $\mathbf{A}^{\sharp\intercal} \cdot \mathbf{A}^{\sharp}$ appearing in this quadratic form. Introducing the conjugate semi-diameters $\vec{g} = \mathbf{P}^{-1} \cdot \vec{l}$ and $\vec{h} = \mathbf{P}^{-1} \cdot \vec{m}$ defined in (75), it must be noted that the eigenvectors of $\mathbf{A}^{\intercal} \cdot \mathbf{A}$ are in general not transported to those of $\mathbf{A}^{\sharp\intercal} \cdot \mathbf{A}^{\sharp}$ since $\vec{g}$ is in general not orthogonal to $\vec{h}$. The identification of the ellipse defined by $\mathbf{A}^{\sharp}$, namely the axes $\vec{l}^{\sharp}$ and $\vec{m}^{\sharp}$, and the radii $a^{\sharp}$ and $b^{\sharp}$ ($a^{\sharp} \geqslant b^{\sharp}$), requires then to perform the diagonalization

$$\mathbf{A}^{\sharp\intercal} \cdot \mathbf{A}^{\sharp} = a^2\, \vec{g} \otimes \vec{g} + b^2\, \vec{h} \otimes \vec{h} = a^{\sharp 2}\, \vec{l}^{\sharp} \otimes \vec{l}^{\sharp} + b^{\sharp 2}\, \vec{m}^{\sharp} \otimes \vec{m}^{\sharp} \tag{139}$$

After the previously identified expression of $\vec{n}^{\sharp}$ in (72), closed-form expressions of $a^{\sharp}$, $b^{\sharp}$, $\vec{l}^{\sharp}$ and $\vec{m}^{\sharp}$ can fully be derived here.

In order to specify the relationships between initial and transformed radii, a first equation is obtained by taking the trace of (139)

$$a^{\sharp 2} + b^{\sharp 2} = a^2\, \|\vec{g}\|^2 + b^2\, \|\vec{h}\|^2 \tag{140}$$

Another equation is obtained from the formula of surface vector transformation

$$a^{\sharp}\, b^{\sharp}\, \vec{n}^{\sharp} = \pm a\, b\, \vec{g} \wedge \vec{h} = a\, b\, \frac{\mathbf{P}^{\intercal} \cdot \vec{n}}{|\det \mathbf{P}|} \tag{141}$$

since the cofactor (Nanson) identity gives

$$\vec{g} \wedge \vec{h} = (\mathbf{P}^{-1} \cdot \vec{l}) \wedge (\mathbf{P}^{-1} \cdot \vec{m}) = \frac{\mathbf{P}^{\intercal} \cdot (\vec{l} \wedge \vec{m})}{\det \mathbf{P}} = \frac{\mathbf{P}^{\intercal} \cdot \vec{n}}{\det \mathbf{P}} \tag{142}$$

Note that the $\pm$ sign and the absolute value sign affecting $\det \mathbf{P}$ in (141) just aim at choosing the orientation between the normal and its opposite without any consequence on the results of the paper. It is interesting to note that (141) is then consistent with (72). Eventually the second relationship involving $a^{\sharp}$ and $b^{\sharp}$ is given by taking the norm of (141)

$$a^{\sharp}\, b^{\sharp} = a\, b\, \|\vec{g} \wedge \vec{h}\| = a\, b\, \frac{\|\mathbf{P}^{\intercal} \cdot \vec{n}\|}{|\det \mathbf{P}|} \tag{143}$$

Recalling that $b^{\sharp} \leqslant a^{\sharp}$ by convention, (140) and (143) can be exploited in the expressions

$$a^{\sharp} = \frac{\sqrt{a^{\sharp 2} + b^{\sharp 2} + 2\, a^{\sharp}\, b^{\sharp}} + \sqrt{a^{\sharp 2} + b^{\sharp 2} - 2\, a^{\sharp}\, b^{\sharp}}}{2} \quad \text{and} \quad b^{\sharp} = \frac{\sqrt{a^{\sharp 2} + b^{\sharp 2} + 2\, a^{\sharp}\, b^{\sharp}} - \sqrt{a^{\sharp 2} + b^{\sharp 2} - 2\, a^{\sharp}\, b^{\sharp}}}{2}$$

which deliver the closed-form radii $a^{\sharp}$ and $b^{\sharp}$ reported in Section 3.1 in (73) and (74).

Owing to the symmetrical roles played by $\mathscr{P}$ and $\mathscr{P}^{\sharp}$, equations (73) and (74) can readily be inverted if necessary. Introducing the conjugate semi-diameters of the inverse mapping $\vec{g}^{\sharp} = \mathbf{P} \cdot \vec{l}^{\sharp}$ and $\vec{h}^{\sharp} = \mathbf{P} \cdot \vec{m}^{\sharp}$ (symmetric to (75) under $\mathbf{P} \leftrightarrow \mathbf{P}^{-1}$ and $\vec{l} \leftrightarrow \vec{l}^{\sharp}$), the initial radii read

$$a = \frac{\sqrt{a^{\sharp 2}\, \|\vec{g}^{\sharp}\|^2 + b^{\sharp 2}\, \|\vec{h}^{\sharp}\|^2 + 2\, a^{\sharp}\, b^{\sharp}\, \|\vec{g}^{\sharp} \wedge \vec{h}^{\sharp}\|} + \sqrt{a^{\sharp 2}\, \|\vec{g}^{\sharp}\|^2 + b^{\sharp 2}\, \|\vec{h}^{\sharp}\|^2 - 2\, a^{\sharp}\, b^{\sharp}\, \|\vec{g}^{\sharp} \wedge \vec{h}^{\sharp}\|}}{2} \tag{144}$$

and

$$b = \frac{\sqrt{a^{\sharp 2}\, \|\vec{g}^{\sharp}\|^2 + b^{\sharp 2}\, \|\vec{h}^{\sharp}\|^2 + 2\, a^{\sharp}\, b^{\sharp}\, \|\vec{g}^{\sharp} \wedge \vec{h}^{\sharp}\|} - \sqrt{a^{\sharp 2}\, \|\vec{g}^{\sharp}\|^2 + b^{\sharp 2}\, \|\vec{h}^{\sharp}\|^2 - 2\, a^{\sharp}\, b^{\sharp}\, \|\vec{g}^{\sharp} \wedge \vec{h}^{\sharp}\|}}{2} \tag{145}$$

where the inverse area-stretch factor is $\|\vec{g}^{\sharp} \wedge \vec{h}^{\sharp}\| = |\det \mathbf{P}|\, \|\mathbf{P}^{-\intercal} \cdot \vec{n}^{\sharp}\|$, again by the cofactor identity.

It is further found that

$$\frac{b^\sharp}{b} = \frac{\sqrt{\|\vec{g}\|^2 + \eta^2\,\|\vec{h}\|^2 + 2\,\eta\,\|\vec{g}\wedge\vec{h}\|} - \sqrt{\|\vec{g}\|^2 + \eta^2\,\|\vec{h}\|^2 - 2\,\eta\,\|\vec{g}\wedge\vec{h}\|}}{2\,\eta} \tag{146}$$

and

$$\eta^\sharp = \frac{b^\sharp}{a^\sharp} = \frac{\|\vec{g}\|^2 + \eta^2\,\|\vec{h}\|^2}{2\,\eta\,\|\vec{g}\wedge\vec{h}\|} - \sqrt{\left(\frac{\|\vec{g}\|^2 + \eta^2\,\|\vec{h}\|^2}{2\,\eta\,\|\vec{g}\wedge\vec{h}\|}\right)^2 - 1} \tag{147}$$

obtained by normalizing $b^\sharp$ by b and introducing the initial aspect ratio $\eta = b/a$.

There remains to identify the axes $\vec{l}^\sharp$ and $\vec{m}^\sharp$, which are the eigenvectors of the rank-two symmetric tensor $\mathbf{A}^{\sharp\intercal}\cdot\mathbf{A}^\sharp$, the kernel of which is spanned by $\vec{n}^\sharp$. The diagonalization (139) is therefore a two-dimensional symmetric eigenvalue problem in the plane $\vec{n}^{\sharp\perp}$, which admits a closed-form solution. Introducing the in-plane identity $\mathbf{1} - \vec{n}^\sharp\otimes\vec{n}^\sharp = \vec{l}^\sharp\otimes\vec{l}^\sharp + \vec{m}^\sharp\otimes\vec{m}^\sharp$, the spectral projector onto the major axis reads (provided $a^\sharp \neq b^\sharp$)

$$\vec{l}^\sharp\otimes\vec{l}^\sharp = \frac{\mathbf{A}^{\sharp\intercal}\cdot\mathbf{A}^\sharp - b^{\sharp 2}\,(\mathbf{1} - \vec{n}^\sharp\otimes\vec{n}^\sharp)}{a^{\sharp 2} - b^{\sharp 2}} \tag{148}$$

The vectors $\vec{g}$ and $\vec{h}$ both lie in the plane $\vec{n}^{\sharp\perp}$, since $(\mathbf{P}^\intercal\cdot\vec{n})\cdot\vec{g} = \vec{n}\cdot\vec{l} = 0$ and likewise for $\vec{h}$. Recalling from (139) that $\mathbf{A}^{\sharp\intercal}\cdot\mathbf{A}^\sharp = a^2\,\vec{g}\otimes\vec{g} + b^2\,\vec{h}\otimes\vec{h}$, applying the projector (148) to $\vec{g}$ (resp. $\vec{h}$) delivers a vector parallel to $\vec{l}^\sharp$, namely the candidate $\vec{w}_{\vec{l}}$ (resp. $\vec{w}_{\vec{m}}$) given in (77). As $\vec{g}$ and $\vec{h}$ are linearly independent (since $\mathbf{P}$ is invertible) and span $\vec{n}^{\sharp\perp} = \mathrm{Span}\,(\vec{l}^\sharp, \vec{m}^\sharp)$, they cannot both be orthogonal to $\vec{l}^\sharp$, so that retaining the candidate of larger norm in (77) always provides a non-zero direction, the construction being indeterminate only in the circular case $a^\sharp = b^\sharp$ where the axes are arbitrary. The minor axis then follows as $\vec{m}^\sharp = \vec{n}^\sharp\wedge\vec{l}^\sharp$, which establishes (76) reported in Section 3.1.

6.5.2 Identification of the transformed ribbon

The transformed ribbon can be identified as the limiting case for $a \to +\infty$ of the transformed ellipse considered in Appendix 6.5.1. It results from (73) that

$$a^\sharp \underset{a\to\infty}{\sim} a\|\vec{g}\| \tag{149}$$

Therefore $a^\sharp \to \infty$ and the transformed crack is also of ribbon-like type.

The second radius $b^\sharp$ is deduced from the Taylor series of (74), or even more easily from (143), which delivers the ratio $b^\sharp/b$ (78) reported in Section 3.1, together with its inverse counterpart

$$b \underset{a,a^\sharp\to\infty}{\sim} b^\sharp\,\frac{\|\vec{g}^\sharp\wedge\vec{h}^\sharp\|}{\|\vec{g}^\sharp\|}$$

In the case of a ribbon, the transformed crack can in fact be fully identified (including the eigenvectors $\vec{l}^\sharp$ and $\vec{m}^\sharp$). Indeed, (139) gives, to first order in $\mathbf{A}^{\sharp\intercal}\cdot\mathbf{A}^\sharp$

$$\mathbf{A}^{\sharp\intercal}\cdot\mathbf{A}^\sharp \underset{a,a^\sharp\to\infty}{\sim} a^2\,\vec{g}\otimes\vec{g} \underset{a,a^\sharp\to\infty}{\sim} a^{\sharp 2}\,\vec{l}^\sharp\otimes\vec{l}^\sharp \tag{150}$$

The quadratic form is therefore consistent with (149) and, together with (72), delivers the eigenvectors $\vec{l}^\sharp$ and $\vec{m}^\sharp$ (78) reported in Section 3.1.

6.5.3 On the transformed polar decomposition

In order to proceed to a decomposition similar to (99), it is first recalled that (71) implies that $\mathbf{A}$ and $\mathbf{A}^\sharp$ share the same image so that the orthonormal vectors $\vec{U}^\sharp$ and $\vec{V}^\sharp$, playing the same role for $\mathbf{A}^\sharp$ as $\vec{U}$ and $\vec{V}$ for $\mathbf{A}$, both belong to $\operatorname{Im}\mathbf{A}$ which is also the hyperplane normal to $\vec{W}$. Thus, up to a change of sign of $\vec{U}^\sharp$ or $\vec{V}^\sharp$, it is possible to assume that $\vec{W} = \vec{U}^\sharp \wedge \vec{V}^\sharp$. The decomposition of $\mathbf{A}^\sharp$ then writes

$$\mathbf{A}^\sharp = \mathbf{R}^\sharp \cdot \mathbf{S}^\sharp \quad \text{with} \quad \left\{ \begin{array}{lcl} \mathbf{R}^\sharp & = & \vec{U}^\sharp \otimes \vec{l}^\sharp + \vec{V}^\sharp \otimes \vec{m}^\sharp + \vec{W} \otimes \vec{n}^\sharp \\ \mathbf{S}^\sharp & = & a^\sharp\, \vec{l}^\sharp \otimes \vec{l}^\sharp + b^\sharp\, \vec{m}^\sharp \otimes \vec{m}^\sharp \end{array} \right. \tag{151}$$

and $\mathbf{A}^\sharp$ itself

$$\mathbf{A}^\sharp = a^\sharp\, \vec{U}^\sharp \otimes \vec{l}^\sharp + b^\sharp\, \vec{V}^\sharp \otimes \vec{m}^\sharp \quad \text{with} \quad \operatorname{Im}\mathbf{A}^\sharp = \operatorname{Im}\mathbf{A} = \operatorname{Span}(\vec{U}^\sharp, \vec{V}^\sharp) = \operatorname{Span}(\vec{U}, \vec{V}) = \vec{W}^\perp \tag{152}$$

Note that $\vec{U}^\sharp$ and $\vec{V}^\sharp$ are then related to $\vec{U}$ and $\vec{V}$ by a rotation around $\vec{W}$ which is not straightforward nor useful to precise particularly for later developments of the present work. On the contrary the following relationship giving the projection on $\operatorname{Im}\mathbf{A} = \vec{W}^\perp$ will prove important

$$\mathbf{A} \cdot \mathbf{A}^\dagger = \vec{U} \otimes \vec{U} + \vec{V} \otimes \vec{V} = \mathbf{1} - \vec{W} \otimes \vec{W} = \mathbf{A}^\sharp \cdot \mathbf{A}^{\sharp^\dagger} \tag{153}$$

Replacing $\mathbf{A}$ by $\mathbf{A}^\sharp \cdot \mathbf{P}^\intercal$, equation (153) becomes

$$\mathbf{A}^\sharp \cdot \left(\mathbf{P}^\intercal \cdot \mathbf{A}^\dagger - \mathbf{A}^{\sharp^\dagger} \right) = \mathbf{0} \tag{154}$$

which means that the image of $\mathbf{P}^\intercal \cdot \mathbf{A}^\dagger - \mathbf{A}^{\sharp^\dagger}$ belongs to the kernel of $\mathbf{A}^\sharp = \operatorname{Span}(\vec{n}^\sharp)$ so there exists a vector $\vec{X}$ such that

$$\mathbf{P}^\intercal \cdot \mathbf{A}^\dagger = \mathbf{A}^{\sharp^\dagger} + \vec{n}^\sharp \otimes \vec{X} \tag{155}$$

Recalling from (100) that $\mathbf{A}^\dagger = \mathbf{S}^\dagger \cdot \mathbf{R}^\intercal$ and thus $\mathbf{A}^{\sharp^\dagger} = \mathbf{S}^{\sharp^\dagger} \cdot \mathbf{R}^{\sharp\intercal}$, equation (155) can be rearranged as

$$\mathbf{P}^\intercal \cdot \mathbf{S}^\dagger = \mathbf{S}^{\sharp^\dagger} \cdot \mathbf{R}^{\sharp\intercal} \cdot \mathbf{R} + \vec{n}^\sharp \otimes \vec{Y} \tag{156}$$

where $\mathbf{R}^{\sharp\intercal} \cdot \mathbf{R}$ is a rotation sending $\vec{n}$ to $\vec{n}^\sharp$ and $\vec{n}^\perp$ to $\vec{n}^{\sharp\perp}$ and $\vec{Y}$ is an undefined vector. This equation shows a great importance in the derivation of the transformed COD tensor in Section 3.2.

Acknowledgements

Special thanks are due to Prof. S. Brisard (Aix Marseille Univ, LMA) for the valuable discussions, insightful comments, and constant support throughout the preparation of this manuscript. His help greatly contributed to improving the clarity and quality of this work.

During the preparation of the revision of this work, the author used Claude (Anthropic) only to assist in writing the validation scripts and in refining the wording of marginal parts of the text. All theoretical developments, analytical derivations, modelling, initial script implementations, and the interpretation and validation of the results are entirely the author's work, the numerical results being obtained with established software (`FEniCSx`, `Gmsh`, `Echoes`). The author reviewed and edited all output and takes full responsibility for the content of the published article.

References

Abramowitz, M., Stegun, I.A., 1972. Handbook of Mathematical Functions. National Bureau of Standards - Applied Mathematics Series - 55, Washington D.C.

Adessina, A., Barthélémy, J.-F., Lavergne, F., Ben Fraj, A., 2017. Effective elastic properties of materials with inclusions of complex structure. International Journal of Engineering Science 119, 1–15. https://doi.org/10.1016/j.ijengsci.2017.03.015

Baratta, I.A., Dean, J.P., Dokken, J.S., Habera, M., Hale, J.S., Richardson, C.N., Rognes, M.E., Scroggs, M.W., Sime, N., Wells, G.N., 2023. DOLFINx: The next generation FEniCS problem solving environment. https://doi.org/10.5281/zenodo.10447666

Barnett, D.M., Asaro, R.J., 1972. The fracture mechanics of slit-like cracks in anisotropic elastic media. Journal of the Mechanics and Physics of Solids 20, 353–366. https://doi.org/10.1016/0022-5096(72)90013-0

Barthélémy, J.-F., 2026. Echoes: Extended Calculator of HOmogEnization Schemes. https://doi.org/10.5281/zenodo.19679057

Barthélémy, J.-F., 2020. Simplified approach to the derivation of the relationship between Hill polarization tensors of transformed problems and applications. International Journal of Engineering Science 154, 103326. https://doi.org/10.1016/j.ijengsci.2020.103326

Barthélémy, J.-F., 2009. Compliance and Hill polarization tensor of a crack in an anisotropic matrix. International Journal of Solids and Structures 46, 4064–4072. https://doi.org/10.1016/j.ijsolstr.2009.08.003

Barthélémy, J.-F., Sevostianov, I., Giraud, A., 2021. Micromechanical modeling of a cracked elliptically orthotropic medium. International Journal of Engineering Science 161, 103454. https://doi.org/10.1016/j.ijengsci.2021.103454

Barthélémy, J.-F., Sevostianov, I., Giraud, A., Vilchevskaya, E., 2023. Compliance of a crack embedded in a transformed transversely isotropic material. Mathematics and Mechanics of Solids 1–30. https://doi.org/10.1177/10812865221150771

Budiansky, B., O'Connell, R.J., 1976. Elastic moduli of a cracked solid. International Journal of Solids and Structures 12, 81–97. https://doi.org/10.1016/0020-7683(76)90044-5

Destuynder, P., Djaoua, M., 1981. Sur une Interprétation Mathématique de l'Intégrale de Rice en Théorie de la Rupture Fragile. Mathematical Methods in the Applied Sciences 3, 70–87. https://doi.org/10.1002/mma.1670030106

Deude, V., Dormieux, L., Kondo, D., Maghous, S., 2002. Micromechanical approach to nonlinear poroelasticity: Application to cracked rocks. Journal of engineering mechanics 128, 848–855. https://doi.org/10.1061/(ASCE)0733-9399(2002)128:8(848)

Dormieux, L., Kondo, D., 2016. Micromechanics of Fracture and Damage. Wiley. https://doi.org/10.1002/9781119292166

Dormieux, L., Kondo, D., 2009. Stress-based estimates and bounds of effective elastic properties : The case of cracked media with unilateral effects. Computational Materials Science 46, 173–179. https://doi.org/10.1016/j.commatsci.2009.02.027

Du, K., Cheng, L., Barthélémy, J.-F., Sevostianov, I., Giraud, A., Adessina, A., 2020. Numerical computation of compliance contribution tensor of a concave pore embedded in a transversely isotropic matrix. International Journal of Engineering Science 152, 103306. https://doi.org/10.1016/j.ijengsci.2020.103306

Eshelby, J.D., 1957. The determination of the elastic field of an ellipsoidal inclusion, and related problems. Proceedings of the Royal Society of London. Series A. Mathematical and Physical Sciences 241, 376–396. https://doi.org/10.1098/rspa.1957.0133

Fabrikant, V.I., 1987. The stress intensity factor for an external elliptical crack. International Journal of Solids and Structures 23, 465–467. https://doi.org/10.1016/0020-7683(87)90011-4

Gel'fand, I.M., Shilov, G.E., 1964. Generalized functions - Vol I Properties and Operations. Academic press, New-York; London.

Geuzaine, C., Remacle, J.-F., 2009. Gmsh: A 3-D finite element mesh generator with built-in pre- and postprocessing facilities. International Journal for Numerical Methods in Engineering 79, 1309–1331. https://doi.org/10.1002/nme.2579

Gruescu, C., Montchiet, V., Kondo, D., 2005. Eshelby tensor for a crack in an orthotropic elastic medium. C. R. Mécanique 333, 467–473.

Hoenig, A., 1978. The behavior of a flat elliptical crack in an anisotropic elastic body. International Journal of Solids and Structures 14, 925–934. https://doi.org/10.1016/0020-7683(78)90068-9

Irwin, G.R., 1957. Analysis of Stresses and Strains Near the End of a Crack Traversing a Plate. Journal of Applied Mechanics 24, 361–364. https://doi.org/10.1115/1.4011547

Kachanov, M., 1993. Elastic Solids with Many Cracks and Related Problems. Advances in Applied Mechanics 30, 259–445. https://doi.org/10.1016/S0065-2156(08)70176-5

Kachanov, M., 1992. Effective Elastic Properties of Cracked Solids: Critical Review of Some Basic Concepts. Applied Mechanics Reviews 45, 304–335. https://doi.org/10.1115/1.3119761

Kachanov, M., Sevostianov, I., 2018. Micromechanics of Materials, with Applications, Solid Mechanics and Its Applications. Springer International Publishing, Cham. https://doi.org/10.1007/978-3-319-76204-3

Kachanov, M., Shafiro, B., Tsukrov, I., 2003. Handbook of Elasticity Solutions. Springer Netherlands, Dordrecht. https://doi.org/10.1007/978-94-017-0169-3

Kanaun, S.K., 1981. On the problem of a three-dimensional crack in an anisotropic elastic medium. Journal of Applied Mathematics and Mechanics 45, 262–269. https://doi.org/10.1016/0021-8928(81)90045-9

Kanaun, S.K., Levin, V.M., 2009. Elliptical cracks arbitrarily oriented in 3D-anisotropic elastic media. International Journal of Engineering Science 47, 777–792. https://doi.org/10.1016/j.ijengsci.2008.12.014

Kassir, M.K., Sih, G.C., 1968. Three-dimensional stresses around elliptical cracks in transversely isotropic solids. Engineering Fracture Mechanics 1, 327–345. https://doi.org/10.1016/0013-7944(68)90006-4

Kassir, M.K., Sih, G.C., 1966. Three-Dimensional Stress Distribution Around an Elliptical Crack Under Arbitrary Loadings. Journal of Applied Mechanics 33, 601–611. https://doi.org/10.1115/1.3625127

Kunin, I.A., 1983. Elastic Media with Microstructure II, Proceedings of the National Academy of Sciences, Springer Series in Solid-State Sciences. Springer Berlin Heidelberg, Berlin, Heidelberg. https://doi.org/10.1007/978-3-642-81960-5

Kushch, V.I., Sevostianov, I., 2020. Ellipsoidal inhomogeneity in elliptically orthotropic elastic solid. International Journal of Solids and Structures 206, 282–291. https://doi.org/10.1016/j.ijsolstr.2020.09.025

Laws, N., 1985. A short note on penny-shaped cracks in transversely isotropic materials. Mech. Mater. 4, 209–212.

Li, F.Z., Shih, C.F., Needleman, A., 1985. A comparison of methods for calculating energy release rates. Engineering Fracture Mechanics 21, 405–421. https://doi.org/10.1016/0013-7944(85)90029-3

Li, Y., Qin, Q.-H., Zhao, M., 2020. Analysis of 3D planar crack problems of one-dimensional hexagonal piezoelectric quasicrystals with thermal effect. Part II: Numerical approach. International Journal of Solids and Structures 188–189, 223–232. https://doi.org/10.1016/j.ijsolstr.2019.10.020

Masson, R., 2008. New explicit expressions of the Hill polarization tensor for general anisotropic elastic solids. International Journal of Solids and Structures 45, 757–769. https://doi.org/10.1016/j.ijsolstr.2007.08.035

Mauge, C., Kachanov, M., 1994b. Effective elastic properties of an anisotropic material with arbitrarily oriented interacting cracks. Journal of the Mechanics and Physics of Solids 42, 561–584. https://doi.org/10.1016/0022-5096(94)90052-3

Mauge, C., Kachanov, M., 1994a. Anisotropic material with interacting arbitrarily oriented cracks. Stress intensity factors and crack-microcrack interactions. International Journal of Fracture 65, 115–139. https://doi.org/10.1007/BF00032283

Mura, T., 1987. Micromechanics of Defects in Solids, Second Edition. Kluwer Academic. https://doi.org/10.1007/978-94-009-3489-4

Nemat-Nasser, S., Hori, M., 1999. Micromechanics: Overall Properties of Heterogeneous Materials 2nd Edition, North Holland. ed. North Holland, Amsterdam, The Netherlands.

Pouya, A., 2007. Green's function solution and displacement potentials for Transformed Transversely Isotropic materials. European Journal of Mechanics - A/Solids 26, 491–502. https://doi.org/10.1016/j.euromechsol.2006.09.002

Pouya, A., 2000. Une transformation du problème d'élasticité linéaire en vue d'application au problème de l'inclusion et aux fonctions de Green. C. R. Acad. Sci., Série IIb 328, 437–443.

Pouya, A., Zaoui, A., 2006. A transformation of elastic boundary value problems with application to anisotropic behavior. Int. J. Solids Struct. 43, 4937–4956. https://doi.org/10.1016/j.ijsolstr.2005.06.046

Rice, J., 1989. Weight Function Theory for Three-Dimensional Elastic Crack Analysis, in: Fracture Mechanics: Perspectives and Directions (Twentieth Symposium). ASTM International100 Barr Harbor Drive, PO Box C700, West Conshohocken, PA 19428-2959, pp. 29–57. https://doi.org/10.1520/stp18819s

Rice, J.R., 1975. Continuum mechanics and thermodynamics of plasticity in relation to microscale deformation mechanisms, in: Argon, A. (Ed.), Constitutive Equations in Plasticity. MIT Press, Cambridge, pp. 23–79.

Rice, J.R., 1968. A Path Independent Integral and the Approximate Analysis of Strain Concentration by Notches and Cracks. Journal of Applied Mechanics 35, 379–386. https://doi.org/10.1115/1.3601206

Schwartz, L., 1966. Théorie des distributions (in French). Hermann, Paris.

Sevostianov, I., Kachanov, M., 2021. Evaluation of the incremental compliances of non-elliptical contacts by treating them as external cracks. European Journal of Mechanics - A/Solids 85, 104114. https://doi.org/10.1016/j.euromechsol.2020.104114

Sevostianov, I., Kachanov, M., 2002. On elastic compliances of irregularly shaped cracks. International Journal of Fracture 114, 245–257. https://doi.org/10.1023/A:1015534127172

Sevostianov, I., Kushch, V.I., 2020. Compliance contribution tensor of an arbitrarily oriented ellipsoidal inhomogeneity embedded in an orthotropic elastic material. International Journal of Engineering Science 149, 103222. https://doi.org/10.1016/j.ijengsci.2020.103222

Sevostianov, I., Yilmaz, N., Kushch, V., Levin, V., 2005. Effective elastic properties of matrix composites with transversely-isotropic phases. International Journal of Solids and Structures 42, 455–476. https://doi.org/10.1016/j.ijsolstr.2004.06.047

Shih, C.F., Moran, B., Nakamura, T., 1986. Energy release rate along a three-dimensional crack front in a thermally stressed body. International Journal of Fracture 30, 79–102. https://doi.org/10.1007/BF00034019

Tsukrov, I., Kachanov, M., 2000. Effective moduli of an anisotropic material with elliptical holes of arbitrary orientational distribution. International Journal of Solids and Structures 37, 5919–5941. https://doi.org/10.1016/S0020-7683(99)00244-9

Villani, G., Belardi, V.G., Salvini, P., Vivio, F., 2023. Energetic approach to predict the elliptical crack growth. Procedia Structural Integrity 47, 873–881. https://doi.org/10.1016/j.prostr.2023.07.032

Willis, J.R., 1977. Bounds and self-consistent estimates for the overall properties of anisotropic composites. Journal of the Mechanics and Physics of Solids 25, 185–202. https://doi.org/10.1016/0022-5096(77)90022-9

Willis, J.R., 1968. The stress field around an elliptical crack in an anisotropic elastic medium. International Journal of Engineering Science 6, 253–263. https://doi.org/10.1016/0020-7225(68)90025-6

Zhao, M., Fan, C., Yang, F., Liu, T., 2007. Analysis method of planar cracks of arbitrary shape in the isotropic plane of a three-dimensional transversely isotropic magnetoelectroelastic medium. International Journal of Solids and Structures 44, 4505–4523. https://doi.org/10.1016/j.ijsolstr.2006.11.039

Zhao, M.H., Shen, Y.P., Liu, Y.J., Liu, G.N., 1998. The method of analysis of cracks in three-dimensional transversely isotropic media: Boundary integral equation approach. Engineering Analysis with Boundary Elements 21, 169–178. https://doi.org/10.1016/S0955-7997(98)00033-2